Experimental Modeling of NOx and PM Generation from Combustion of Various Biodiesel Blends for Urban Transport Buses

MNTRC Report 12-62

MNTRC
MINETA NATIONAL TRANSIT RESEARCH CONSORTIUM

THE UNIVERSITY OF TOLEDO
1872

MINETA TRANSPORTATION INSTITUTE
LEAD UNIVERSITY OF MNTRC

The Mineta Transportation Institute (MTI) was established by Congress in 1991 as part of the Intermodal Surface Transportation Equity Act (ISTEA) and was reauthorized under the Transportation Equity Act for the 21st century (TEA-21). MTI then successfully competed to be named a Tier 1 Center in 2002 and 2006 in the Safe, Accountable, Flexible, Efficient Transportation Equity Act: A Legacy for Users (SAFETEA-LU). Most recently, MTI successfully competed in the Surface Transportation Extension Act of 2011 to be named a Tier 1 Transit-Focused University Transportation Center. The Institute is funded by Congress through the United States Department of Transportation's Office of the Assistant Secretary for Research and Technology (OST-R), University Transportation Centers Program, the California Department of Transportation (Caltrans), and by private grants and donations.

The Institute receives oversight from an internationally respected Board of Trustees whose members represent all major surface transportation modes. MTI's focus on policy and management resulted from a Board assessment of the industry's unmet needs and led directly to the choice of the San José State University College of Business as the Institute's home. The Board provides policy direction, assists with needs assessment, and connects the Institute and its programs with the international transportation community.

MTI's transportation policy work is centered on three primary responsibilities:

Research

MTI works to provide policy-oriented research for all levels of government and the private sector to foster the development of optimum surface transportation systems. Research areas include: transportation security; planning and policy development; interrelationships among transportation, land use, and the environment; transportation finance; and collaborative labor-management relations. Certified Research Associates conduct the research. Certification requires an advanced degree, generally a Ph.D., a record of academic publications, and professional references. Research projects culminate in a peer-reviewed publication, available both in hardcopy and on TransWeb, the MTI website (http://transweb.sjsu.edu).

Education

The educational goal of the Institute is to provide graduate-level education to students seeking a career in the development and operation of surface transportation programs. MTI, through San José State University, offers an AACSB-accredited Master of Science in Transportation Management and a graduate Certificate in Transportation Management that serve to prepare the nation's transportation managers for the 21st century. The master's degree is the highest conferred by the California State University system. With the active assistance of the California Department of Transportation, MTI delivers its classes over a state-of-the-art videoconference network throughout the state of California and via webcasting beyond, allowing working transportation professionals to pursue an advanced degree regardless of their location. To meet the needs of employers seeking a diverse workforce, MTI's education program promotes enrollment to under-represented groups.

Information and Technology Transfer

MTI promotes the availability of completed research to professional organizations and journals and works to integrate the research findings into the graduate education program. In addition to publishing the studies, the Institute also sponsors symposia to disseminate research results to transportation professionals and encourages Research Associates to present their findings at conferences. The World in Motion, MTI's quarterly newsletter, covers innovation in the Institute's research and education programs. MTI's extensive collection of transportation-related publications is integrated into San José State University's world-class Martin Luther King, Jr. Library.

REPORT 12-62

EXPERIMENTAL MODELING OF NOX AND PM GENERATION FROM COMBUSTION OF VARIOUS BIODIESEL BLENDS FOR URBAN TRANSPORT BUSES

Ashok Kumar, Ph.D., P Eng., BCEE
Dong-Shik Kim, Ph.D., PE
Hamid Omidvarborna, Ph.D.
Manideep Yarlagadda
Sudheer Kumar Kuppili
Nader Majed Sawtarie

August 2016

A publication of
Mineta National Transit Research Consortium

College of Business
San José State University
San José, CA 95192-0219

TECHNICAL REPORT DOCUMENTATION PAGE

1. Report No. CA-MNTRC-16-1245	**2. Government Accession No.**	**3. Recipient's Catalog No.**
4. Title and Subtitle Experimental Modeling of NO_x and PM Generation from Combustion of Various Biodiesel Blends for Urban Transport Buses		**5. Report Date** August 2016 **6. Performing Organization Code**
7. Authors Ashok Kumar, Ph.D., P Eng., BCEE, Dong-Shik Kim, Ph.D., PE, Hamid Omidvarborna, Ph.D., Manideep Yarlagadda, Sudheer Kumar Kuppili, Nader Majed Sawtarie		**8. Performing Organization Report** MTI Report 12-62
9. Performing Organization Name and Address Mineta National Transit Research Consortium College of Business San José State University San José, CA 95192-0219		**10. Work Unit No.** **11. Contract or Grant No.** DTRT12-G-UTC21
12. Sponsoring Agency Name and Address U.S. Department of Transportation Office of the Assistant Secretary for Research and Technology University Transportation Centers Program 1200 New Jersey Avenue, SE Washington, DC 20590 The University of Toledo College of Engineering Nitschke Hall, MS 310 1610 N. Westwood Toledo, OH 43607		**13. Type of Report and Period Covered** Final Report **14. Sponsoring Agency Code**
15. Supplemental Notes		

16. Abstract

Biodiesel has diverse sources of feedstock and the amount and composition of its emissions vary significantly depending on combustion conditions. Results of laboratory and field tests reveal that nitrogen oxides (NOx) and particulate matter (PM) emissions from biodiesel are influenced more by combustion conditions than emissions from regular diesel. Therefore, NOx and PM emissions documented through experiments and modeling studies are the primary focus of this investigation. In addition, a comprehensive analysis of the feedstock-related combustion characteristics and pollutants are investigated. Research findings verify that the oxygen contents, the degree of unsaturation, and the size of the fatty acids in biodiesel are the most important factors that determine the amounts and compositions of NOx and PM emissions.

17. Key Words Biodiesel feedstocks; combustion; particulate matter; nitrogen oxides; modeling analysis	**18. Distribution Statement** No restrictions. This document is available to the public through The National Technical Information Service, Springfield, VA 22161		
19. Security Classif. (of this report) Unclassified	**20. Security Classif. (of this page)** Unclassified	**21. No. of Pages** 79	**22. Price** $15.00

Form DOT F 1700.7 (8-72)

Library of Congress Catalog Card Number:
2016948759

To order this publication, please contact:

Mineta National Transit Research Consortium
College of Business
San José State University
San José, CA 95192-0219

Tel: (408) 924-7560
Fax: (408) 924-7565
Email: mineta-institute@sjsu.edu

transweb.sjsu.edu/mntrc/

080916

ACKNOWLEDGMENTS

This study is based upon work supported by the U.S. Department of Transportation's University Transportation Centers Program under Grant Number DTRT12-G-UTC21. The assistance provided by Mineta National Transit Research Consortium (MNTRC) is gratefully acknowledged. The authors would like to extend their sincere appreciation to Toledo Area Regional Transit Authority (TARTA), United Oil Inc., and White Mountain Biodiesel for providing us samples of ultra-low sulfur diesel (ULSD) and biodiesel. The contents of this report reflect the views of the authors, who are responsible for the facts and accuracy of the information presented herein. This document is disseminated under the sponsorship of the U.S. Department of Transportation's University Transportation Centers Program, in the interest of information exchange. The U.S. government assumes no liability for the contents or use thereof.

The authors thank MTI staff, including Executive Director Karen Philbrick, Ph.D.; Publication Support Coordinator Joseph Mercado; Executive Administrative Assistant Jill Carter; and Editor and Webmaster Frances Cherman.

TABLE OF CONTENTS

LIST OF FIGURES

LIST OF TABLES

EXECUTIVE SUMMARY

Although it is generally accepted that biodiesel fuel contributes to the reduction of pollutants, biodiesel still needs more study for better control of emissions and engine performance. Biodiesel has very diverse sources of feedstock, and due to various blends and chemical components, the amount and composition of its emissions vary significantly depending on combustion conditions. Particularly in real tests, nitrogen oxides (NO_x) and particulate matter (PM) emissions from biodiesel are more influenced by combustion conditions than emissions from regular diesel. Therefore, NO_x and PM emissions are the primary focus of the current investigation. In addition, a comprehensive analysis of the feedstock-related combustion characteristics and pollutants are investigated as well.

On the other hand, as demand climbs for more fuel-efficient vehicles, a new strategy known as low-temperature combustion (LTC) may soon lead auto manufacturers and consumers to broader use of cleaner diesel engines in the United States. LTC addresses NO_x emissions from engines by recirculating some of the exhaust gases back into the engine's cylinders, whereby heat is absorbed from combustion through the dilution effect. The method, called "exhaust gas recirculation" (EGR), has proven to be a very effective and practical NO_x reduction technique resulting from lower combustion temperatures, which significantly reduces NO_x formation.

The focus of the research lies on generation mechanisms of NO_x and PM emissions from combustion of different biodiesel feedstocks. First, this aim was achieved by experiments comparing the emissions of biodiesel of different grades (B0, B20, B50, and B100 biodiesel) with ultra-low sulfur diesel (ULSD) for three types of biodiesel feedstocks: soybean methyl ester (SME), tallow oil (TO), and waste cooking oil (WCO). Laboratory studies were performed by burning biodiesel and then analyzing the exhaust emissions. The exhaust gas was analyzed for NO_x and collected PM was used for further analyses. For chemical characterization of PM, the collected samples from the reactor were analyzed by using inductively coupled plasma mass spectrometry (ICP-MS) for their possible elements. For further characterization of PM formed in the laboratory reactor, scanning electron microscope (SEM), transmission electron microscope (TEM), Fourier transform infrared spectroscopy (FTIR), and thermogravimetric analysis (TGA) were used. The exhaust gas was analyzed using a NO_x analyzer to correlate the fuel's properties with NO_x emissions.

Combustion analysis showed that neat biodiesel fuels had longer ignition delays and lower ignition temperatures compared to ULSD. The unsaturation of biodiesel samples and their blends with ULSD were analyzed for their effects on NO_x emissions. The results showed that biodiesel containing more unsaturated fatty acids emitted higher levels of NO_x than did biodiesel with more saturated fatty acids. A paired t-test showed that neat TO, WCO, and WCO-B50 significantly reduced the formation of NO_x compared with ULSD and SME-B20. It can be concluded that less unsaturated fatty acid methyl esters (FAMEs) such as TO and WCO would be preferable when reduction of NO_x emissions is desired.

Combustion of biodiesel fuels to better understand the effects of feedstock type on carbon emissions in the forms of carbon dioxide (CO_2), carbon monoxide (CO), and methane (CH_4) were conducted under fuel-rich conditions. ULSD showed the highest emission of CO and

the lowest emissions of CO_2 and CH_4 among the fuels studied. Compared to ULSD, it was found that the use of pure biodiesel fuels reduced CO by a factor of 0.33 and enhanced CO_2 emissions by a factor 3. Biodiesel fuel with a high degree of unsaturation and high portion of long methyl esters appeared to produce more CO and less CO_2 emissions than those with low degrees of unsaturation and short chain length (such as WCO and TO). Biodiesel fuels with long and unsaturated chains released more CH_4 than fuels with short and less unsaturated chains. It is thought that the length of FAMEs affects the carbon emissions because shorter chains, which contain less unsaturated structures, have a high oxygen-to-carbon ratio.

Experiments using a laboratory combustion chamber showed significantly lower soot emissions with biodiesel fuel compared to ULSD. For neat biodiesel, no soot particles were observed from combustion regardless of their feedstock origins. The overall morphology of soot particles showed that the average diameter of ULSD soot particles was greater than the average soot particles from biodiesel blends. Eight elements were detected as the marker metals in biodiesel soot particles. In a laboratory combustion chamber, unsaturated methyl esters and the high oxygen content of biodiesel are thought to be the major factors that help reduce the formation of soot particles.

Secondly, experiments on both PM and NO_x emissions were conducted on real engines. The Federal Transit Administration has identified engines in idle mode as a pollution source for future regulatory plans. Field experiments using Toledo Area Regional Transit Authority (TARTA) buses were performed on buses equipped with EGR and non-EGR engines. A novel method was introduced to analyze size distribution of PMs emitted from heavy duty engines. For better comparison of real engines, NO_x emissions were analyzed in both off-road (idle) and on-road tests.

The performance of a bus that ran on blended biodiesel (B5) was found to be very similar to that of ULSD, and drivability was not an issue with blended biodiesel. In addition, a simplified model was developed by using an Artificial Neural Network (ANN) to predict NO_x emissions from TARTA buses via available parameters.

There are very few robust NO_x formation models due to the complexity of combustion processes. Thousands of interactions are involved in a combustion process, making it extremely difficult to model. Thus, instead of choosing the high degrees of freedom needed for successful NO_x modeling, a simple biodiesel surrogate was selected and main pathways were derived. A stochastic simulation algorithm (SSA) approach was implemented with the components of a simplified biodiesel surrogate to predict NO_x (NO and NO_2) emission concentrations from the combustion of biodiesel. The main reaction pathways were obtained by simplifying the previously derived skeletal mechanisms, including saturated methyl decenoate (MD), unsaturated methyl 5-decanoate (MD5D), and n-decane (ND). ND was added to match the energy content and the C/H/O ratio of actual biodiesel fuel. The MD/MD5D/ND surrogate model was also equipped with detailed H_2/CO/C_1 formation mechanisms and a NO_x formation mechanism. The predicted model results are in good agreement with a limited number of experimental data at LTC conditions for three different biodiesel fuels consisting of various ratios of unsaturated and saturated methyl esters. The SSA model shows the potential to predict NO_x emission concentrations, when the

peak combustion temperature increases through the addition of ULSD to biodiesel. The SSA method used in this study demonstrates the possibility of reducing the computational complexity in biodiesel emissions modeling.

Modeling is expected to help us determine major intermediates and reaction pathways that play important roles in biodiesel emissions under LTC. Engine manufacturers may use this model to establish advanced combustion strategies and design engines with high efficiency. Based on these findings, it can be concluded that both the use of alternative renewable fuels (biodiesel blends) as well as a LTC condition are suitable choices for existing diesel engines to reduce pollutant emissions.

I. INTRODUCTION

BIODIESEL STUDY

Recently, it has become more attractive to utilize biodiesel as an alternative fuel to meet both emission reduction and energy security objectives. Biodiesel has inherent characteristics that allow its use in modern diesel engines without significant modifications (Kumar et al., 2014). Biodiesel, as defined in Standard ASTM D6751, is a non-petroleum-based diesel fuel made by transesterification of mono-alkyl esters of fatty acid methyl esters (FAMEs) from vegetable oils and animal fats. Biodiesel and its blends in general are known to produce lower emissions of carbon monoxide (CO), soot, and hydrocarbons (HCs), but higher emissions of nitrogen oxides (NO_x) when compared with regular diesel (Kumar et al., 2014; Omidvarborna et al., 2014; Omidvarborna et al., 2015a). Lower emissions from biodiesel combustion have been a key driving force for biodiesel fuel use in the transportation sector (Kegl, 2011). Biodiesel is commonly blended with diesel in different proportions; most commonly, a mix of 20% biodiesel and 80% diesel (volume based) is used, which is referred to as B20 (Omidvarborna et al., 2014). An essential characteristic of biodiesel fuels is its fatty acid profile, which corresponds to its principal feedstocks. Therefore, the main structural features of fatty acids are associated with their characteristics, e.g., chain length, oxygen content, and number of double bonds (unsaturated content).

SOOT AND NO_x EMISSIONS

Diesel, as a fuel, is known as a source of emission species such as particulate matter (PM), polycyclic aromatic hydrocarbons (PAHs), heavy metals, and NO_x (Krzyzanowski et al., 2005; Omidvarborna et al., 2014; Shandilya and Kumar, 2014). These species are produced during combustion and found mainly in the form of aerosols, which are recognized as health hazards (Kaden et al., 1979). Among these diesel emission species, PM has garnered serious concern as a hazard to human health due to its direct and broad impact on the respiratory organs. In the past, health professionals associated PM_{10} (diameter £10 μm) with chronic lung disease, lung cancer, influenza, asthma, and increased mortality rate (Stöber and Abel, 1996). However, recent scientific studies suggest that these correlations are more closely linked with fine particles ($PM_{2.5}$) and ultra-fine particles ($PM_{0.1}$) (Schwartz, 1994), which can penetrate deep into the lungs. To address these problems, a great deal of air quality research has been performed on the toxicity and chemistry of PM over the past decades. It is generally reported that the majority of PM originates from soot, which is usually formed in fuel-rich or low-oxygen regions of a diesel engine (Omidvarborna et al., 2015a).

Along with the fatty acid profile, equal importance must be given to the extent of the contribution from biodiesel pollution, because biodiesel usage in the transportation sector has been gradually increasing. PM emissions from motor vehicles are the major contributors of urban atmospheric PM, especially $PM_{2.5}$ (Kleeman et al., 2000; Laden et al., 2000; Robert et al., 2007). PM released from diesel engines also contains various organic and inorganic compounds (Betha and Balasubramanian, 2013; Shah et al., 2004). It is necessary to measure the PM size distribution released from vehicles in order to quantify the source contribution and elucidate the possible health effects (Laden et al., 2000; Robert et al., 2007). Numerous epidemiologic studies have found that increased exposure

to atmospheric PM also increases human mortality rate and various adverse health effects (Betha and Balasubramanian, 2013; Riediker et al., 2004; Robert et al., 2007; Rounce et al., 2012; Su et al., 2013) and diesel engines are a significant source for PM emissions (Su et al., 2013). Ultrafine particles emitted from diesel engines are reported to have caused higher health impacts than $PM_{2.5}$ (Betha and Balasubramanian, 2013). The characterization of PM emission data is also needed as fuels, engines, and vehicle technologies evolve over time (Kleeman et al., 2000). Alternative fuels such as biodiesel have been found to be more attractive when trying to reduce PM emissions (Fazal et al., 2011; Lapuerta et al., 2008a; Lapuerta et al., 2008b; Xue et al., 2011). During biodiesel combustion, the amount of PM released decreases as biodiesel blend percentage is increased, e.g., B100 releases less PM than B50 (Fazal et al., 2011; Lapuerta et al., 2008; Xue et al., 2011).

Current research on PM has been categorized and concentrated on specific characteristics such as size, number, and composition of the particles (Su et al., 2013). Progress in engine combustion research now facilitates the reduction of PM and other exhaust gases even before their release from the vehicles, e.g., by lowering combustion temperature, by using exhaust gas recirculation (EGR) and catalytic converters (Rounce et al., 2012).

Soot consists of carbonaceous material accompanied by various organic and inorganic compounds. It is widely accepted that during diesel combustion, the formation of soot particles can be depicted in five sequential steps (Omidvarborna et al., 2015a): (1) soot precursors formation (e.g., acetylenes and PAHs), (2) nucleation, i.e., transition from gaseous media in a combustion process to heavy molecules that eventually turn into nascent soot, (3) mass growth by attracting and interacting with HCs, (4) coagulation and agglomeration to form spherical soot particles and large aggregates with chain-like structures, respectively, and finally (5) oxidation to reduce the mass and size of soot particles. To meet the increasingly stringent regulations on soot emissions, numerous efforts have been made to control diesel soot emissions by modifying engine systems (Omidvarborna et al., 2014; Omidvarborna et al., 2015b; Shandilya and Kumar, 2014).

NO_x formation during biodiesel combustion is associated with a number of factors such as the properties of the biodiesel fuel and combustion conditions. In real engines, many more parameters are involved in NO_x formation such as load percent, engine speed, etc. The reduction of NO_x emissions is one of the most important technical challenges facing biodiesel usage, especially in light of the progressively strict exhaust emissions regulations on diesel engines (Knothe et al., 2006). Combustion temperature influences on thermal NO_x emissions have been reported (Hoekman and Robbins, 2012; Kumar et al., 2014; Omidvarborna et al., 2014). Low temperature may help with thermal NO_x formation and PM reduction (by lowering combustion flame temperature) during combustion, leading to low-temperature combustion (LTC) technology (Hill and Smoot, 2000; Varatharajan and Cheralathan, 2012).

CARBON EMISSIONS (CO, CO_2, AND CH_4)

According to the United States Environmental Protection Agency (USEPA), the majority of carbon emissions from the transportation sector can be attributed to carbon dioxide (CO_2) and relatively small amounts of other components, e.g., CO and methane (CH_4) resulting from the combustion of petroleum-based products (diesel and gasoline) in engines (Kumar et al., 2014; USEPA 2016). Although CH_4 is not toxic, it has a global warming potential, as reported by Environment Canada in 2011 that is 25 times higher than that of CO_2. Technological improvements in engines over the last few decades have greatly reduced carbon emissions (Omidvarborna et al., 2015a); however, energy consumption and CO_2 emissions have experienced a sustained increase mainly due to population growth. Therefore, advanced technologies such as LTC with the implementation of alternative fuels are currently under extensive research and development to reduce emissions. In addition, advances and research in molecular biology make it possible to improve the profile of biofuel feedstocks to enhance fuel properties and reduce emissions (Durrett et al., 2008).

Biodiesel has received considerable attention for its potential to reduce emissions in the transportation sector, where it offers advantages by lowering tailpipe emissions over emissions from ultra-low sulfur diesel (ULSD) fuel (Omidvarborna et al., 2014; Omidvarborna et al., 2015c; Shandilya and Kumar, 2013). It is reported that the contribution from traffic to CO_2 emissions is as high as 23% (GHG Data, 2006). Therefore, the benefits of biodiesel on greenhouse gas emissions are especially significant, because CO_2 released during biofuel combustion is offset by CO_2 captured by the plants from which biodiesel is produced. Thus, biodiesel is very attractive as a means for reducing CO_2 emissions (Barabas et al., 2010).

LITERATURE REVIEW

The type and proportion of the FAME molecules are thought to be the most important factors that affect fuel emissions. As mentioned earlier, the number of double bonds (e.g., the degree of unsaturation) and the oxygen content of biodiesel plays an important role in soot emissions (Benjumea et al., 2011; Salamanca et al., 2012a). According to the USEPA report (2002), biodiesel's impact on pollutant emissions is mostly related to biodiesel feedstocks and the chemical composition of the diesel used to prepare the blends (Salamanca et al., 2012b). Biodiesel lacks sulfur and aromatics, which are considered to be critical precursors for the initial formation of PAHs leading to soot (Lapuerta et al., 2008a; Lapuerta et al., 2008b; Omidvarborna et al., 2015a; Salamanca et al., 2012a; Song et al., 2006). The complex reaction mechanisms of biodiesel fuel combustion are described not only as a function of the size of the fuel molecules and degree of unsaturation, but also as a consequence of the additional reactions of the oxygen-containing species (Kohse-Höinghaus et al., 2010).

The diameter of soot particles from diesel engines has been reported elsewhere (Lapuerta et al., 2007; Neer and Koylu, 2006). Engine speed and air/fuel ratio have been reported to influence the size of soot particles. Increasing air/fuel ratio leads to a decrease in the diameter of the soot particles due to soot oxidation. For neat methyl esters, the oxygen content slightly increases with the degree of unsaturation because of the decrease in the

molecular weight associated with the displacement of two hydrogen atoms by each double bond (Benjumea et al., 2010). Sarathy et al. (2007) found that the unsaturated methyl ester fuel led to the generation of higher levels of oxygenated species. Lapuerta et al. (2008a) reported that as the biodiesel fuel became more unsaturated, soot emissions decreased by 20%. They also concluded that unsaturated biodiesel fuels showed a smaller mean particle diameter than less unsaturated fuels. Boehman et al. (2005) found that soot samples collected from the combustion of B20 blend had a lower oxidation temperature than that of diesel, whereas amorphous carbon was found in the inner core of soot particles. The hollow internal structure of soybeen methyl ester (SME) soot, likely created by the fuel-bonded oxygen, enables a much higher oxidation rate than the soot generated by diesel (Song, 2006). In this study, the chemical functional groups of biodiesel and associated PM emissions from a diesel engine were determined by Fourier Transform Infrared (FTIR) spectroscopy (Chien et al., 2008). Compared to diesel fuel, the FTIR spectra of the PM emissions from biodiesel PM showed the oxygenated functional group at 1747 cm^{-1} (Chien et al., 2008). Lapuerta et al. (2012) found that the morphology and reactivity of the soot emitted by a diesel engine was affected more by fuel composition (diesel and animal fat biodiesel) than by engine operation mode (temperature). Animal fat biodiesel soot was observed to be nano-sized and more reactive with oxygen than the diesel soot. Biodiesel fuels with different saturation levels were tested in a diesel engine and the results showed that PM emissions were reduced by 50% for all of the fuels (Hass et al., 2001).

Due to lower energy content (calorific value) of biodiesel fuels, more fuel was needed to produce the same amount of power (Omidvarborna et al., 2015c). The oxygen-to-carbon ratio of biodiesel fuel is higher than that of diesel fuel, because biodiesel has more than 10% oxygen by mass in its molecular structure (Zheng et al., 2008). In addition, due to fuel-borne oxygen in biodiesel, a larger amount of carbon was oxidized to CO_2 rather than partially oxidized to CO. Moreover, the oxygen-carbon ratio is also higher for biodiesel than for regular diesel fuel (Bari, 2014). The higher oxygen-carbon ratio promotes more complete combustion and little to no formation of CO, PM, and HCs. Although emissions of many species decrease by using biodiesel, NO_x emissions slightly increase. The production of NO_x is significantly influenced by the in-cylinder gas temperature, availability of oxygen, and residence time of fuel. NO_x emissions were greater at lower speeds than at higher speeds for both fuels because the torque was higher at higher speeds, which produces higher exhaust temperatures, indicating higher in-cylinder combustion temperatures (Bari, 2014). Bari reported that at lower speed, 1000 rpm, the residence time for NO_x formation would be twice as long at higher speed, 2000 rpm. As supported by Zheng et al. (2008), a longer residence time led to higher NO_x emissions. Therefore, the combination of higher in-cylinder temperatures, longer residence times, and increased oxygen content biodiesel not only produced the most NO_x at lower speeds but produced more NO_x emissions than diesel at all speeds. On average, this increase was 4.8% higher than with ULSD. This increase in NO_x emissions from biodiesel-fueled engines has been documented in the literature (Chattopadhyay and Sen, 2013; Macor et al., 2011; Wang et al., 2000).

A number of attempts have been made to reduce NO_x emissions from diesel and biodiesel engines through combustion modification methods (Abd-Alla, 2002; Saleh, 2009; Szybist et al., 2007). No single theory provides an adequate explanation for the relationship between biodiesel properties and NO_x emissions under various conditions, including combustion

temperature. However, it has been suggested that the degree of unsaturation of biodiesel plays an important role in NO_x formation during combustion (Benjumea et al., 2010; Lapuerta et al., 2009; Puhan et al., 2010). Although using biodiesel fuels usually increases the formation of NO_x in engines (Fernando et al., 2006; Hoekman and Robbins, 2012; Szybist et al., 2005; Yamane et al., 2001), LTC helped to reduce thermal NO_x emissions (Hill and Smoot, 2000; Kumar et al., 2014; Omidvarborna et al., 2014; Yamane et al., 2001; Zeldovich, 1946). EGR has proven to be a very effective and practical NO_x reduction technique (Agarwal et al., 2004; Zheng et al., 2004; Taghavifar et al., 2014). EGR in diesel combustion reduces NO_x emissions essentially by lowering the peak combustion temperature, using diluent gases of high specific heat (containing substantial levels of H_2O and CO_2), and low oxygen levels in the cylinder (Agarwal et al., 2011; Hountalas et al., 2008). In addition, EGR also eliminates the NO_x emissions from the exhaust gas before releasing it into the environment (Majewski, 2001; Morimune et al., 1998; Rosenberg et al., 1980).

Combustion emissions of various biodiesel feedstocks are very complicated, and vary mainly according to the type of chemical characteristics of the fuels (Omidvarborna et al., 2015c). Reductions in total hydrocarbons and CO emissions have been reported with increases in biodiesel chain length (Knothe et al., 2006; Schönborn et al., 2009). Several researchers have looked at the impact of biodiesel on exhaust emissions. Although a few publications have discussed the effect of fatty acid compositions and properties of emission components, no clear conclusion has been reached on the unsaturation level of fatty acids (Benjumea et al., 2010; Knothe et al., 2006; Omidvarborna et al., 2015b; Schönborn et al., 2009). Furthermore, ineffective mixing of air and fuel, lack of excess air, locally rich zones in the combustion chamber, deficiency of ignition delay time, etc., are reported as contributing factors to more exhaust emissions such as CO (Abdel-Rahman, 1998).

OBJECTIVES

Experiments were carried out in a laboratory combustion chamber fueled with different biodiesel feedstocks and their blends with ULSD. The physical and chemical characteristics of biodiesel samples were discussed and compared with those of ULSD (Kumar et al., 2014). The originality of this study lies in the methodology used for characterizing PM size, and the study of fundamental combustion chemistry of biodiesel fuels from various feedstocks under simplified conditions. The goal was to gain a better understanding of biodiesel combustion characteristics and to help develop more realistic emission generation models.

The first goal was defined as finding the relationship between the chemical structure of biodiesel fuel on soot, carbon, and NO_x emission characteristics in a set of laboratory experiments. Therefore, three types of relatively common biodiesel fuels used in the US, and their blends with ULSD were tested to represent various degrees of unsaturation. NO_x, carbon, and soot emissions from the biodiesel blends were compared to each other to determine the samples with the most significant reduction in emissions. With regard to carbon and NO_x emissions, the main objective was to determine the effect of the biodiesel molecular structure on the emission properties of NO_x, CO, CO_2, and CH_4 to facilitate recommendations for the most effective biodiesel fuel formulations.

The detailed morphologic, structural, and compositional features thus revealed a much

improved understanding of the characteristics of soot, providing a rigorous assessment of the influence of biodiesel fuel structure in soot formation process. Numerous analytic techniques are available for combustion emission characterization. Chemical structure and elemental composition, especially for toxicity and trace metals of soot, were analyzed using FTIR and ICP-MS, respectively. Transmission electron microscopy (TEM) was used to ascertain the nanostructure and fractal properties of soot particles, as well as to determine the sizes and distributions of the primary soot and aggregates (Koylu et al., 1995; Neer and Koylu, 2006). Thermogravimetric analysis (TGA) was used to identify and determine the chemical structure of formed soot particles and measure the oxidation ability of soot particles. To the best knowledge of the authors, only a few publications have described the oxidation of soot from different biodiesel feedstocks using TGA (Salamanca et al., 2012a; Salamanca et al., 2012b; Stratakis and Stamatelos, 2003).

The second goal was defined as understanding the actual soot formation and NO_x emissions in engines, which are very complex and associated with engine operation and environmental conditions as well as fuel structure and composition. Therefore, it is reasonable to speculate that these emissions would be influenced only by biodiesel specifications in a laboratory combustion chamber without having to consider external effects.

Various procedures and methodologies have been developed to characterize the size of PM released from vehicular emissions. However, most of them involve either suspending the emissions directly from the tail pipe into a liquid and then measuring the PM concentration and size, or placing an instrument near the vehicle's tail pipe to collect the PM samples on quartz filter papers. As a part of the field experimental study, a novel method was proposed to measure the size distribution of the PM released from heavy duty TARTA buses, which ran on SME-B20. The new method included PM collection, suspension, and finally characterization using a NICOMP 380 ZLS zeta potential analyzer. Only a limited number of studies were available that were slightly similar to this methodology.

In this study, transit buses were tested on their real routes, and NO_x emissions were measured in both running and idle modes. One of the objectives was to correlate the in-cylinder combustion data with the emissions of the engine. Results are discussed with the perspective of adding new information on the diesel bus performance with the blended fuel, and also to compare this with other research on engines tested so far. The bus was tested using both ULSD for the baseline operation and 5% biodiesel blended with 95% ULSD.

In addition to the experiments with the laboratory combustion chamber and transit buses, the third goal was to conduct a modeling study of both the laboratory setup and field experiment. ANN is a powerful technique with the ability to model highly nonlinear and complex systems that can be simpler than other approaches (Adi et al., 2009; Kiani et al., 2010; Obodeh and Ajuwa, 2009). To the best of the authors' knowledge, there is no literature that reports the application of ANN to predict and model NO_x emissions from engines operating in EGR and idle mode. This modeling technique can be applied to estimate the desired model output parameters if sufficient experimental data are provided.

The modeling of biodiesel combustion emissions using stochastic approaches is further discussed. This model prediction of NO_x is performed by selecting appropriate

reaction pathways of a biodiesel surrogate. Chemical reaction mechanisms are used as an appropriate approach to model biodiesel combustion emissions. The reaction mechanisms also help in selecting the appropriate blends for mobile sources used around the globe, and also provide insights into selecting a proper biodiesel fuel in diesel combustion. A simplified biodiesel surrogate model based on a previously published biodiesel mechanism (60 species and 172 reactions) (Chang et al., 2015) is used with the components of n-decane (ND), methyl decanoate (MD), and methyl-5-decanoate (MD5D). The low complexity of the simplified reaction mechanism enables it to be integrated into the stochastic simulation algorithm (SSA) model to simulate the combustion characteristics. The predicted concentration values of combustion byproducts were compared with the concentrations observed in the laboratory experiments that simulated single cycle combustion in a combustion chamber. The experimental conditions included combustion of three different biodiesel fuels at LTC (below 700 K), where the initial pressure and air-fuel ratio (Φ) values were 200 psi and 1, respectively. More details on the methodology and experimental procedure are presented later.

II. EXPERIMENTAL STUDIES

FUEL SPECIFICATIONS

Most commercial biodiesel fuels are mainly composed of medium- to long-chain FAMEs. The major fatty acid structures and compositions for neat biodiesel samples used in this study are presented in Table 1 and their structures are depicted in Figure 1. As shown in Figure 1, oleic acid (C18:1), linoleic acid (C18:2), and linolenic acid (C18:3) have 18 carbon atoms and 1, 2, or 3 double bonds within their structure, respectively. The degree of unsaturation of a biodiesel is an indicator of the number of double bonds present in its fatty acid chain, with a higher number of double bonds representing a higher degree of unsaturation (Benjumea et al., 2010).

In this context, the test fuels were SME, waste cooking oil (WCO), and tallow oil (TO) and their blends at 20% and 50% by volume with ULSD. The chemical composition of the test fuels is given in Table 1. As shown in Table 1, SME is predominantly unsaturated (85.1%) with significant contents of mono-unsaturated (22.8% C18:1), di-unsaturated (53.7% C18:2) and tri-unsaturated (8.6% C18:3) methyl esters. Compared with SME, WCO is relatively unsaturated (67.2%), and contains mono-unsaturated 52.9% oleic acid and 13.5% di-unsaturated linoleic acid. TO is characterized as having a balance between total saturated (45.6%) and total unsaturated (46.2%) methyl esters. Therefore, among the biodiesel samples used in this study, SME is the most unsaturated, WCO is moderately unsaturated, and TO is the least unsaturated. Due to the presence of mostly 18 carbon atoms in the saturated and unsaturated FAMEs, the effects of chain length on NO_x emissions are considered insignificant compared to the degree of unsaturation. The specification of each biodiesel fuel was reported in Kumar et al. (2014).

Table 1. Major Fatty Acid Composition of the Feedstocks in Mass Percent

Fatty acids	Chemical formula	Chemical structure*	SME	WCO	TO
Lauric	C12H24O2	C12:0	0.1	0.0	0.1
Myristic	C14H28O2	C14:0	0.1	0.9	2.8
Palmitic	C16H34O2	C16:0	10.2	20.4	23.3
Stearic	C18H38O2	C18:0	3.7	4.8	19.4
Oleic	C18H36O2	C18:1	22.8	52.9	42.4
Linoleic	C18H34O2	C18:2	53.7	13.5	2.9
Linolenic	C18H32O2	C18:3	8.6	0.8	0.9
Total saturated			14.1	26.1	45.6
Total unsaturated			85.1	67.2	46.2
CN (ASTM D 613)			47.0	49.3	NR**

Notes:

**C12:*0 describes a molecule with a HC chain of 12 carbon atoms and 0 double bonds.

***NR:* not reported by the supplier.

CN, Cetane Number; SME, soybean methyl ester; TO, tallow oil; WCO, waste cooking oil.

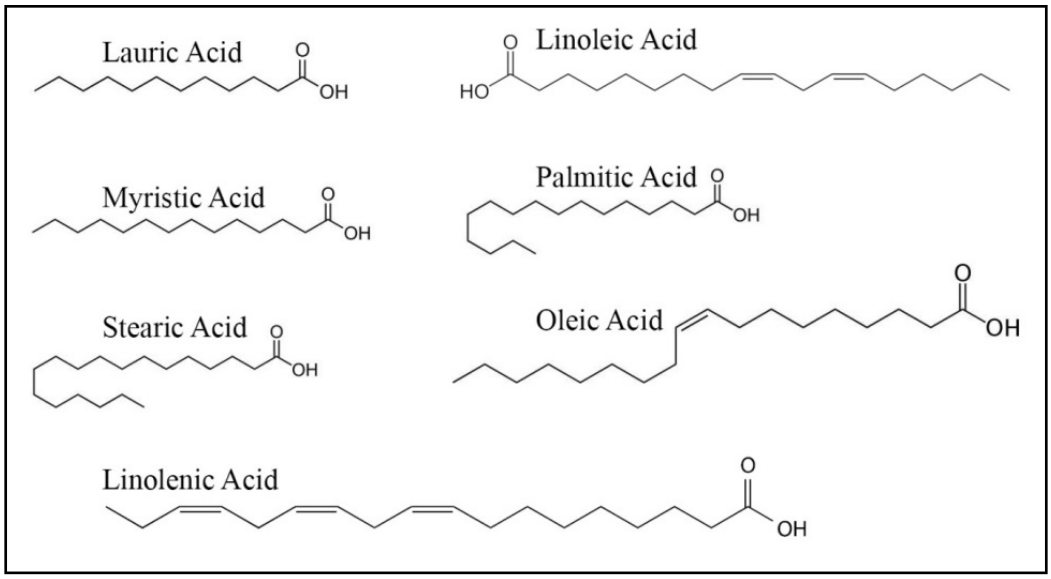

Figure 1. Seven Fatty Acid Molecules Commonly Found in Biodiesel

Note: (Herbinet et al., 2008; Lai et al., 2011).

LABORATORY EXPERIMENTS

Combustion tests were carried out in a laboratory scale combustion chamber (300 mL purchased from Parr Instrument Company). The combustion chamber included a stainless steel reactor (2.5″ inside diameter with 4.0″ inside depth) that was placed in an electrically heated chamber. A J-type thermocouple was placed inside the reactor for monitoring combustion temperature, and a temperature controller was installed to preserve reaction conditions at the predetermined values. With this arrangement, the reaction temperature was controlled and monitored to a precision of 0.1°C. A compressed air tank was used to maintain the stoichiometric combustion conditions. A schematic diagram of the entire experimental setup is shown in Figure 2.

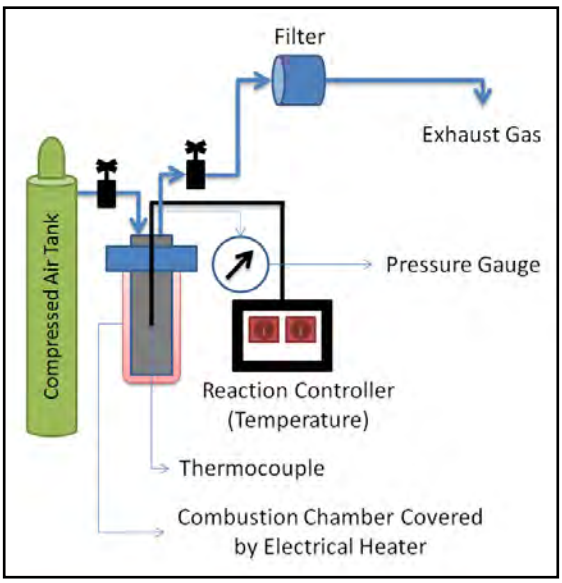

Figure 2. Schematic Diagram of Experimental Setup

EXPERIMENTAL PROCEDURE

The tested samples were neat SME, TO, and WCO and their blends of 20 and 50 (volume percent) with ULSD. ULSD (B0, as a control fuel) and SME were acquired from the TARTA Company (purchased from Peter Cremer), TO from United Oil Inc., and WCO obtained from White Mountain Biodiesel Inc. Experiments were conducted in a combustion chamber to represent a single cycle of combustion in an engine cylinder. The amounts of fuel and air were determined in order to keep the air–fuel equivalence ratio, λ at one. To obtain an estimate of λ, stoichiometric conditions were calculated from a mixture of various esters as a representative for biodiesel fuel as shown in Table 1 (Lai et al., 2011; Lapuerta et al., 2008b; Leung and Guo, 2006; Yaakob et al., 2014). The amount of O_2 in the fuel is added while calculating λ. The test fuel of 1 mL was placed inside the reactor at room temperature, and air was injected from a high-pressure air tank (dried air purchased from Airgas®) into the reactor, with pressure being monitored. The process used could be called a premixed combustion process because the oxygen was allowed to come into contact with the fuel before combustion. The heater was then turned on to elevate the temperature until the fuel ignited. The ignition point of combustion was determined by observing the combustion peak for temperature and pressure via a computer software program and pressure gauge provided by Parr Instrument. The elapsed time from turning on the heater to observation of the ignition temperature peak was termed “ignition delay” and the peak temperature was termed “ignition temperature,” as shown in Figure 3. After ignition terminated, the combustion gases were released and allowed to pass through a polytetrafluoroethylene (PTFE) membrane filter capsule with a 0.2-μm pore, which was placed before the NO_x analyzer. NO_x data were recorded as the gases passed through the detector until the reactor depressurized.

For carbon emission analysis, the chamber was closed after adding fuel and then helium was injected from a high-pressure tank (from Airgas®) into the chamber to pressurize the chamber to the set pressure, 300 to 400 psi. The heater was turned on to elevate the temperature until the fuel ignited. To prevent any blockage in the gas chromatography (GC) column, the combustion gases were released and allowed to pass through a PTFE membrane filter capsule with 0.2-μm pore size, which was placed before the GC inlet.

Various techniques and methods were implemented for laboratory soot particle analyses which are presented here. All instruments were calibrated with standard protocols provided by the manufacturers prior to testing. A satisfactory result, which fulfills the requirement to have reproducible values within an acceptable range, was achieved by conducting multiple experiments, and then repeating each experiment to make sure that it is reproducible.

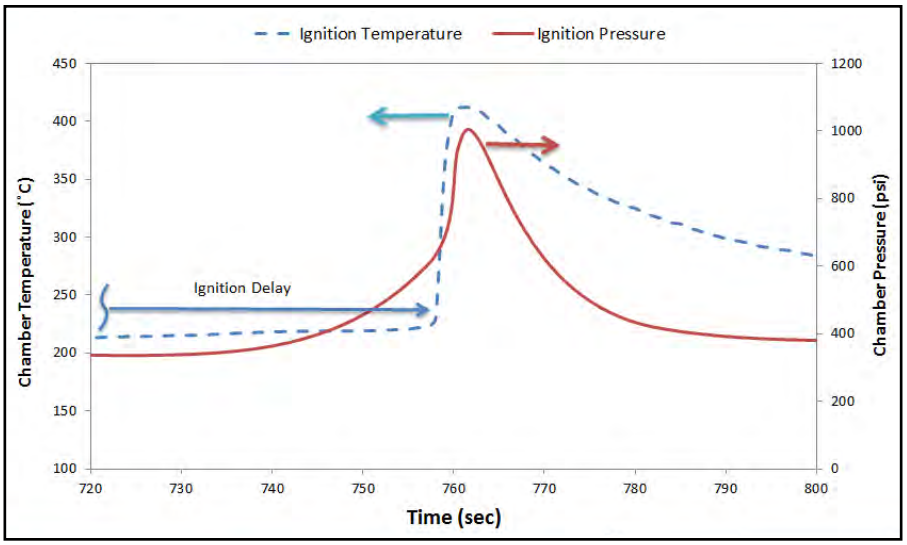

Figure 3. Example of Defined Ignition Delay and Ignition Temperature Measurement

FTIR Analysis of Biodiesel Fuels and Soot

FTIR (UMA-600 Microscope, Varian Excalibur Series, Digilab) analysis was conducted on biodiesel liquid samples using maximum scans with resolutions of 1 cm^{-1} in the range between 650 and 4000 cm^{-1}. Also, FTIR spectroscopy for soot samples, collected from the combustion chamber, were carried out using a PerkinElmer Frontier™ FTIR spectrophotometer (PerkinElmer, Waltham, MA) equipped with the Spectrum 10.4.2™ software suite (accumulation, 100 scans) within the range of 800 to 4000 cm^{-1}. Samples were prepared in the form of pressed wafers (1% sample in potassium bromide [KBr]) for analysis.

TEM Analysis of Soot Particles

Information on the size and morphology of soot was obtained using TEM. First, a small amount of soot was transferred to a separate centrifuge tube and well mixed with isopropanol. Then, a drop of sonicated suspension was deposited on PELCO® TEM grid support films of carbon (300 mesh Au) and placed in a Hitachi HD-2300A (Hitachi, Tokyo, Japan) microscope operated at a voltage of 200 kV. The particle size of soot in the randomly collected images was measured using a software program, Quartz PCI (version 8) at 110 K magnification.

Elemental Analysis of Soot Particles

Inductively coupled plasma–mass spectrometry (ICP-MS) is a highly sensitive and accurate method for quantifying the elemental composition of soot particles. ICP-MS analyses were performed on a quadruple instrument (XSeries II, Thermo Fisher Scientific, Inc., Bremen, Germany). It is worth mentioning that the data obtained using ICP-MS corresponds to a bulk analysis and not a surface analysis (such as energy dispersive X-ray (EDX) spectroscopy). Therefore, all of the interpretations based on this technique

are quantitative. Due to the high ionization potential and low sensitivity of the instrument on sulfur content, sulfur is not detected by ICP-MS.

TGA Analysis of Soot Particles

TGA analysis of the collected soot was performed using a Q50 TGA (TA Instruments, Wood Dale, IL) under two different media. The soot was placed in a platinum pan and the temperature was then ramped up from room temperature to about 400°C under nitrogen atmosphere and then to about 750°C under an oxygen atmosphere at a heating rate of 5°C/min. A balance purge flow of 40 mL/min and sample purge flow of 60 mL/min were used for analysis. It is expected that at this high temperature all the dry carbon materials present in soot would be oxidized. For measurement reliability and repeatability with respect to the instrument and sample, all instruments, especially TGA, were calibrated with the predefined standard operating procedures prior to any tests.

Carbon Emission Analysis

A Shimadzu 2010 (Shimadzu, Kyoto, Japan) GC device equipped with a pulsed discharge helium ionization detector was used for carbon emission analysis. The column used for GC was Carboxene 1010 PLOT (Sigma-Aldrich, USA), 30 m in length and 0.53 mm in diameter.

FIELD EXPERIMENTS

PM Sampling

Field experiments were conducted on two transit buses, both running on B20 from two different series of TARTA buses (701 and 802). A total of six samples for both hot and cold idling tests (e.g., minimum load, zero acceleration and zero velocity) were collected from each bus. The cold idle test includes samples collected in the morning before the buses leave the garage. In the hot idle test, samples were collected late in the evening after the bus has reached the garage. The same bus was used for each PM sampling under both cold and hot idling conditions, so as to maintain the same engine conditions and emission release conditions for the samples collected.

To avoid the influence of any possible contaminants in the garage, sampling was conducted in an open area outside the garage. Sampling was conducted by fixing a quartz filter paper of 12-cm (4.75 inches) diameter to a Catch-Can, which was placed into the exhaust pipe to capture the PM emissions as shown in Figure 4 (Omidvarborna et al., 2014; Shandilya and Kumar, 2013). PM was collected on the quartz filter paper for 15 minutes, similar to previous studies (Kumar and Nerella, 2009; Shandilya and Kumar, 2013; Omidvarborna et al., 2014; Vijayan, 2007). The effect of ambient air and humidity on the PM collected was considered to be negligible because the PM was collected at high temperatures and placed close to the tail pipe of the bus tested. The exhaust flow rate data were obtained for the 700 Series (701) bus from a Donaldson Engine Exhaust Flow Guide, and for the 800 Series (802) bus from Energy Service Insite software provided by Cummins Inc. Table 2 summarizes the specifications of the engines of the two buses tested.

Table 2. Engine Specifications of the Tested Buses

Bus series / number	Engine	Chassis	Year of manufacture	Gross vehicle weight (lbs)	Engine capacity	Maximum power	Maximum torque	Emission certifications	Mileage
700/701	Cummins ISL6LTAA	Gillig	2003	39,000	8.9L	289HP @ 2000 RPM	900 ft-lbs @ 1300 RPM	2007	150-200 K
800/802	Cummins ISL-07	Eldorado National	2010	42,760	8.9L	280HP @ 2200 RPM	900 ft-lbs @ 1300 RPM	2007	100-150 K

PALLflex tissuquartz 2500 membrane quartz filters, which have a 99.9% retention rate for PM of size 0.3 µm, were used for field experiments. Therefore, it can capture any PM >0.3 µm in size. Before sampling, quartz filter papers were stored in vacuum desiccators for 24 to 72 hours to equilibrate the filters and then weighed using a gravimetric mass balance. A certified Mettler Toledo XP105 microbalance (maximum capacity: 31 g/120 g; accuracy: 0.01 mg/0.1 mg) placed on a vibration-free table was used for weighing the filter papers. After the collection of PM, filter papers were equilibrated again and then gravimetrically weighed. The difference between the weight of the filter paper before and after collecting the PM gives the amount of PM collected.

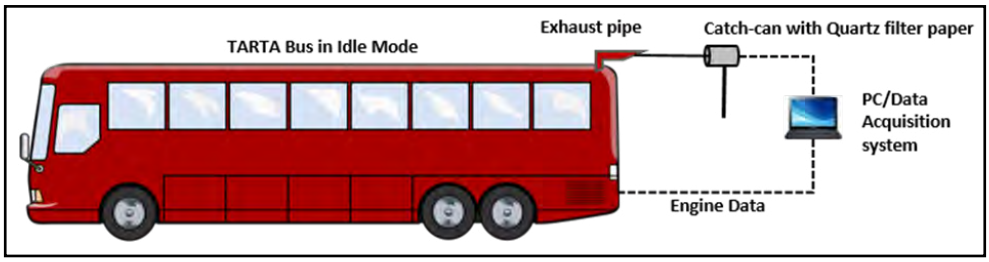

Figure 4. Schematic Diagram of PM Sample Collection from Tarta Buses on a Quartz Filter Paper by Using a Catch-Can

Suspension of PM

The PM distribution on quartz filter paper has been assumed to be even. Therefore, a sample of 1 square inch (2.54 × 2.54 cm) was cut out of the filter paper to use for the PM suspension, consisting of 50 mL of isopropanol. A Branson 2510 sonicator was used for the suspension. The 1-square-inch filter paper was placed in a container that was covered with paraffin to avoid contamination. The container with filter paper was sonicated for 10 minutes. A maximum time limit of 10 minutes was followed for sonication of filter paper, based on pervious sensitivity testing. Sonication was performed for filter papers with PM deposited from a 700 series (701) bus for 30 minutes (i.e., three repetitions of 10 minutes sonication) and with PM deposited from an 800 series (802) bus, only for 10 minutes. The 800 series buses are equipped with EGR, therefore, their PM emissions are significantly less than those from non-EGR 700 series buses. It is also assumed that sonication causes 100% of the PM to be dissolved and suspended into isopropanol from the filter paper.

Particle Sizing

Based on the solution's intensity of particles, 1.2 mL of PM suspended isopropanol was diluted. Of this isopropanol solution, 1.2 mL was placed in the NICOMP 380 ZLS Zeta Potential/Particle Sizer and run for particle sizing (Figure 5). This instrument is operated using PSS ZPW388 0.1 software, and the results can be used with the required data using this software. The NICOMP 380 zls works on the electrophoretic light scattering (ELS) method, which is based on the scattering of light from particles that move in the liquid under the influence of an applied electric field. This instrument can detect particles as small as 0.3 nm up to 50 µm in size.

Figure 5. A NICOMP 380ZLS Zeta Potential/Particle Sizer

NO_x Emissions

NO_x emissions were measured using a NO_x gas analyzer (MEXA-720, Horiba, Kyoto, Japan). The gas analyzer was a direct-installation gas analyzer using a zirconia ceramic sensor with a response time of about 0.7 seconds. The NO_x analyzer was directly attached at the tip of exhaust pipes to capture NO_x emissions continuously. As shown in Figure 6, for NO_x emissions from field experiments, sampling was conducted outside the garage in an open area during idling before the buses left for their daily route (cold idle). The engines were connected to the data acquisition systems provided by Cummins, so that several operating parameters could be simultaneously measured. Standard laboratory instruments and procedures provided by the company were used to calibrate the NO_x analyzer. The main specifications of the NO_x gas analyzer are given in Table 3.

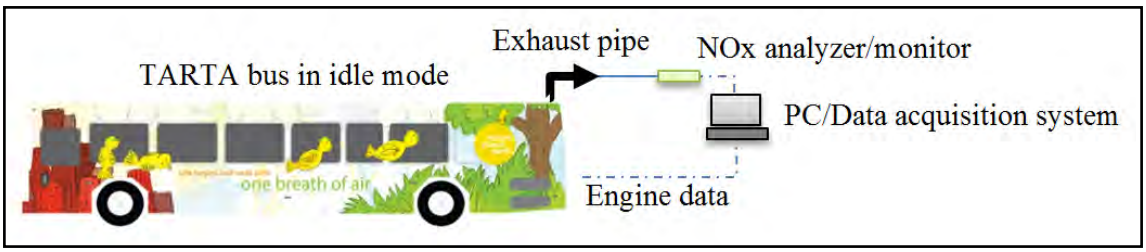

Figure 6. Schematic Diagram of Collecting NO_x Data from Bus Engines at Tarta Garage

Table 3. Specification of the Horiba NO_x Analyzer

Component	NO_x
Ranges	0-3 K ppm
Accuracy	0-1000 ppm: ±30 ppm with 3-point calibration 1001-2 K ppm: ±3% of reading with 3-point calibration
Warm-up time	Approximately 3 minutes after starting the engine
Sample gas conditions	Stoichiometric to lean for diesel or lean-burn engines Measurement gas temperature: -7 to 800°C
Ambient conditions	<80% relative humidity For main unit: 5°C to 45°C; (operating), -10°C to 70°C (storage)

To evaluate NO_x emissions from the bus in running mode, a real-time experiment was carried out on a transit bus in the city of Toledo from Franklin Park Mall to Jefferson Avenue. Experimental investigation was conducted on transit buses running on B5. The numbers assigned to the vehicles tested were 701 and 802. Route number 22F was selected for this study as it is the longest route in the city of Toledo. The route started from Franklin Park Mall and ended at Jefferson Street in downtown Toledo. Testing time for each run was approximately 70 minutes, which included 35 minutes during the trip from Franklin Park Mall to Jefferson Street and 35 minutes on the return trip from Jefferson Street to Franklin Park Mall. There were about 25 traffic signal points and several TARTA bus stops on this route. The bus left the TARTA garage at 7:25 a.m. and returned to the garage by 10:30 p.m. after finishing its route. A diagram of the test run route is shown in Figure 7.

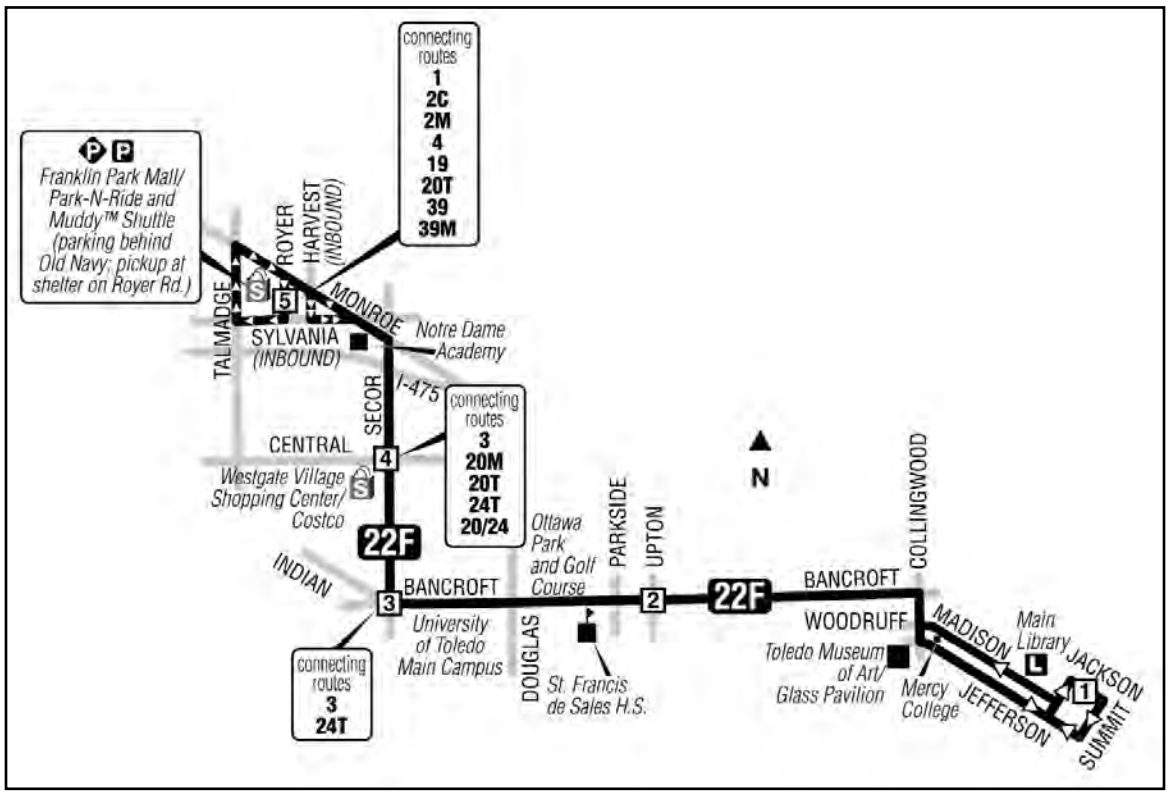

Figure 7. Route Map of the Test Run

The equipment was installed on the bus while parked in the garage on the day of testing, as shown in Figure 8. It takes approximately 20 minutes for installation and 15 minutes for removal of setup from the bus. Proper precautions should be taken while removing the equipment, because the sensor temperature may be approximately 88°C to 116°C. A place right next to the driver in the bus was chosen to set up the instrument because of its proximity to a power supply unit. The tailpipe is covered with an aluminum heating shield and the probe of the instrument is clamped to the tailpipe to measure the exhaust concentrations. The Cummins in-site toolbox consists of equipment that is used to collect engine data. One end of the 9-pin plug connector is connected to the laptop computer through a USB connector, while the other end is connected to the diagnostic read ports in the bus through the 9-pin plug. All the engine parameters, including engine speed and load, are recorded during the test and the file is stored for later use.

Figure 8. NO_x Analyzer (a) Probe Setup on the Tail Pipe, (b) Instrument Setup Inside, and (c) 9-Pin Plug Connector

III. MODELING APPROACH

ANN APPROACH

Neural networks are a type of artificial intelligence system that simulates the manner in which neurons work in the human brain. Neurons, which can learn from examples, are able to deal with nonlinear problems, and once trained, they can make predictions and generalizations. In the present work, variable parameters such as time, fuel temperature, intake air temperature, and percent fuel for non-EGR engine (four input variables) that influence exhaust emissions from idle engines operating with B5 fuel (Hountalas et al., 2008; Maiboom et al., 2008), were considered for NO_x modeling. For the EGR engine in idle mode, time, catalyst intake temperature after treatment, the diesel particulate filter intake/outlet temperature after treatment, EGR temperature, fuel flow rate, and the intake air temperature were included (seven input variables) in the ANN. The output of the system was the concentration of NO_x from each engine.

Engine load is one of the most important parameters affecting engine performance and exhaust emissions (Kumar et al., 2014; Marques et al., 2007). However, in idle mode, engine load was kept constant at 10% and engine speed remained at 1000 rpm; therefore, they were not considered as input variables.

Table 4. Measured/Calculated Statistical Engine Data Including NO_x Emissions with Respect to the Four Input Parameters in a Non-EGR Engine

Parameters (non-EGR engine)	Dimension	Min	Max	Avg.	Median	Mode	Std. deviation
Inputs:							
Fuel temperature	°C	11.2	27.3	20.3	20.9	25.5	4.8
Intake manifold temperature	°C	9.9	13.1	11.8	11.9	12.1	0.9
Percent fuel	%	5.3	13.1	7.6	7.0	6.9	1.8
Time	sec						
Output:							
NO_x Concentration	ppm	217.0	1208.0	571.6	526.0	479.0	149.0

Initially, independent models were developed for both engines because they had different inputs variables. For the non-EGR and EGR engines, of more than 1500 data points, 70% were used for the training set, 15% for the validation set, and the remaining 15% for testing both models. The range of variations of the operating parameters and the corresponding values of NO_x emissions are listed in Tables 4 and 5 together with their statistics (including minimum, maximum, average, median, mode, and standard deviation (SD)), respectively. Diesel particulate parameters (oxidation catalyst temperature and particulate intake/outlet temperature) in the EGR engine were incorporated in NO_x modeling because the engine exhaust gas (including NO_x), was recirculated either continuously or periodically during thermal regeneration. During this process, the exhaust gas including NO_x and unreacted O_2 reacts with trapped soot particles and produces mainly CO_2 (Majewski, 2001).

Table 5. Measured/Calculated Statistical Engine Data Including NO_x Emissions with Respect to the Seven Input Parameters in an EGR Engine

Parameters (EGR engine)	Dimension	Min	Max	Avg.	Median	Mode	Std. deviation
Inputs:							
After treatment diesel oxidation catalyst intake temperature	°C	87.9	111.2	107.9	109.7	110.3	4.7
After treatment diesel particulate filter intake temperature	°C	73.1	104.1	99.1	102.8	103.3	7.6
After treatment diesel particulate filter outlet temperature	°C	31.2	96.7	76.2	83.1	94.7	19.4
EGR temperature	°C	27.8	55.1	42.8	41.8	41.4	7.7
Fuel flow rate commanded	gph	1.6	3.2	2.4	2.4	2.4	0.2
Intake manifold air temperature	°C	19.7	30.9	25.1	25.9	19.7	3.4
Time	sec						
Output:							
NO_x Concentration	ppm	80.0	659.0	106.8	108.0	118.0	35.1

Achieving an optimal ANN structure is an essential part of neural network study to harness the maximum capabilities of the computational intelligence of the network. The neural network toolbox of MATLAB 8.0.1 was used to form the ANN model. A simple structure of the ANN used is shown in Figure 9. This structure consists of three layers of the network, namely: input layer, hidden layer, and output layer (Najafi et al., 2009; Yusaf et al., 2010). Operating parameters of the engines were fed into the network as inputs, and NO_x emissions were the outputs of the network. The network was trained using the Levenberg-Marquardt (LM) training algorithm (trainlm) to find the optimum number of neurons in the hidden layer for which the error was minimum (Roweis, 2004; Taghavifar et al., 2014). The activation function for the hidden layer was selected to be logsig (Ghobadian et al., 2009; Kiani et al., 2010; Yusaf et al., 2010).

Most of the ANN studies related to emission performance of engines (Ghobadian et al., 2009; Najafi et al., 2009; Yusaf et al., 2010) evaluated the validity of their models against statistical error measures. A commonly used statistical analysis is the root mean squared error (RMSE) and is defined as follows:

$$RMSE = \sqrt{\frac{1}{n}\sum_{i=1}^{n}\left(y_{exp} - y_{cal}\right)^2} \quad (1)$$

where n is the number of the points in the data set, y_{exp} is actual (expected) output, and y_{cal} is predicted (calculated) output.

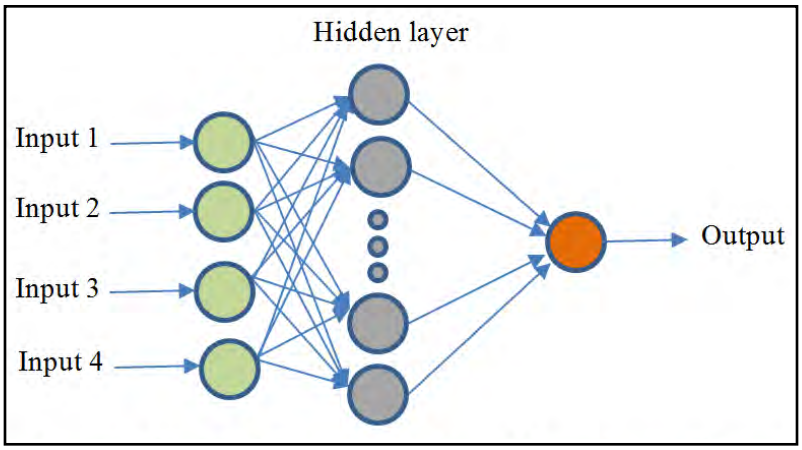

Figure 9. Schematic Diagram of the ANN Structure to Model Engines with a Single Output

SSA APPROACH

Due to the large size and complexity of the combustion reactions associated with FAMEs, the main components of biodiesel fuels, the combustion mechanism is extremely complicated, and modeling it is a challenging task. Westbrook et al. (2011) developed a detailed mechanism for biodiesel combustion with more than 4,800 species and nearly 20,000 reactions. In practice, this complexity is often reduced by replacing it with a single and relatively simple species called a surrogate, which exhibits similar characteristics to the actual FAMEs. A suggested surrogate should be small enough to be readily investigated with simple calculations and large enough to represent the actual combustion mechanisms and emissions accurately. Accordingly, a few detailed mechanisms (Chang et al., 2015; Fisher et al., 2000; Gaïl et al., 2007; Herbinet et al., 2008; Westbrook et al., 2011) were proposed as the base mechanisms to derive the main combustion pathways of simple surrogates with lower associated computational costs (Fisher et al., 2000; Westbrook et al., 2011). In addition, it has been reported that computational run times on a single processor are proportional to the square of the number of species and the square of the number of computational grid points (Aceves et al., 2001). Thus, alternative methods with simpler approaches are favored to investigate the combustion mechanisms of large biodiesel molecules. In this study, the SSA method was used with one surrogate to predict NO_x emissions from laboratory experiments. Preliminary information regarding the SSA method is presented below.

In the SSA approach, it is believed that collisions in a system of molecules in equilibrium occur in an essentially random manner. Gillespie developed the SSA approach to model networks of reactions via Monte Carlo methods (Gillespie, 1976; Gillespie, 1977). In the SSA method, a system involves operating on one reaction at a time, choosing a specific reaction to perform, and changing the counts of reactant and product molecules via their stoichiometric coefficients. In doing so, the system advances by appropriate intervals, and updates the probability distribution of future reactions to reflect the outcome of the selected reaction. Furthermore, the type of reaction that occurs in the next step and the time at which it occurs are determined using random numbers and probabilistic rules that

ensure accurate sampling. However, the SSA approach often slows down the calculation because it simulates every reaction step. In the SSA, a propensity that is computed for each reaction is proportional to its probability of occurrence relative to other reactions (Gillespie, 1976; Gillespie, 1977; Slepoy et al., 2008). Detailed description of the SSA method and application of the Monte Carlo methods to generate model parameters (e.g., time interval) are presented elsewhere (Ahn et al., 2008; Gillespie, 1976; Gillespie, 1977).

Biodiesel Surrogate

The surrogate components used in the modeling are methyl esters and normal alkane. Methyl ester is introduced to simulate the oxidation characteristics of ester groups of biodiesel, whereas normal alkane is used to compensate for the energy content and C/H/O ratio of actual biodiesel. It was found that a surrogate model containing n-alkanes better represented the C/H/O ratio and the energy content of actual biodiesel fuel (Brakora et al., 2009; Ismail et al., 2013). Most previous surrogate models considered only methyl butanoate as a representative of saturated methyl esters (Dooley et al., 2008; Golovitchev and Yang, 2009; Ismail et al., 2013; Liu et al., 2013; Ng et al., 2013). Methyl butanoate, a C_5 species, is of a manageable size for simulation and has a similar $RC(=O)OCH_3$ chemical structure to biodiesel (Brakora et al., 2009).

Only a few reduced mechanisms with long-chain esters are available at present, and almost all the recent mechanisms were obtained by reducing the mechanism described by Herbinet et al. (2008), which consists of n-heptane, MD, and methyl-9-decenoate, with 8580 reactions and 3034 species. Due to the recent emergence of a new database for various physicochemical properties of biodiesel, different biodiesel surrogates and their reaction pathways have been introduced (Omidvarborna et al., 2014; Omidvarborna et al., 2015c; Omidvarborna et al., 2016a). However, due to the complicated molecular structure of these components, it is still a significant challenge to develop either a comprehensive combustion mechanism or a simplified mechanism that accurately represents biodiesel fuels.

Skeletal Mechanism

Recent studies highlight the fact that biodiesel surrogate fuels with large molecules represent actual biodiesel fuels better for combustion modeling and simulation (Brakora et al., 2009; Luo et al., 2012). These large surrogate molecules are neither as complex as those of long-chain methyl esters nor as small as methyl butanoate and are more manageable for combustion calculations compared to larger molecules (Fisher et al., 2006; Gaïl et al., 2008). Feasibility of these surrogate molecules was validated under various experimental conditions (Chang et al., 2013). Although the combustion mechanisms of these surrogates are by no means completely accurate, it is thought that the surrogates are sufficient enough to provide qualitative insight into the reaction pathways in the biodiesel combustion. In the current work, the combustion mechanism modeling and simulation are performed using a surrogate molecule, MD, MD5D, and ND, and the results are analyzed in terms of the mole fraction of NO_x in the exhaust emissions.

The most recent combustion mechanism for biodiesel surrogates was obtained by Chang et al. (Chang et al., 2015) by merging the large-molecule submechanisms of

ND (Chang et al., 2013), MD, MD5D, reduced C_2–C_3 mechanism (Patel et al., 2004), and H_2/CO/C_1 mechanism (Klippenstein et al., 2011), which are shown in Figure 10. Figure 10 also demonstrates the main reaction pathways for the main components of the biodiesel surrogate. The R_{11}-R_{20}, R_{21}-R_{28}, R_{31}-R_{38}, and R_{41}-R_{46} reactions represent the simplified pathways for ND, MD, MD5D, and MP2D (ester group) reactions, respectively. A decoupling method was used to depict the oxidation of the small molecules (i.e., H_2/CO/C_1), and a simplified mechanism was used for C_2–C_n species (n is the number of carbon atoms in the fuel molecule) (Chang et al., 2013). Because of the size of the simplified mechanism, the Chang et al. model significantly reduced the number of species involved in the combustion, where no isomers for large-molecule radicals were considered (Chang et al., 2015). Although the SSA method remains a computationally demanding approach with limited applicability, especially for large reaction networks required for modeling more realistic networks, the size of the simplified mechanism can be well controlled. The SSA method takes time steps of variable length, based on the rate constants and population size of each chemical species (Burrage et al., 2004).

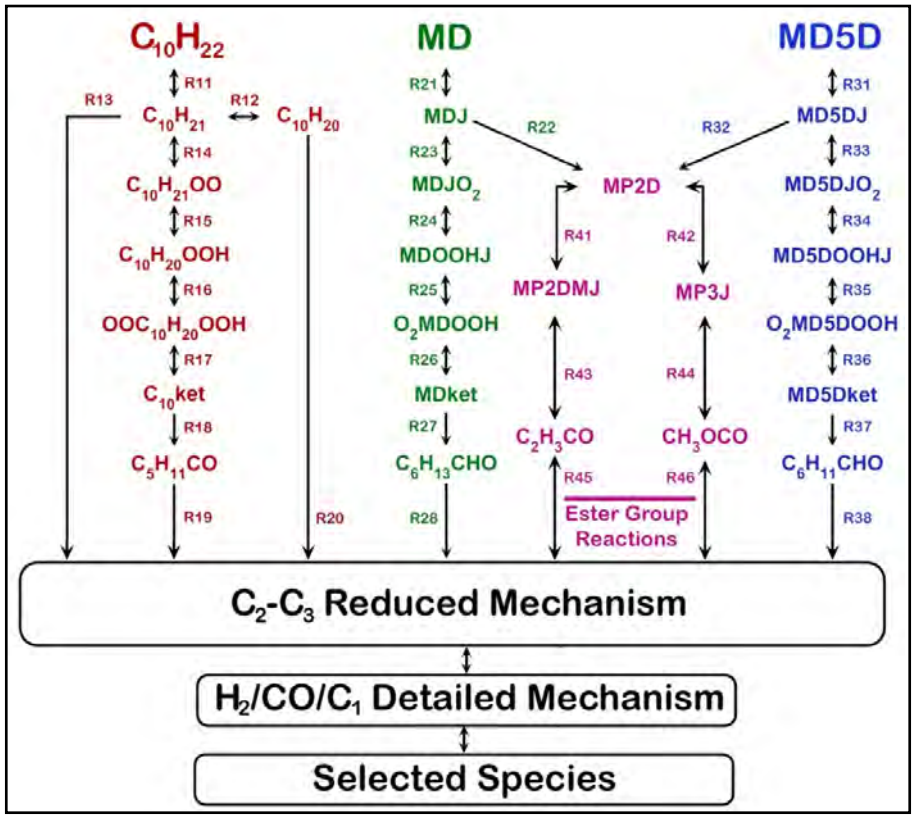

Figure 10. Simplified Reaction Pathways for the Skeletal Mechanism of the Proposed Biodiesel Surrogate

Note: Chang et al., 2015.

According to the literature (Gillespie, 1976, Metropolis et al., 1953), MD and MD5D mainly produce alkyl-ester radicals through H-abstraction reactions (R_{21} and R_{31}), as shown in Figure 11. This reaction happens via H-abstraction through the carbon atom in the ester group, which results in MDJ formation from MD, MDJ, MD5DJ, and MP2D. The H-abstraction reaction generates intermediate oxygenated species that lead to lighter

HCs such as $C_6H_{13}CHO$, $C_6H_{11}CHO$, C_2H_3CO, and methoxycarbonyl (CH_3OCO) through radical reactions, as presented in Figure 11. Light HCs form CH_3O, CH_2CO, and CH_3O, which become methyl aldehyde (CH_2O), then CHO, and finally CO and CO_2. CH_3OCO is an important intermediate product in biodiesel combustion (Lapuerta et al., 2008b), because it finally produces CO_2 (Dooley et al., 2008; Gaïl et al., 2007), which is a unique characteristic of methyl esters (Herbinet et al., 2008; Lapuerta et al., 2008b). Therefore, if a biodiesel surrogate has a short chain length, it may form more oxygenated products such as CO, CO_2, CH_4, and CH_2O, and fewer carbon atoms are left to form unsaturated HCs such as ethane and acetylene which are thought to be PAH precursors (Dooley et al., 2008; Gaïl et al., 2007). Moreover, as shown in Figures 10 and 11, the two oxygen atoms of the ester group finally lead to CO_2 formation in the pathways of ester group reaction. It means that two oxygen atoms of the ester group capture the carbon atoms from a pool of carbon atoms that may form PAH precursors otherwise (Omidvarborna et al., 2016a). This oxygen reaction of the ester group with carbon could be the reason for the higher CO_2 formation in biodiesel combustion than in regular diesel. The main molecular reaction mechanisms for MD and MP2D are illustrated briefly in Figure 11.

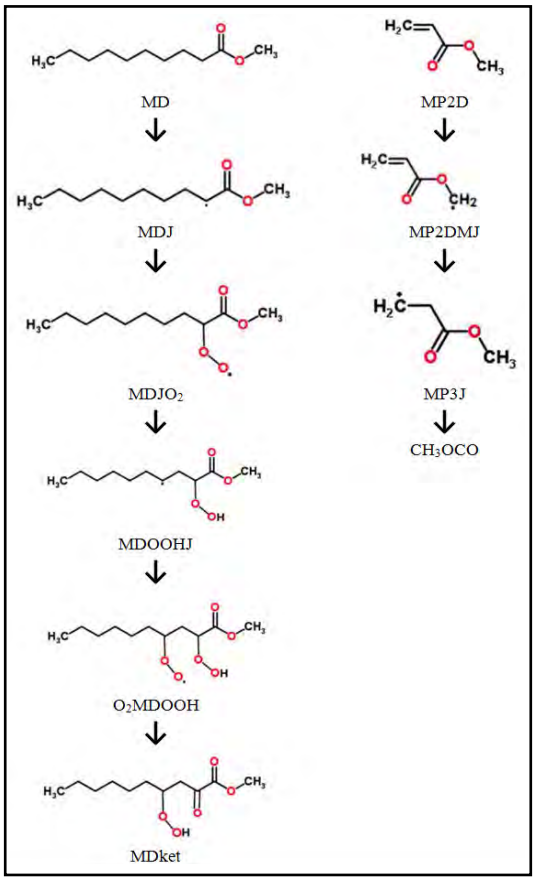

Figure 11. Detailed Chemical Pathway of Major Species in MD Submechanisms with their Structures

A relatively detailed MP2D mechanism is included because the MP2D-related reactions are the major ester group reactions, which are important for the oxidation of methyl esters (Diévart et al., 2012). The light HCs such as C_3H_6, C_2H_4, and C_2H_2 species are also

included because they can potentially contribute to NO_x formation. Finally, a reduced NO_x submechanism (Brakora et al., 2009; Diévart et al., 2012) is added to investigate NO_x emission formation as tabulated in Table 6.

As shown in Table 6, of the various NO_x formation mechanisms, Reaction N1: $CH + N_2 \leftrightarrow HCN + N$ is an important one, with a lower activation energy than thermal NO_x reactions (Liberman, 2010). Moreover, the oxygen atoms bound to one carbon atom in the methyl ester moiety lead to the increase of CO/CO_2 formation. In addition, the double bond in methyl ester leads to a high-combustion temperature (Szybist et al., 2005), and possibly to the increase of thermal NO_x formation (Shu et al., 2013). Therefore, in the modeling study, the role of methyl ester moiety in increased NO_x formation is very important, and is included in the combustion mechanism accordingly.

The main Arrhenius rate constants used in the simplified mechanisms are also summarized in Table 6. The ND, MD, and MD5D submechanisms are described in detail in Chang et al. (2015), and Ng et al. (2013). Optimization of reaction rate constants for the biodiesel surrogate can be found elsewhere (Chang et al., 2013; Chang et al., 2015).

Table 6. Main Reaction Kinetics Used in this Study

		Arrhenius rate constants		
No.	**Reaction**	**A**	**B**	**E_a**
R11	$C_{10}H_{22} + O_2 = C_{10}H_{21} + HO_2$	2.00E+15	0.00	50,150
R12	$C_{10}H_{21} + O_2 = C_{10}H_{20} + HO_2$	3.16E+11	0.00	6,000
R13	$C_{10}H_{21} = 2C_3H_6 + C_2H_5 + C_2H_4$	4.00E+13	0.00	28,810
R14	$C_{10}H_{21} + O_2 = C_{10}H_{21}OO$	2.00E+11	0.00	0
R15	$C_{10}H_{21}OO = C_{10}H_{20}OOH$	5.51E+13	0.00	19,000
R16	$C_{10}H_{20}OOH + O_2 = OOC_{10}H_{20}OOH$	2.00E+11	0.00	0
R17	$OOC_{10}H_{20}OOH = C_{10}ket + OH$	8.91E+10	0.00	17,000
R18	$C_{10}ket = CH_2O + C_5H_{11}CO + OH + C_3H_6$	1.98E+16	0.00	41,000
R19	$C_5H_{11}CO + O_2 = C_3H_7 + C_2H_3 + CO + HO_2$	3.16E+13	0.00	10,000
R20	$C_{10}H_{20} + O_2 = 2C_3H_6 + C_2H_5 + CH_2O + HCO$	3.16E+13	0.00	10,000
R21	$MD + O_2 = MDJ + HO_2$	3.00E+14	0.00	43,150
R22	$MDJ = C_3H_7 + 2C_2H_4 + MP2D$	8.00E+13	0.00	28,800
R23	$MDJ + O_2 = MDJO_2$	2.00E+11	0.00	0
R24	$MDJO_2 = MDOOHJ$	5.51E+13	0.00	19,000
R25	$MDOOHJ + O_2 = O_2MDOOH$	2.00E+11	0.00	0
R26	$O_2MDOOH = MDket + OH$	8.91E+10	0.00	17,000
R27	$MDket = C_6H_{13}CHO + CH_2CO + CH_3OCO + OH$	1.98E+15	0.00	41,000
R28	$C_6H_{13}CHO + O_2 = C_3H_7 + C_3H_6 + CO + HO_2$	3.16E+13	0.00	10,000
R31	$MD5D + O_2 = MD5DJ + HO_2$	6.00E+14	0.00	40,150
R32	$MD5DJ = C_3H_5 + 2C_2H_4 + MP2D$	8.00E+12	0.00	28,700
R33	$MD5DJ + O_2 = MD5DJO_2$	2.00E+11	0.00	0
R34	$MD5DJO_2 = MD5DOOHJ$	5.51E+13	0.00	19,000
R35	$MD5DOOHJ + O_2 = O_2MD5DOOH$	2.00E+11	0.00	0

No.	Reaction	Arrhenius rate constants A	B	E_a
R36	O_2MD5DOOH = MD5Dket +OH	8.91E+10	0.00	17,000
R37	MD5Dket = $C_6H_{11}CHO$ + CH_3OCO + CH_2CO + OH	8.98E+15	0.00	43,000
R38	$C_6H_{11}CHO$ + O_2 = C_3H_5 + C_3H_6 + CO + HO_2	3.16E+13	0.00	10,000
R41	MP2D + OH = MP2DMJ + H_2O	7.02E+07	1.60	-35
R42	MP2D + H = MP3J	1.00E+13	0.00	2,900
R43	MP2DMJ = C_2H_3CO + CH_2O	5.75E+23	-2.80	23,540
R44	MP3J = C_2H_4 + CH_3OCO	2.91E+13	0.17	33,670
R45	C_2H_3CO + M = C_2H_3 + CO + M H_2O/16.25/ CO/1.875/ CO_2/3.75/ CH_4/16.25/	8.60E+15	0.00	23,000
R46	CH_3OCO = CH_3 + CO_2	7.98E+12	0.33	15,640
N1	CH_2 + N_2 = HCN + N	3.12E+09	0.90	20,130
N2	N + O_2 = NO + O	9.00E+09	1.00	6,500
N3	N + OH = NO + H	3.36E+13	0.00	385
N4	HO_2 + NO = NO_2 + OH	2.11E+12	0.00	-480
N5	HCN + OH = NH_2 + CO	5.96E+05	3.20	8,210
N6	NH_2 + O = H_2 + NO	3.90E+13	0.00	0

Note: * Arrhenius equation, k = A·Tn·e(-E/RT). The units of A are cm3/mol/sec, T is in K, and E is in cal/mol (Chang et al., 2013; Chang et al., 2015; Metcalfe et al., 2007; Yoshikawa and Reitz, 2009).

IV. RESULTS AND DISCUSSION

LABORATORY STUDY

FTIR Spectra of Biodiesel Fuels and ULSD

In order to investigate the unsaturation and functional groups of neat biodiesel fuels and ULSD, FTIR spectra from the fuels were measured. The FTIR spectra of neat SME, TO, and WCO samples and ULSD are shown in Figure 12(a). The absorption peaks at 700 to 750 cm^{-1} suggested the out-of-plane bending of CH_2. CH_2 and its relevant species, acetylene, is one of the main parts in soot formation and it prompts NO_x formation. The NO_x mechanism results from N_2 being in contact with light HC radicals (CH and CH_2) where they react with species containing N and get further oxidized to NO_x. The spectra of C-O bonds (e.g., esters) normally appear at 1000 to 1300 cm^{-1}, and they represent the difference between biodiesel and ULSD. The double bond region (e.g., the C=O stretching bond of methyl ester that is mainly a monoalkyl ester) is distributed at 1700 to 1800 cm^{-1}. According to Figure 12(b), the biodiesel samples showed more unsaturated bonds in the range of 1700 to 1800 cm^{-1} than ULSD. These molecules in the double bond region are generally considered oleic (C18:1), linoleic (C18:2), and linolenic (C18:3) fatty acids. This unsaturated carbonyl signal was observed at 1742 cm^{-1} in the FTIR spectrum for SME, TO, and WCO and compared with ULSD in Figure 12(b). As shown in Figure 12(b), the absorbance peak for unsaturated SME at 1742 cm^{-1} was 0.37%, and the absorbance peaks for medium saturated WCO and low saturated TO were about 0.34%.

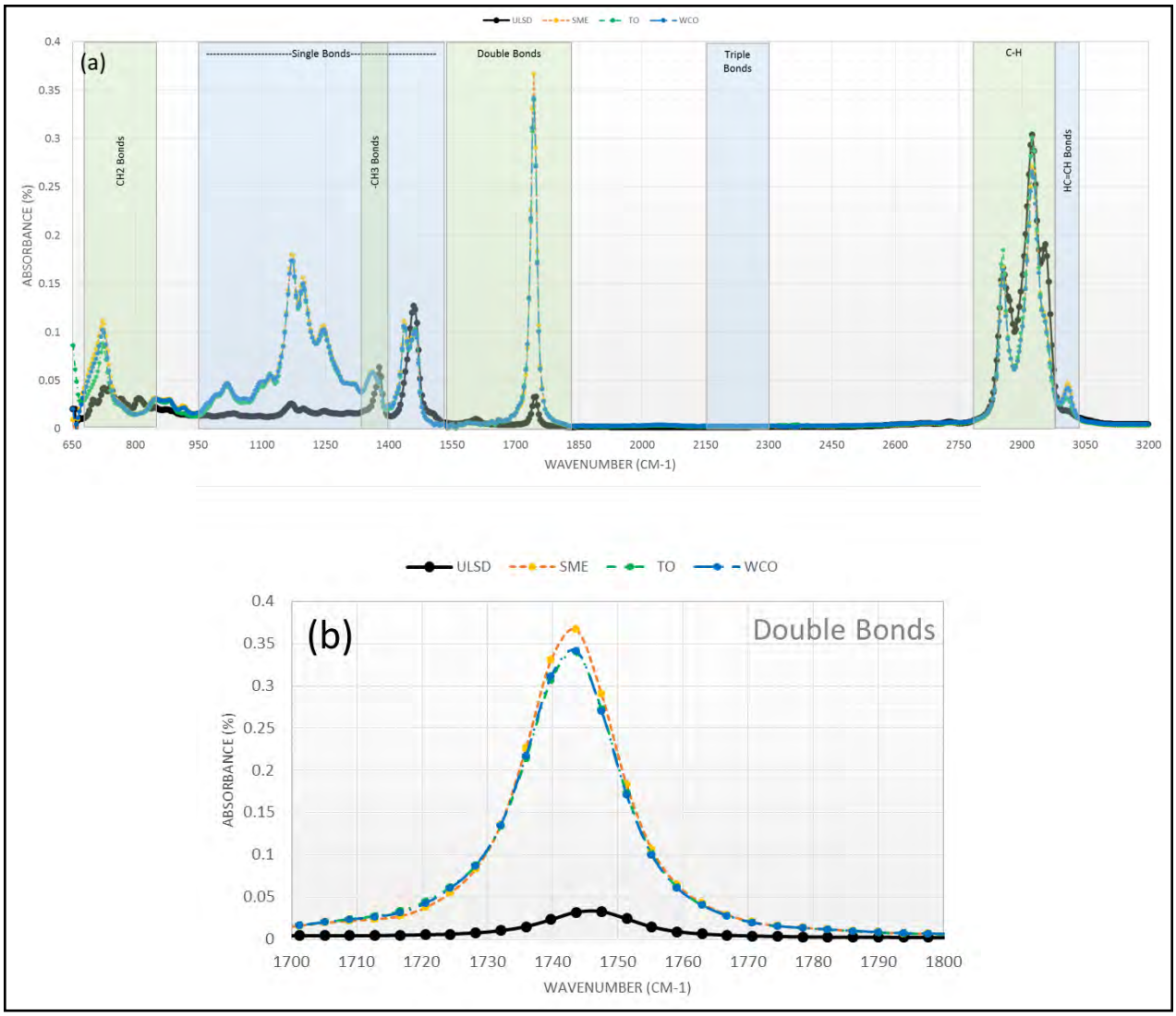

Figure 12. (A) General FTIR Spectra of Selected Neat Biodiesel Fuels and ULSD Used in the Study, (B) FTIR Spectra of Unsaturated Compounds

The absorbance near 3000 cm^{-1} indicated the HC=CH bond association, and the absorbance at around 1375 cm^{-1} indicated the $-CH_3$ bond (Chien et al., 2008). The main components of biodiesel samples are aliphatic HCs (their structures are similar to long-chain carbons), which is shown as C-H in the shaded area. The aliphatic hydrogen bond is shown in Figure 12(a) at 2800 to 3200 cm^{-1} which represents the higher carbon content of ULSD compared with biodiesel fuels. The higher carbon content is the reason for ULSD having higher energy content than any other biodiesel fuels.

Differences between the biodiesel samples and ULSD appear significant, whereas the biodiesel samples had almost the same chemical structure when compared to each other. Comparison of the biodiesel fuels with the other biodiesel feedstocks indicates that although the chemical structure of SME has a higher degree of unsaturation (Table 6), it is not possible to establish any significant difference on degree of unsaturation with the WCO and TO under FTIR study.

Ignition Delay and Temperature

Ignition temperature and ignition delay were defined to determine their relation to the degree of unsaturation of the fuel. The average values of ignition delay and ignition temperature along with their SDs are shown in Figure 13(a,b), respectively. Unsaturated structures and relatively long-chain fatty acids in biodiesel fuels are reported to nonlinearly slow down combustion compared with a saturated fuel such as ULSD. The results showed that the ignition delay of ULSD occurred about 2 minutes earlier than the three biodiesel samples under test conditions (as confirmed in Figure 13(a)). SME has a higher percentage of unsaturation, giving it a longer ignition delay than TO and WCO. The longer ignition delay may be due to the contribution of linoleic and linolenic fatty acids, which are relatively higher in SME biodiesel, than that of TO and WCO biodiesel.

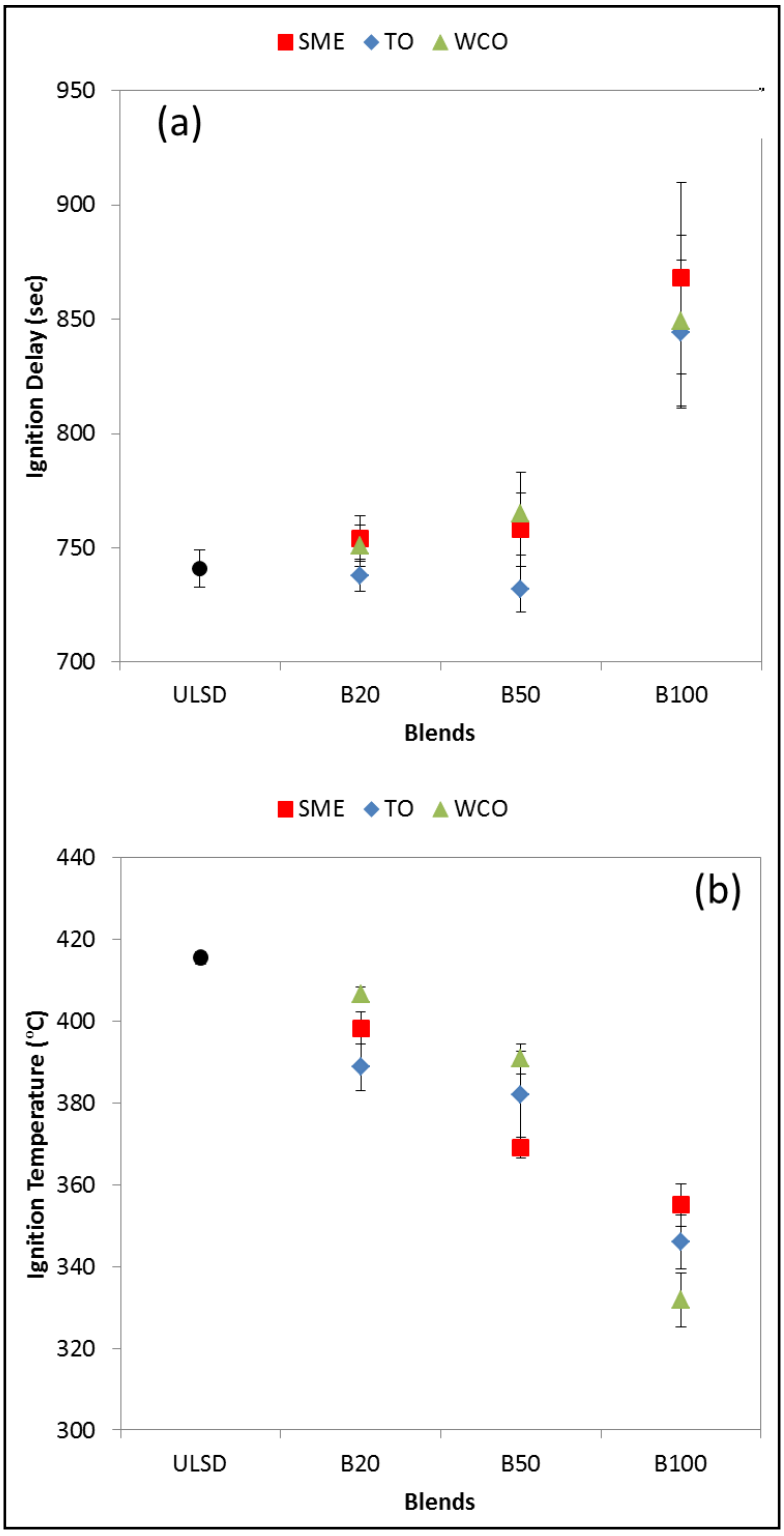

Figure 13. (A) The Ignition Delay and (B) Ignition Temperature of Different Biodiesel Fuels Blended with ULSD

Figure 13(b) shows that ULSD released higher energy at the ignition point than the other biodiesel samples, which indicates its higher heating value compared to biodiesel fuels (Agarwal, 2001; Demirbas, 2007; Knothe, 2005). The higher the ignition temperature,

the shorter is the ignition delay (Basha et al., 2009; Caresana et al., 2011). As shown in Figure 13(b), the ignition temperature of ULSD reached 415.6 ± 2.9°C, whereas for the biodiesel combustion, the average ignition temperature barely reached 355.1 ± 10.3°C, 346.1 ± 13.2°C, and 331.8 ± 13.4°C for SME, TO, and WCO, respectively. As the content of biodiesel increased in the blends, the ignition temperatures decreased. In other words, as the oxygen content of the fuels increased in the blends, the ignition temperature decreased due to their low carbon content and the low heating values of methyl esters (less C-H and C-C bonds than ULSD) (Knothe, 2005). In general, the heat of combustion of biodiesel fuels are within the range of 75.6% to 89.9% of that of regular diesel (Ng et al., 2010). Highly unsaturated biodiesel exhibited maximum ignition temperature for neat biodiesel fuels. Comparison between the graphs clearly shows that combustion reactions for saturated fuels are faster at higher temperatures, thus shortening the ignition delay.

TEM Analysis of Soot Particles

Understanding the characteristics and differences among diesel soot and soot from various biodiesel feedstocks is crucial for evaluating their impact on human health and the environment. As particles become smaller, it is much easier for them to diffuse into ambient air, absorb more hazardous substances, and subsequently be inhaled into the lungs. Once inhaled, they can affect both the heart and lungs and cause serious health problems.

The size of soot particles from the laboratory study was investigated by TEM images (Figure 14). At least 10 images were taken, and average diameters were obtained by measuring the diameters of 100 soot particles. TEM images for size distribution analysis were taken on the same scale and the results showed that most particle sizes ranged from 50 to 150 nm. Using TEM, it can be observed that soot particles were smaller for biodiesel samples than for ULSD. Soot particles were nearly spherical in shape and aggregate to form agglomerate structures. As shown in Figure 14, the clusters of particles per unit area involve the continuous bonding of particles to form a large network of carbon soot particles.

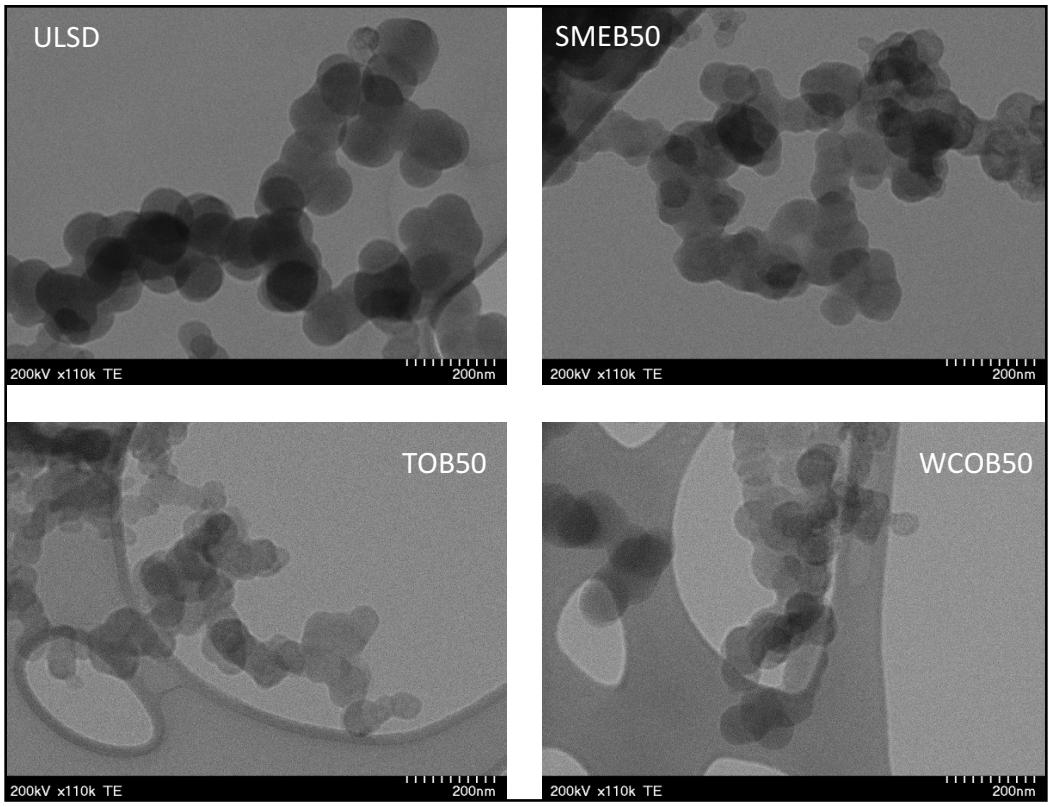

Figure 14. Tem Images of Soot Particles from Combustion of Biodiesel and ULSD

The average diameters of the soot particles and their SDs are listed in Table 7. A significant reduction in the mass of soot was observed in the biodiesel combustion for all of the biodiesel samples compared with the ULSD result. For neat biodiesel samples (B100), no soot was observed inside the combustion chamber. As shown in Table 7, soot from the ULSD sample had the greatest diameter (95.2 nm). For biodiesel samples, the soot particles from B20 samples were slightly larger than B50 soot. In addition to lower emission of soot inceptors and mass growth species in biodiesel fuels (Omidvarborna et al., 2015a; Shandilya and Kumar, 2014), it is speculated that soot particles were further oxidized when the portion of oxygenated fuel (e.g., biodiesel) in the blends was increased (Kohse-Höinghaus et al., 2010). The results were in agreement with those of previous studies (Harris and Maricq, 2001; Ishiguro et al., 1991), which concluded that the oxidation process may influence the signature size distributions for soot particles.

Table 7. Details on Size Distribution of Collected Soot from Different Feedstocks and Blends with ULSD

Fuel	ULSD	SMEB20	SMEB50	TOB20	TOB50	WCOB20	WCOB50
Average (nm)	95.2	88.3	87.9	93.7	92.5	91.8	90.1
SD	35.9	26.3	24.0	21.9	21.4	24.5	22.7

Unlike ULSD soot, it was observed that SME, TO, and WCO blends produced normal distributions in the range of 50 to 150 nm. As shown in Figure 15, soot particles larger than

175 nm were formed only in the combustion of ULSD. The average sizes for biodiesel-blended soot were slightly lower than ULSD (Table 7). Size distribution of ULSD did not follow the same trend as other biodiesel-blended fuels which exhibited a quasi-monodispersed structure (Smekens et al., 2005). Increases in the diameter of the soot particles for ULSD can be applied here because combustion takes place with higher pressure and temperature levels in the combustion chamber when compared with biodiesel fuels (ULSD has higher heating value than biodiesel fuels). Such local conditions, apart from contributing to soot nucleation, promote the growth of the existing soot by means of soot growth species such as PAHs (Lapuerta et al., 2007; Omidvarborna et al., 2015a).

Numerous findings support the idea that degree of unsaturation has an impact on soot emissions in diesel engines (Boehman et al., 2004; Cardone et al., 2002; Lapuerta et al., 2012). The high degree of unsaturation results in an earlier start of the combustion process, which increases the residence time of soot particles in the combustion chamber. Therefore, the soot particles undergo further oxidation, leading to reduction in soot mass emissions and size distribution (Cardone et al., 2002). The laboratory results also confirmed that the more unsaturated biodiesel fuel (such as SME) had the smallest average soot particles compared with medium (WCO) and low (TO) unsaturated feedstocks for both B20 and B50. This finding was in agreement with those of Lapuerta et al. (2008a) that increasing the unsaturation degree (proportion of biodiesel in blends) results in a decrease in mean particle diameter. Therefore, it can be concluded that degree of unsaturation is closely related to soot oxidation and oxygen content in biodiesel feedstocks (Benjumea et al., 2010).

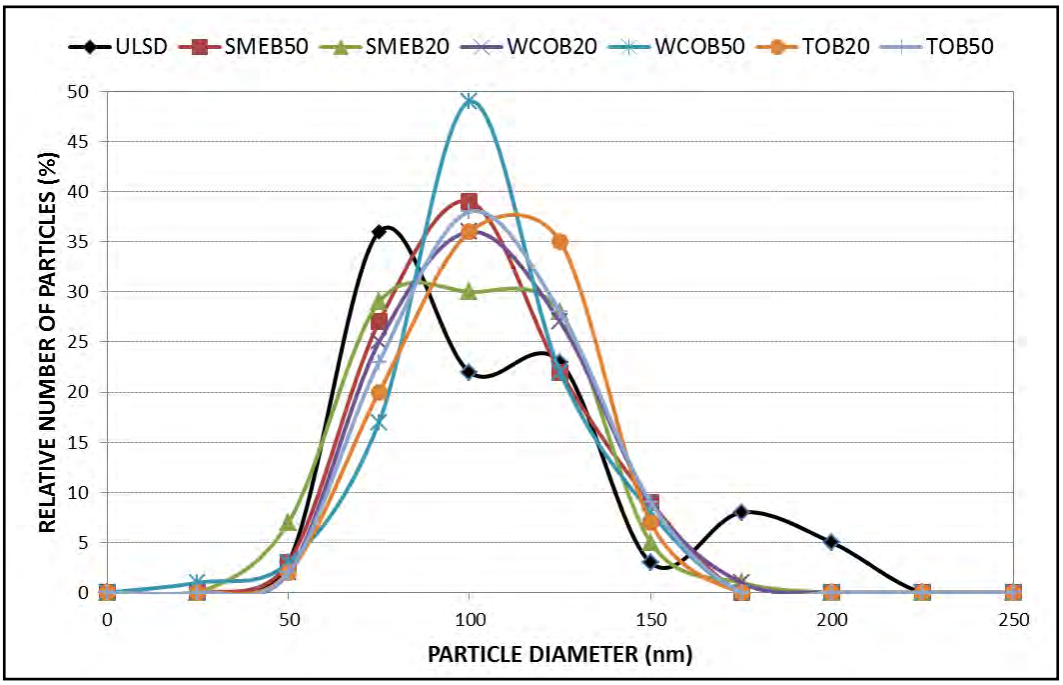

Figure 15. Size Distribution of the Soot Particles of the Different Biodiesel Feedstocks and Blends with ULSD

Structure of Oxidized Soot in Biodiesel Combustion

Biodiesel soot, produced especially from high percentage biodiesel blends, is reported to exhibit fast and capsule-type oxidation by burning, which makes it hollow inside (Song et al., 2006). Eventually the depletion of the inner core leads to a more disordered arrangement in the structure of the outer shell (Song et al., 2006). In Figures 16(a-c), the arrows indicate oxidation deformation in the structures of soot from the combustion of all biodiesel blends. In the combustion of biodiesel fuels, biodiesel's extra oxygen molecules are involved in various side reactions that may cause interference in the formation of soot by eliminating soot inceptors (Omidvarborna et al., 2015a). When one of the main soot inceptors, PAH, is not formed during the soot inception and growth process, a soot particle transforms into an ordered morphology (typical shell-core structure) (Omidvarborna et al., 2015a). Differences in any step of soot mechanism (e.g., inception and mass growth) may lead to disorder in the soot structure (Vander and Tomasek, 2004). During oxidation, a uniform structure of soot may be deformed from the inside to a nonuniform structure. Song et al. (2006) described the process of soot oxidation as follows: the soot oxidation mechanism starts with the development of microporosity in a soot particle during the course of the early stages of oxidation through the partial removal of the amorphous aliphatic carbon-rich sections present at the outermost shell. Once sufficient micropores have been developed to penetrate to the particle core, the soot is likely to become hollow inside through burning of the more reactive internal carbon, thereby forming a capsule (Song et al., 2006). More details are presented to support the oxidation of soot particles in Figures 16(d-f) which shows the magnified images of deformed soot particles at 100K, 200K, and 400K magnification. Any specific difference was not observed among oxidized soot particles based on their saturation levels.

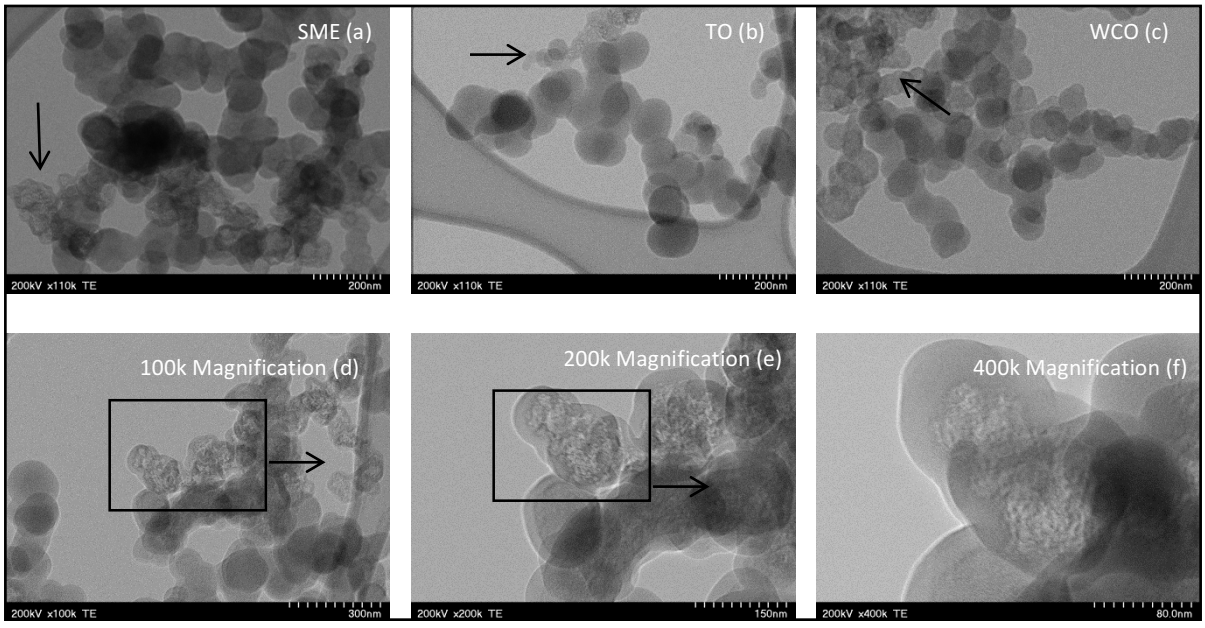

Figure 16. Possible Soot Oxidation Step in Soot Formation Process from Different Feedstocks

Notes: (a-c) Deformation observed in the structure of soot particles by oxidation process for SME, TO, and WCO, respectively. (d-f) Images of oxidized soot particles at magnifications of 100K, 200K, and 400K, respectively. Arrows indicate enlargement of the selected area, which is presented in the next images for better comparison.

Elemental Analysis of Collected Soot Particles

The following section describes the composition change of emissions depending on the type of feedstock and the ratio of biodiesel and ULSD within the blends. The source of many elements may be from organic and inorganic components or complexes present in various feedstocks. These elements can be converted into aerosols during the combustion process in vehicles. Alkali (Na) and alkaline earth (Ca) elements can come from the transesterification process in biodiesel production. Figure 17 summarizes the results of the elemental analysis of soot obtained from the blend of various feedstocks which are presented in pie charts. Eight major elements were detected in the elemental analysis of the exhaust soot: aluminum (Al), calcium (Ca), cupper (Cu), iron (Fe), magnesium (Mg), molybdenum (Mo), sodium (Na), and potassium (P). Compared with the existing data collected from field tests, which include elements originating from engine parts and oils (Kumar et al., 2014; Omidvarborna et al., 2014; Shandilya and Kumar, 2014), all the elements detected in this study came from the tested fuel itself and represented the type and amount of different elements produced at the tested conditions. Some authors have reported that elements such as zinc (Zn) and chromium (Cr) may be produced from the unwanted combustion of lubricants and their additives (Shandilya and Kumar, 2014). These elements were not detected here because of the absence of lubricants in the laboratory combustion chamber. Due to the strong dependency on higher temperature, the chance of releasing higher concentrations of these elements increases at higher combustion temperature, which often occurs in hot idle mode (Omidvarborna et al., 2014; Salamanca et al., 2012a).

The sulfur that appears in soot normally comes from regular diesel. Sulfur content is not reported due to its high ionization potential and low sensitivity of the instrument. As shown in Figure 17, the ratios between detected elements do not show a significant difference except for Mo which encompasses the highest portion in TOB20 soot. The main source of the detected elements is from the feedstocks and the production process. Another source for elements such as Al, Ca, Cu, Mg, Mo, Na are fuel additives to promote specific characteristics (Korn et al., 2007). This means that the concentration of elements might be related to various parameters such as biodiesel portion in the blends and the amount of additives used. The type of biodiesel feedstocks (in other words, fuel unsaturation) did not show any significant difference in the number and amount of elements detected under the conditions of this study. This finding suggests that Na, Mg, Ca, Fe, Mo, and even Cu, Al, and P in very low percentage could be candidates for marker metals of both ULSD and biodiesel blends (from SME, TO, WCO feedstocks).

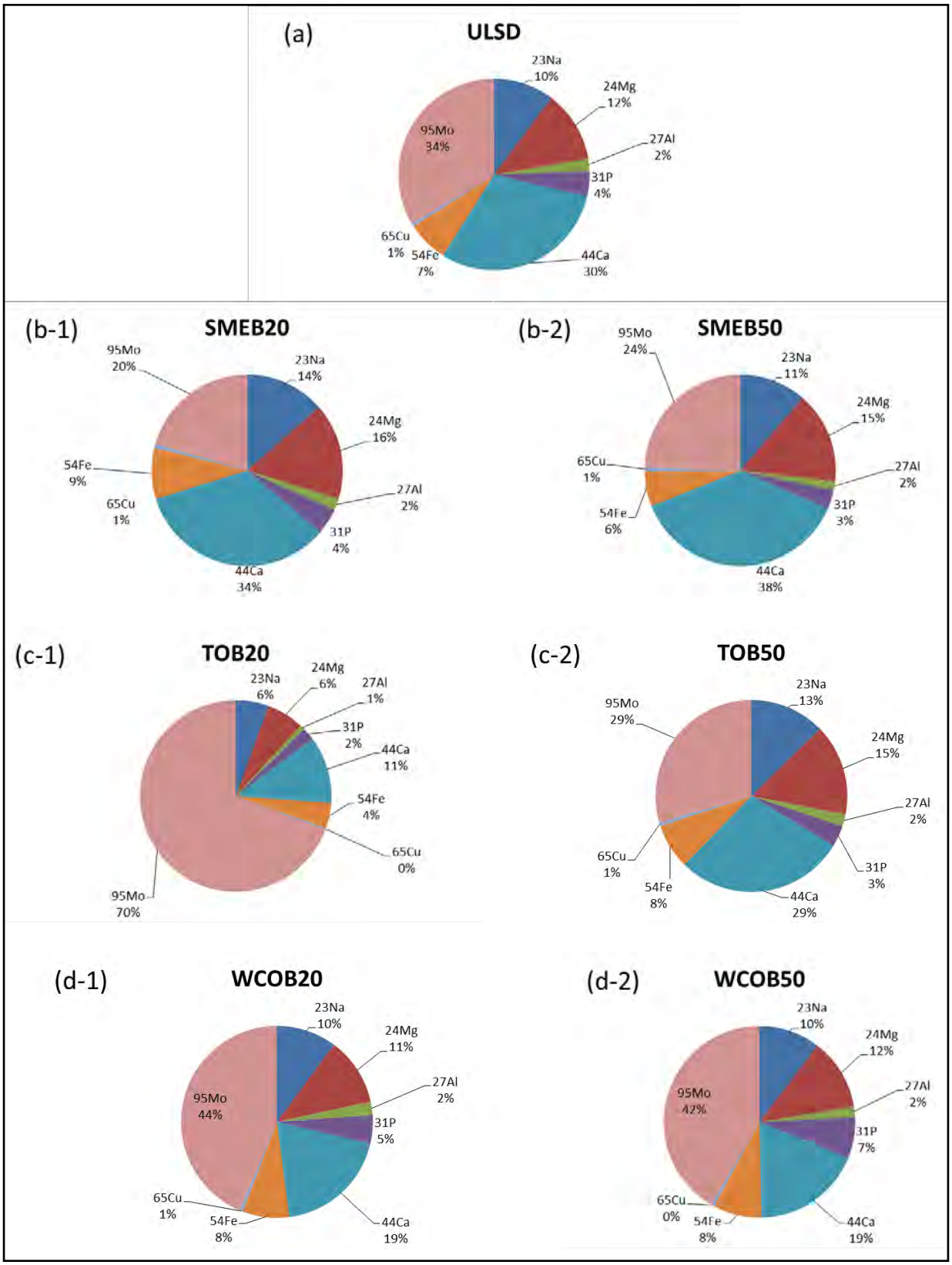

Figure 17. Elemental Analysis of the Collected Soot from Different Feedstocks and Blends with ULSD

Notes: (a) ULSD, (b-1) SMEB20, (b-2) SMEB50, (c-1) TOB20, (c-2) TOB50, (d-1) WCOB20, and (d-2) WCOB50.

FTIR Spectra of Collected Soot Particles

The functional groups of soot particles were characterized using FTIR analysis. The FTIR spectra of collected soot from the combustion of ULSD and three different B20 biodiesel fuels are presented in Figure 18. In the diesel soot spectra, the most characteristic signals are sulfate groups (S-O) (Salamanca et al., 2012b). The sulfate groups reported by Cain et al. (2010) were detected around 1000 and 1100 cm^{-1} (Figure 18(a)). The origin of this signal is attributed to the sulfur present in the ULSD, though sulfur is not detected in the liquid ULSD when using FTIR. Thus, it can be inferred that sulfur-derived species were adsorbed into the soot particles after combustion.

The absorbance peak for all biodiesel soot samples were weak, and this absorbance peak may represent the amount of ULSD used in their blends. Other weak signals in the range of 1350 to 1370 cm^{-1} and 1475 to 1550 cm^{-1} are related to alkanes (C-H) and nitro compounds (N-H), respectively. In Figure 18(a), the weak aromatic signals are observed at around 1500 cm^{-1} (C-C aromatics in-ring) and around 1610 cm^{-1} for stretching aromatics. The larger the aromatic related signal, the lower is the hydrogen content, thus indicating that the aromatic C-H bonds (2800 to 3000 cm^{-1}) are not as intense or in some cases undetected by FTIR.

The presence of aliphatic groups (C-H) helps to maintain the interconnection of PAHs within the network (Santamaria et al., 2010). The presence of an aliphatic spectrum may also come from the unburned HCs condensed on the surface of particles at low temperature (Schönborn et al., 2009; Vander Wal et al., 2010). Literature review showed that the presence of aliphatic bonds increases the mass of soot during the mass growth process (step 3) (Kumar et al., 2014; Omidvarborna et al., 2015a). As shown in Figure 18(a), the carbonyl content (esters, saturated aliphatic, alpha- and beta-unsaturated esters, etc. at around 1665 to 1760 cm^{-1}) of soot samples when compared with ULSD was negligible. Thus, it can be concluded that carbonyl bonds (C=O) were completely involved during reaction pathways for all biodiesel fuels.

Figure 18(b) shows the spectra corresponding to aliphatic groups present in the soot produced from B20 of SME, TO, and WCO at 2850 to 3000 cm^{-1}, which represent weak signals of C-H stretched compounds. The prominent, broad, and intense bond observed in the spectrum of Figure 18(b) between 3100 cm^{-1} and 3640 cm^{-1} is a contribution from a variety of -OH stretching modes. The OH spectrum may be a signature of the absorption of many different chemical compounds which most likely have alcohol groups in their structure. The OH spectrum of SME may be related to its degree of unsaturation. As biodiesel fuels become more unsaturated, the oxygen content may increase. The increase in oxygen content may be due to the decrease in molecular weight associated with the displacement of two hydrogen atoms by each double bond (Benjumea et al., 2010).

From the collected spectra in Figure 18(a,b), it can be concluded that the obtained spectra for ULSD and all three B20 fuels were weak in most cases. Although the signal strength of biodiesel fuels was significant and comparable with that of ULSD for some regions (e.g., 1000–1100 cm^{-1} and 3100–3640 cm^{-1}), soot obtained from the biodiesel samples showed relatively lower sulfur content, but higher oxygen content compared with the

ULSD soot. The low sulfur content of biodiesel may be attributed to soot reduction. In addition, the oxygen content detected in biodiesel soot may help improve the performance of posttreatment processes that reduce emissions by increasing the oxidation of soot.

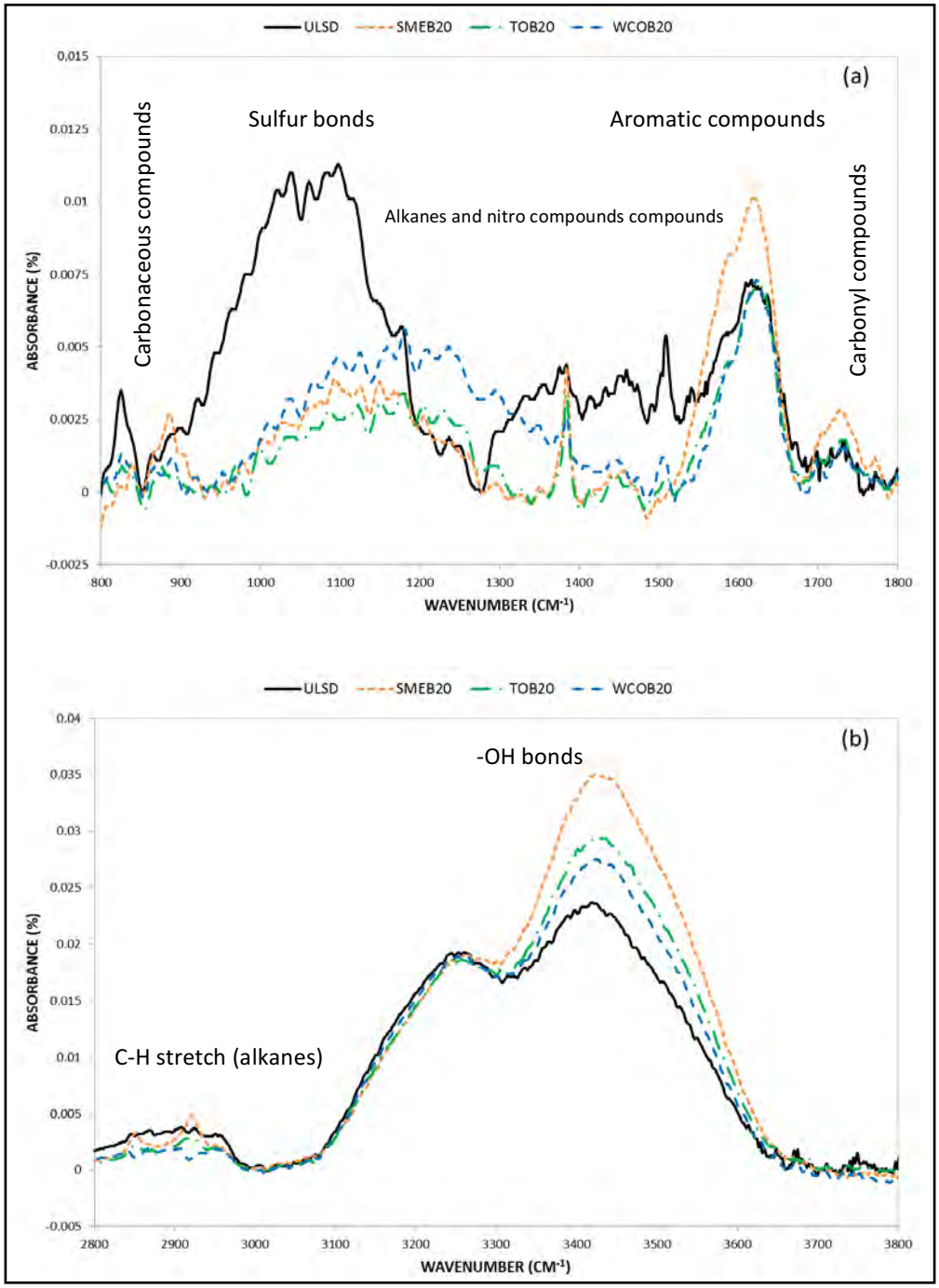

Figure 18. Infrared Spectra of Soot Produced From ULSD and Its Blends with 20% of Various Biodiesel Samples

Notes: (a) from 800 to 1800 cm^{-1} and (b) from 2800 to 3800 cm^{-1}.

TGA Analysis of Collected Soot

A set of TGA experiments was performed to investigate the diesel soot volatile organic fraction (VOF), carbon fraction, and oxidation behavior. Table 8 and Figure 19(a,b) show the TGA analysis of collected soot from the combustion chamber for ULSD and B20 of all biodiesel fuels. As mentioned earlier, the mass of soot was reduced by increasing the portion of biodiesel fuel; therefore, only ULSD and B20 fuels produced enough soot to perform this experiment.

The heating program for TGA analysis is presented in section 2 (TGA analysis of soot particles). In the presence of nitrogen, a slow 5°C/min ramp-up was employed to volatilize the vast majority of the organic compounds to 400°C. Before switching to an oxygen atmosphere at 400°C, thermal decomposition usually happens with the formation of gaseous reaction products, where the amount of moisture and VOF could be determined. Biodiesel blends showed around 6% mass loss under these conditions compared with ULSD, indicating an insignificant difference in water content and VOF among all the fuels.

After 400°C, when the media changes from nitrogen to oxygen, the reaction taking place is assumed to be unburned fuel (carbon) oxidation. The oxidation rate of biodiesel fuels was faster and the oxidation occurred sooner than that of ULSD as shown in Figure 19(a). As shown by FTIR analysis, there are indications that soot created during biodiesel combustion is more reactive for oxidation than soot created during ULSD combustion. Therefore, it follows that the oxygen bonds present in biodiesel fuels are involved in the formation of oxygenated bonds in soot particles. Table 8 shows proximate analysis of collected soot determined by TGA analysis. The results indicate that the major content of all collected soot is carbon, while there is no ash remaining after the combustion. The main source for the ash is lubricant oils and other sources in diesel engines.

Table 8. Proximate Analysis of Collected Soot from B20 Biodiesel Fuels and ULSD and their Peak Temperatures by TGA Analysis

Fuel type	Weight loss (%) by 400°C	Weight loss (%) after 400°C	First peak temperature (°C)	Second peak temperature (°C)
ULSD	5.86	94.14	---	624.00
SMEB20	3.91	96.09	517.21	602.97
TOB20	5.82	94.18	512.82	600.47
WCOB20	5.48	94.52	505.31	609.86

By increasing the heater temperature in the presence of air, the soot begins to oxidize. The derivative weight loss curve in Figure 19(b) identifies the point at which weight loss due to soot oxidation is most evident. ULSD had only one peak and the length of peak was longer than those of biodiesel blends because ULSD has more carbon content than biodiesel fuels. Biodiesel fuels showed two peaks, the first obtained from HC oxidation with the second related to carbon oxidation. The values of the ignition peaks were observed at lower temperature for biodiesel blends due to their chemical structure. According to Boehman et al. (2005), biodiesel fueling alters the oxidation reactivity of the soot particles

due to their oxygenated structure and various unsaturation levels. As a result, a more amorphous soot structure is observed, which enhances the rate of soot oxidation. Thus, inherent differences have been seen between ULSD and biodiesel fuel in the reactivity of the soot produced by each.

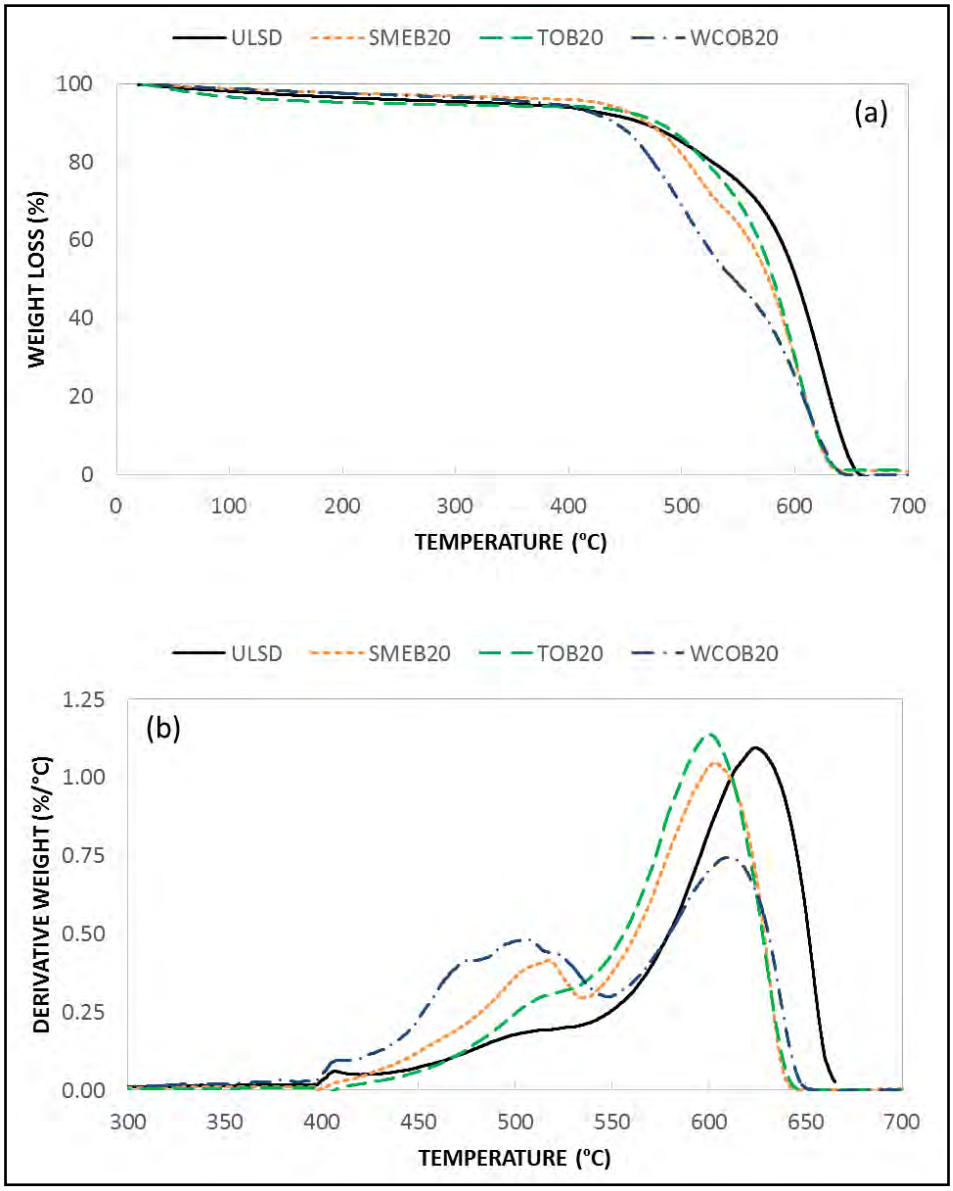

Figure 19. TGA Curves (Weight Loss (A) and Derivative Weight (B)) for Soot Samples Taken Directly from the Combustion Chamber

Note: mass of soot was around 3 mg.

NO_x Emissions

NO_x formation mechanisms are complex and are triggered by a number of coupled mechanisms whose effects may reinforce or cancel one another under different working conditions of an engine as well as fuel characteristics (Mueller et al., 2009). Based on previous work, it can be concluded that temperature and degree of unsaturation are two

major parameters that play important roles on NO_x emissions in a laboratory combustion chamber. Figure 20 represents the average values of five data sets plotted with SDs. In the case of ULSD combustion, due to the presence of more C-C and C-H bonds (higher carbon content which means higher heating value) than biodiesel fuels (Demirbas, 2007), high combustion temperature may be a more influential parameter for NO_x formation than for biodiesel combustion (Plee et al., 1982).

As shown in Figure 20, it is observed that the NO_x emissions varied in terms of the degree of unsaturation of the fuel when biodiesel fuels were included in the samples. In combustion of biodiesel blends, the degree of unsaturation is thought to be the major parameter. Considering the average values of the neat biodiesel samples, SME showed higher NO_x emissions than TO and WCO, which could be expected, because SME has a high degree of unsaturation. Zhang and Boehman (2007) argued that the presence of double bonds in biodiesel leads to the formation of free radicals that advance NO_x formation. The results on LTC were in agreement with those of previous engine studies (Benjumea et al., 2010; Lapuerta et al., 2009; McCormick et al., 2001), which reported that high degrees of unsaturation of biodiesel fuels lead to high NO_x emissions. The observed variations of SD in the combustion and emission results could be due to differences in the fuel's composition in each run.

The results suggest that the indicator for NO_x formations would be the presence of oleic fatty acids (C18:1 to C18:3). This conclusion is readily represented in the NO_x results of SME, TO, and WCO. TO and WCO showed less NO_x than SME, which has the highest amount of linoleic acids (C18:2 or higher in the number of double bonds). The major portion of double bonds in TO and WCO were found in stearate molecules (Table 1). TO and WCO have less or equal portions of C18:1 in the number of double bonds than SME.

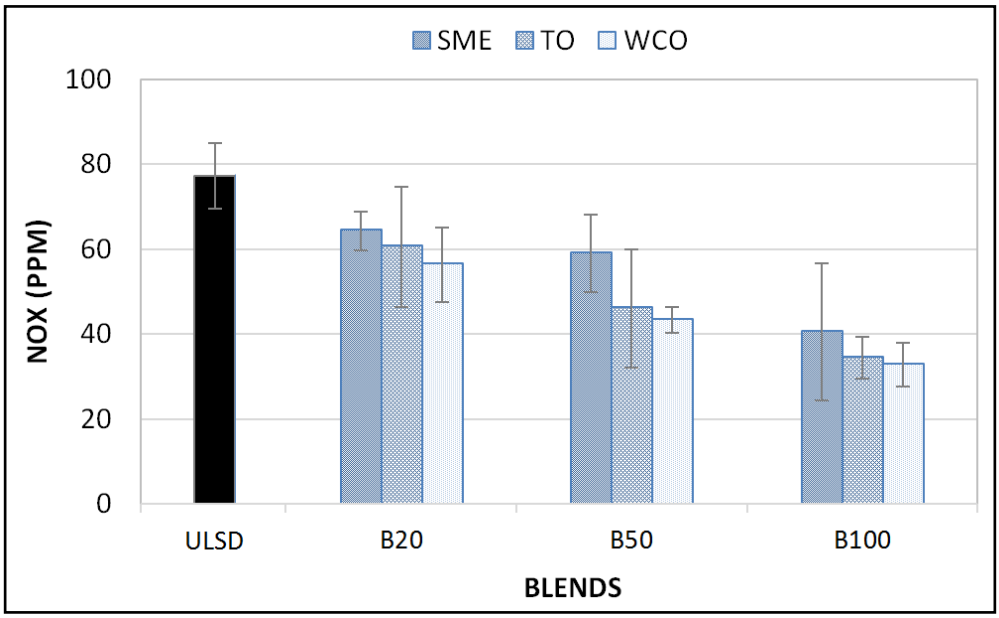

Figure 20. Variation of NO_x Emissions with Respect to their Degree of Unsaturation at LTC

Paired T-Test Analysis on NO_x Emissions

A statistical analysis of the data (paired t-test) was used to assess the differences between the NO_x emissions for the fuel blends. The difference in NO_x emissions among ULSD and all the biodiesel samples were compared statistically based on a paired t-test comparison of the means, assuming equal variance with P-value <0.001 and 95% confidence for all comparisons. For the paired t-test, it was hypothesized that there was a statistically significant difference in the NO_x emissions between two selected samples from different feedstocks where P-value ≤0.001. In addition, it was considered marginally statistically significant when P-value ≤0.05 approximately. Both the p-value and t-value are dimensionless parameters.

Using the simple paired t-test analysis for all samples, the results indicated that the differences between the samples are not considered statistically significant in most cases (presented in cells with white shading) as shown in Table 9. On the other hand, the cases in which the differences appear to be significant and marginally significant are presented in cells with black and grey shading, respectively.

Table 9. Results of Paired T-Test Analysis on Fuels Tested for NO_x Emissions

	SME B20	SME B50	SME B100	TO B20	TO B50	TO B100	WCO B20	WCO B50	WCO B100
ULSD	P = 0.15 t = 1.45	P = 0.13 t = 1.52	P = 0.04 t = 2.07	P = 0.30 t = 1.04	P = 0.05 t = 1.96	P < 0.0001 t = 4.69	P = 0.07 t = 1.80	P <0.0001 t = 4.10	P <0.0001 t = 4.85
SME B20		P = 0.61 t = 0.52	P = 0.15 t = 1.43	P = 0.80 t = 0.26	P = 0.21 t = 1.25	P <0.0001 t =4.49	P = 0.42 t = 0.82	P = 0.0002 t = 3.86	P <0.0001 t = 4.70
SME B50			P = 0.32 t = 1.00	P = 0.93 t = 0.09	P = 0.44 t = 0.78	P = 0.02 t = 2.36	P = 0.83 t = 0.21	P = 0.11 t = 1.63	P = 0.01 t = 2.51
SME B100				P = 0.35 t = 0.94	P = 0.80 t = 0.26	P = 0.72 t = 0.36	P = 0.39 t = 0.87	P = 0.87 t = 0.17	P = 0.64 t = 0.47
TO B20					P = 0.47 t = 0.73	P = 0.08 t = 1.75	P = 0.80 t = 0.25	P = 0.23 t = 1.20	P = 0.07 t = 1.86
TO B50						P = 0.43 t = 0.79	P = 0.53 t = 0.63	P = 0.84 t = 0.20	P = 0.37 t = 0.90
TO B100							P = 0.03 t = 2.19	P = 0.13 t = 1.52	P = 0.81 t = 0.24
WCO B20								P = 0.16 t = 1.42	P = 0.02 t = 2.35
WCO B50									P = 0.08 t = 1.78

The t-test results are summarized in Table 9. No statistically significant differences in the NO_x concentrations were observed among neat biodiesel fuels. ULSD was significantly different from neat TO and WCO, and marginally significantly different from neat SME. Potential significance of the NO_x emission differences between a pair of SME B20 and TO B100 and a pair of WCO B20 and WCO B100 were considered significant and are shown

in the black shaded cells. Also, SMEB20 had significant differences compared with TO and WCO in neat form and even with WCOB50. For the results in the black shaded cells with 95% confidence, the null hypothesis can be rejected. These results suggest that the feedstock type could have a significant effect on the NO_x emissions. Also, some cases in the gray shaded cells represent partially significant effects on the NO_x reduction. The confidence levels of gray shaded cells are less than 95% while they have the potential of being partially significant. The results indicate that TO and WCO reduce NO_x formation significantly when compared to ULSD and SME in many blends.

Carbon Emissions

For biodiesel fuels, the changes in the carbon emissions vary according to the type of chemical characteristics of the feedstocks. Figures 21(a-c) represent the exhaust emissions of CO, CO_2, and CH_4 in relation to the biodiesel percentages, respectively.

The local temperature is not high enough at the early stage of combustion, therefore very few oxidation reactions take place. At this stage, primary reactions can take place and the initial HCs may be produced. In ULSD combustion, the uneven distribution and lack of oxygenated molecules across the combustion chamber may cause local oxygen deficiency and incomplete combustion, which results in more CO formation. A drastic reduction on CO exhaust emissions was observed when biodiesel blends were used instead of ULSD. The results confirmed that ULSD emits higher CO (2.5 mole %) and lower CO_2 (0.7 mole %) than the other blends. For the biodiesel fuels in Figure 21(a), biodiesels' higher oxygen-to-carbon ratios compared to ULSD are thought to be the main reason for the significant decrease in CO emissions. Moreover, the presence of peroxides and hydroperoxides formed during biodiesel combustion may have resulted in the lower emissions of CO in biodiesel than that of ULSD (Monyem and Van Gerpen, 2001). On average, the highest reduction rate for CO was observed in the TOB100 emissions compared to ULSD (~79%). The reductions of CO emission for pure WCO and SME were 64% and 60% less than that of ULSD, respectively.

For the biodiesel fuels, the reduced CO emissions can be explained by the higher oxygen content in the short fatty acid molecules of TO (C16:0 or less), which leads to more complete combustion as stated earlier (Pinzi et al., 2013). Short-chain FAMEs are easier to oxidize than the long-chain FAMEs, and therefore, a further reduction of CO emissions can be achieved using biodiesel fuels containing an increased content of short FAME chains. Moreover, FAMEs with longer chains and unsaturated structure (e.g., SME) have higher boiling and melting points (Pinzi et al., 2013) than shorter chain FAMEs (e.g., TO and then WCO), so they are less likely to be completely vaporized and burnt, thereby increasing CO emissions (Hansen and Jensen, 1997).

CO emissions are reported to increase with an increase in the number of double bonds in the chain lengths of FAMEs (Pinzi et al., 2013). For biodiesel fuels used in this study, the carbon content increases with an increase in the unsaturated contents and chain lengths (especially for C18:0 to C18:3), which means SME possibly emits more CO than WCO and TO, respectively. The obtained emission result in Figure 21(a) is in agreement with the EPA's survey, which reported the reduction of CO emission from pure biodiesel to be 47% on average of the CO emission from ULSD (USEPA 2002).

In contrast with the CO emission reduction, CO_2 emissions in the exhaust increased with the decrease in chain length of FAMEs as shown in Figure 21(b). Higher CO_2 emissions were reported for the pure FAMEs with shorter chains (Pinzi et al. 2013). This trend can be explained by high oxygen content in the shortest fatty acid molecules as well as relatively low carbon content in biodiesel compared with ULSD for the same volume of fuel consumed, which led to more CO_2 emissions (Chauhan et al., 2012; Lapuerta et al., 2008b). As noted earlier, shorter molecular structure of FAMEs helps faster fuel evaporation, which results in possibly more complete combustion. For SME, the CO_2 formation increased by a factor of 2.9, while it increased by a factor of 3.0 and 3.2 on average for WCO and TO from ULSD, respectively.

CH_4 emissions increased as the portion of biodiesel increased in the blends, as shown in Figure 21(c). Although CH_4 may be regarded as an intermediate species in biodiesel combustion, clear trends of CH_4 emissions were observed when the unsaturation level of methyl esters was varied. In accordance with Hansen and Jensen (1997), CH_4 emissions considerably increased with an increasing number of double bonds. Short and less unsaturated FAMEs such as WCO and TO showed lower emissions of CH_4 than unsaturated and longer chain FAMEs such as SME. Although FAMEs take highly complex reaction paths with respect to ULSD, it may be possible to improve CH_4 emissions from biodiesel combustion by increasing the contents of short and saturated FAMEs. The results showed that the average CH_4 formation was increased by a factor of 1.9 for pure biodiesel fuels with respect to ULSD. For pure biodiesel fuels, SME produce the highest CH_4 at 2.7 mol%, WCO at 2.4 mol%, and the TO at 2.3 mol%.

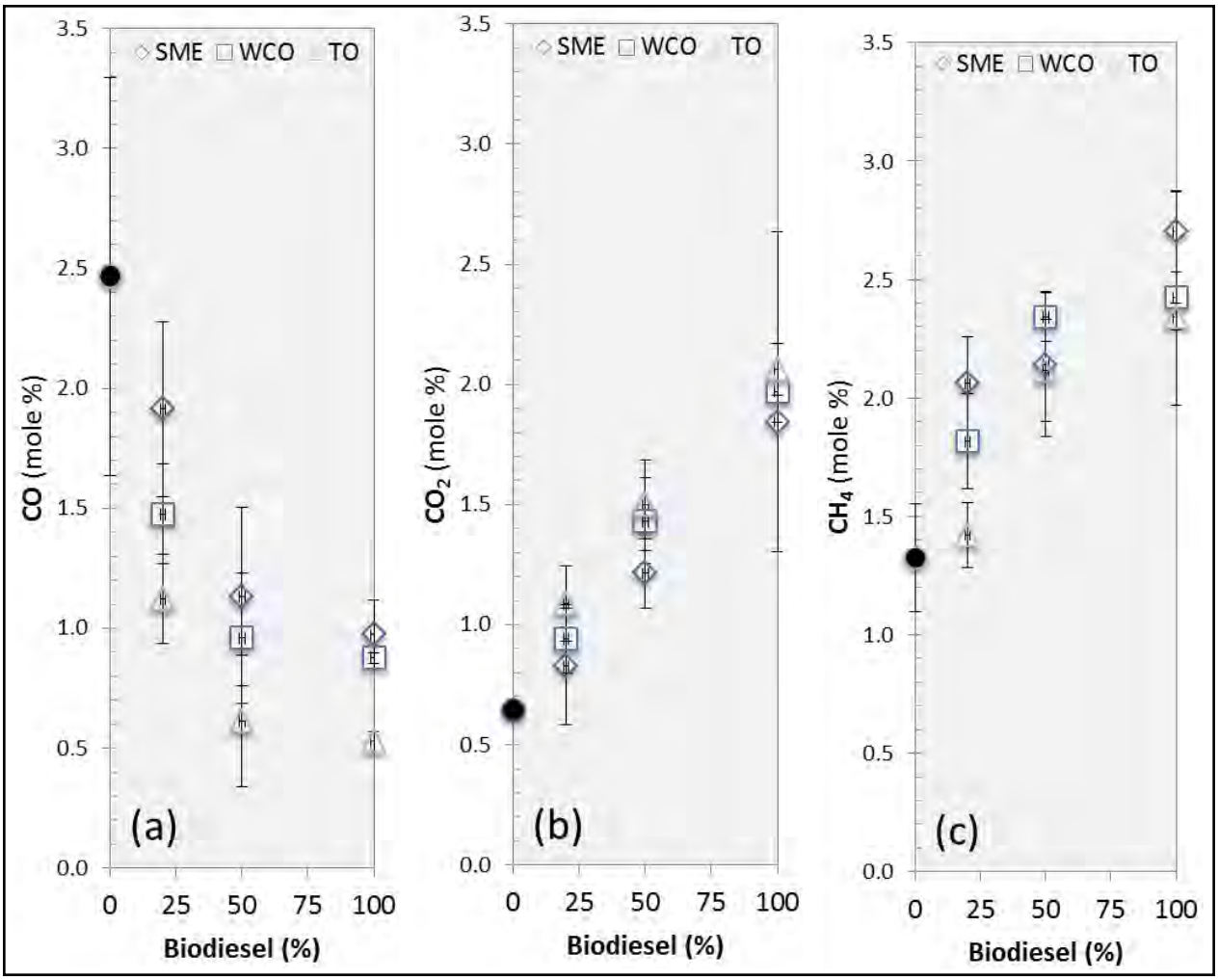

Figure 21. Primary Combustion Gases in Mole Percent Emitted during the Combustion of Fuels

Notes: (a) CO emissions, (b) CO_2 emissions, (c) CH_4 emissions. B0 represents ULSD combustion emissions.

FIELD EXPERIMENTAL RESULTS

Size Characterization of PM

The PM deposited on quartz filter papers were sonicated in isopropanol solution and suspended in the liquid. Figures 22 and 23 show the PM deposited filters before and after sonication for bus 701 and 802 samples, respectively. It is worth mentioning that bus 802 was equipped with EGR, whereas the other (701) was not. Figure 22(a) and Figure 23(a) show PM collected from bus 701 which ran on ULSD and bus 802 which ran on SME B20. The difference between the PM deposition on Figure 22(a,b) and Figure 23(a,b) clearly shows that the methodology followed to transfer deposited PMs to the liquid by using sonication is effective. The PM deposition on the filter papers, especially on the filter paper used for bus 701 (Figure 22(a)), was more than the filter paper used for bus 802 (Figure 23(a)). This difference in deposition quantity can be attested to by the various filters and emission controlling equipment available in bus 802 compared with bus 701. Bus 802 was equipped with the EGR system, diesel particulate filter, and catalytic

converters, whereas bus 701 was only equipped with a catalytic converter. So the higher the PM deposition on the filter paper, the longer is the sonication process. This means, it takes more time to suspend PM deposition on 701 filter paper than 802 filter paper in isopropanol solution through sonication. Even though these experimental runs appear to be successful, different methodologies should be applied to move further in this research.

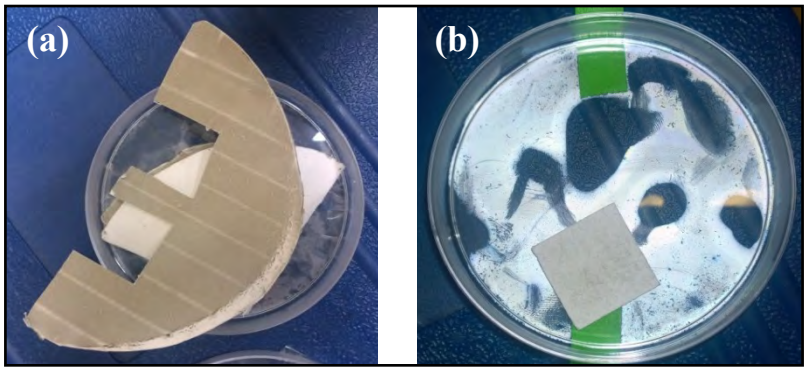

Figure 22. (A) Quartz Filter Paper with PM Suspension from Bus 701 Before Sonication, (B) One Inch^2 Quartz Filter Paper after Sonication

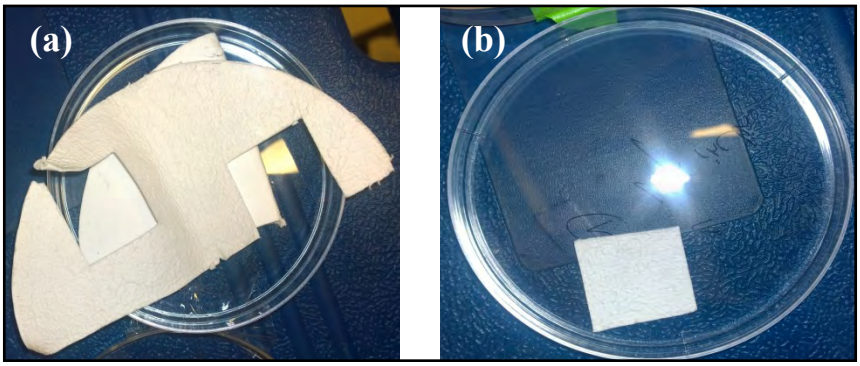

Figure 23. (A) Quartz Filter Paper with PM Suspension from Bus 802 Before Sonication, (B) One Inch^2 Quartz Filter Paper after Sonication

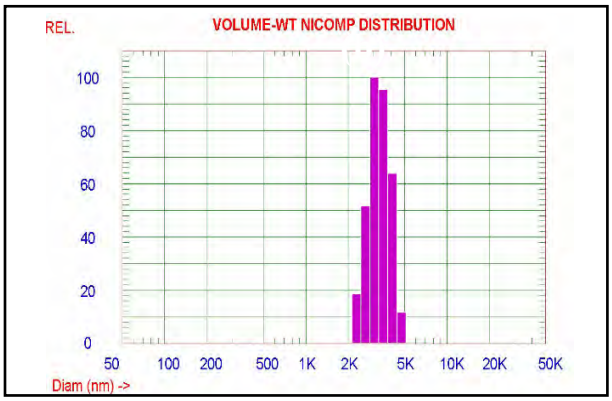

Figure 24. Size Distribution of PM Collected from Bus 701 (cold idling)

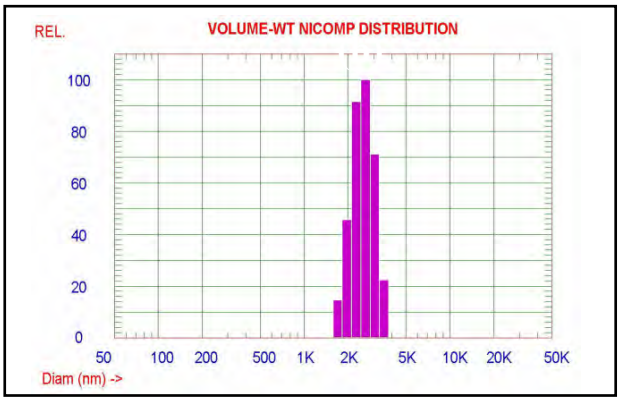

Figure 25. Size Distribution of PM Collected from Bus 701 (hot idling)

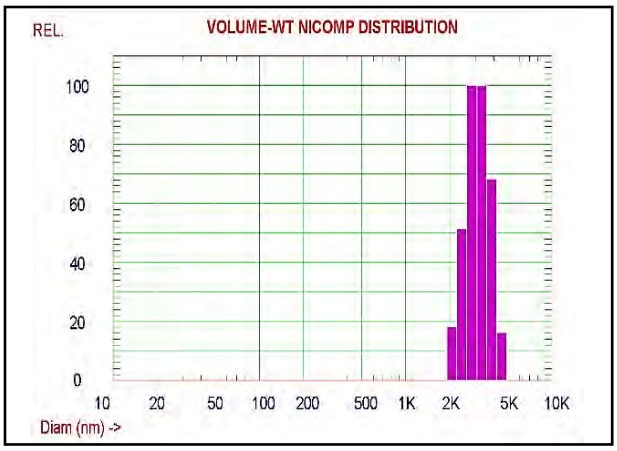

Different types of results can be obtained from NICOMP 380 zls zeta potential/particle size analyzer, but for this study, a volume-to-weight NICOMP distribution histogram is needed. Figures 24 through 27 show the volume-weight NICOMP size distribution histograms of PM, which were collected from buses 701 and 802. In the histograms, the y-axis represents the relative intensity and x-axis represents the diameter of the particles in nanometers (nm). In the histograms, a peak with a 100 value on the relative intensity scale is the highly concentrated PM size, and peaks less than 100 on y-axis represent the PM that are relatively less concentrated.

The size range of the PM detected in the samples from bus 701 was 2 to 5 μm (2000–5000 nm) e.g., values were detected to be $PM_{2.5}$ to PM_{10} (≤2.5 to ≤10 microns in diameter) for cold idling and 1.75 to 4.5 μm (1750–4500 nm) for hot idling. In contrast, emissions from bus 802 had a PM range of 2 to 5 μm (2000–5000 nm) for cold idling and 1.25 to 3.5 μm (1250–3500 nm) for hot idling. Most of the PM samples (both hot and cold idling) of bus 701 are in the range of 2.5 to 4.5 μm (2500–4500 nm). For bus 802, PM samples are in the size range of 2 to 3.5 μm (2000–3500 nm). Each sample was run for three cycles in the instrument, and the results were reported as histograms using PSS ZPW388 0.1 software. It is worth mentioning that the particle size distribution very close to $PM_{2.5}$ and PM_{10} were used to classify PMs.

From Figures 24 through 27, an unraveled consistency can be observed in the size distribution. The peaks observed (>100 nm) in Figures 24 to 27 of PM size distribution are associated with PM samples collected from older vehicles in idle mode. Also, high PM size in the emissions can be associated with vehicle cold starts and warm starts. On the other hand, factors such as maintenance, mileage, EGR effect, and presence of air filtering devices such as catalytic converters, etc., also play a role.

NO_x Emissions from Transit Buses—Idle Mode

Idling was observed when the bus stopped at traffic signals, intersections, or traffic jams. As pointed out earlier, one of the most critical emissions from engines is NO_x. In the combustion of biodiesel fuels, the formation of NO_x is highly dependent on combustion temperature, oxygen content, and residence time (Marques et al., 2007). NO_x formation begins after the start of heat release (combustion). Shortly after the end of heat release, the period of NO_x formation reduces because the temperature of the burned gas decreases (Dieselnet, 2014). Figure 28 plots the cumulative NO_x emissions with time for the engines equipped with EGR and non-EGR, respectively. As shown in Figure 28, NO_x emissions were under better control for the EGR engine than for the non-EGR engine. The non-EGR engine emitted the higher amount of NO_x at the beginning, when it reached 1208 ppm, whereas the NO_x value was 659 ppm for the EGR engine (Tables 4 and 5). After a few seconds, the engine equipped with EGR produced NO_x at a fairly constant rate, while the rate was still elevated for the non-EGR engine (seven times higher than the EGR engine). The total NO_x formation for 1200 seconds is approximately $7x10^5$ ppm for the non-EGR engine and around 10^5 ppm for the EGR engine. The lower NO_x emissions observed in the EGR engine is due to the fact that the EGR can control the formation of NO_x through recirculation of exhaust gas as well as through the regeneration process. In particular, the endothermic dissociation of H_2O results in a decrease in combustion temperature which consequently reduces NO_x emissions.

The results clearly indicate that EGR is an effective method for NO_x control. NO_x emissions from an EGR engine fueled with B5 were found to be comparatively lower than the NO_x emissions from the non-EGR engine. EGR reduces both the combustion temperature and oxygen content of intake air which are the main factors in NO_x reduction (Pradeep and Sharma, 2007; Saleh, 2009). Additionally, in idle mode, diesel engines generally tolerate a higher EGR ratio because recirculating engine exhausts contain high concentration of oxygen and low concentration of carbon dioxide (Agarwal et al., 2011). The EGR ratio is defined as follows (Agarwal et al., 2004):

$$\text{EGR ratio} = \frac{\text{volume of EGR}}{\text{total intake into the cyclinder}} \times 100 \quad (2)$$

Although modern automotive diesel engines are equipped with an EGR cooler, the inlet air temperature increases with the EGR ratio after mixing with recirculated gases, thus, reducing the inlet gas density and in-cylinder trapped mass. This temperature increase tends to increase NO_x emissions (Maiboom et al., 2008), although it is compensated for by other effects of EGR discussed earlier. Therefore, O_2 is available in sufficient quantity in idle mode, but O_2 reduces drastically at high loads, and NO_x is reduced more at higher loads compared to idle mode. Thus, the major influence on NO_x emissions seems to be due to the change in combustion temperature rather than O_2 availability.

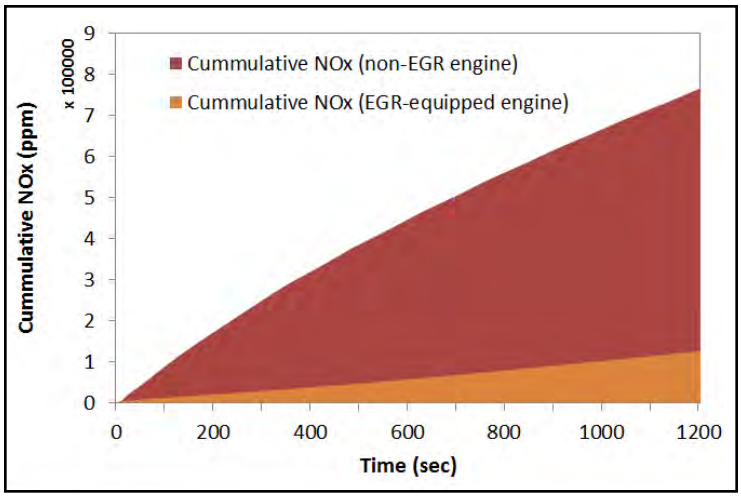

Figure 28. Cumulative NO_x Emissions for Non-EGR and EGR Engines for the City of Toledo, Ohio

Note: Both tests were performed with the minimum load in the morning (a.m.) prior to daily routing of the buses (cold idle).

The graphical representation of NO_x emissions versus time for both EGR and non-EGR engines are plotted in Figure 29. The values of NO_x emissions in idling conditions showed that the non-EGR engine (700 series) emitted more NO_x than the EGR engine (800 series) over the study period. After starting the cold idle test, in about 20 minutes, NO_x emission values tend to decrease and reach a constant point of 200 ppm. The NO_x emission values tend to further decrease beyond this point; however, the rate of change of the emission values with respect to the time will be very low. In a relatively constant engine load (<10%), recirculating a portion of exhaust gas back into the engine helps to absorb the heat from combustion. By using this dilution effect, the combustion temperatures are lower and NO_x formation is significantly reduced.

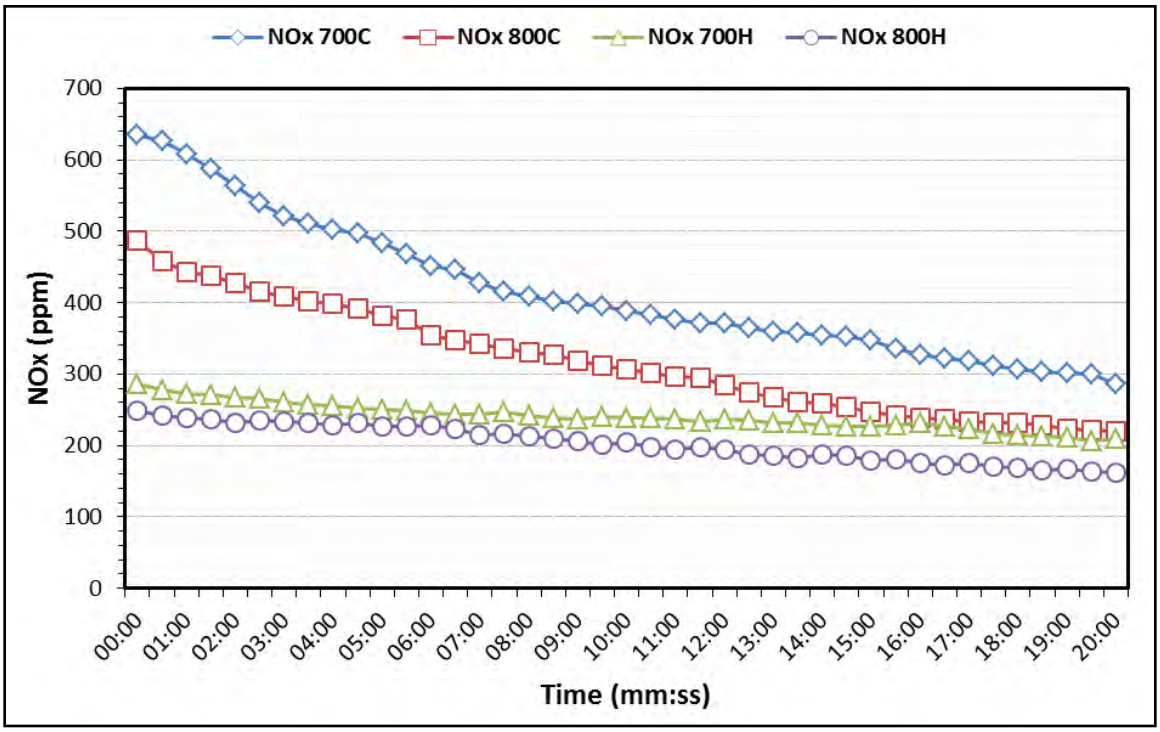

Figure 29. Comparison of NO_x Emissions Among EGR and Non-EGR Engines with Respect to their Idling Modes

NO_x Emissions from Transit Buses – Operating Mode

Factors such as load, acceleration, deceleration, road traffic, traffic signals, and nature of the road affect NO_x emissions. The engine-out discharge of NO_x emissions from B5 fuel is presented in Figure 30.

The decelerating condition is also known as the breaking condition. During deceleration, an extra amount of load will be applied on the engine, which results in reducing the speed of the bus. While decelerating, the fuel consumption will be reduced as well as the NO_x emissions. In the accelerating condition, when the bus starts from a minimum speed after a halt or from a decelerating condition to attain higher speeds, an extra load will be applied on the engine. To attain the acceleration from the rest position, a large amount of fuel is burnt, which in return, increases the NO_x emission concentrations. When the bus is moving at different speeds, different levels of load will be exerted on the engine, causing the NO_x emissions at constant speeds to vary with the varying speeds of the bus. Although the NO_x emissions are, to some extent, stable at constant speeds and do not vary as much as observed with decelerating and accelerating condition of the bus, a particular range can be defined for the NO_x emissions in this case. A graphical representation of NO_x emissions versus engine speed in a decelerating, accelerating, and constant condition are presented in Figure 30.

NO_x emissions in deceleration are the lowest when compared to other conditions. A NO_x emission value of 10 ppm was observed in a decelerating condition at 785 rpm, which was the least for all conditions. In all NO_x emission data points obtained in deceleration, 32 ppm

was the highest value observed at 1140 rpm. A graph for NO_x emissions in deceleration mode was plotted using 54 data points (Figure 30, green points).

At 2095 rpm, the highest value of NO_x emissions (634 ppm) was observed in the accelerating condition. The least value of NO_x emissions observed in acceleration was 408 ppm, which was recorded at 1735 rpm. A graph was plotted for this condition using 63 data points (Figure 30, red points).

At constant speeds, the NO_x emission range experienced more variable speed conditions compared to the rest of the conditions. It was due to the fact that data collection for this condition started from initial acceleration and ended when the bus decelerated. Figure 30 clearly illustrates the constant moving condition drawn using 80 data points. When compared to the initial acceleration condition, the NO_x emissions observed in the constant condition were lower. The highest NO_x emission of 378 ppm was observed at 1707 rpm and the lowest NO_x emission of 98 ppm was observed to be at 1186 rpm. It can be inferred from the graph that larger numbers of NO_x emissions were concentrated in the range of 230 to 360 ppm. The graph also shows limited points from 98 to 160 ppm because of the uneven roads that caused the bus to move slowly.

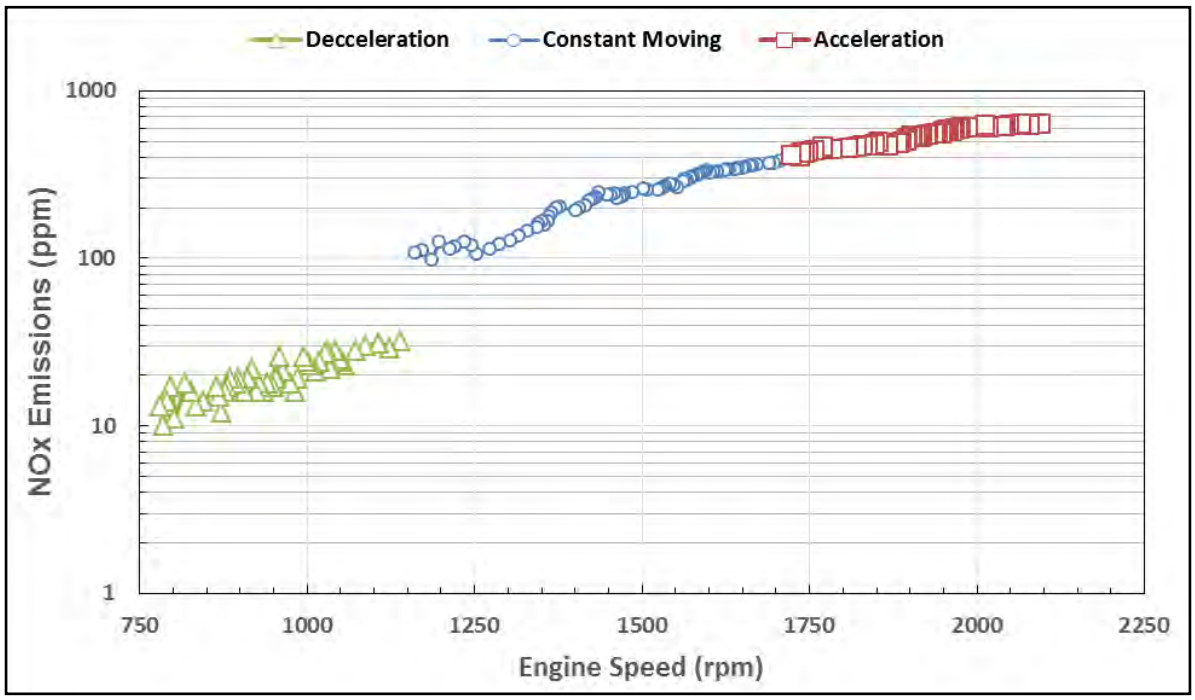

Figure 30. Graph of NO_x Emissions versus Engine Speed in Deceleration, Acceleration, and Constant Moving Condition

The results of combustion analyses obtained from exhaust tail pipe emission data from on-road engines were expected to be different with engine-dynamometer. This discrepancy is because of the fact that the combustion analyses were generally carried out with measurements made inside the combustion chamber. From the study of NO_x emissions from an engine running on SME B5, it can be inferred that the NO_x emission changes were directly proportional with engine speed; that is, NO_x emissions increased with an increase in engine speed and decreased with a decrease in engine speed.

Modeling Results, ANN Study

An ANN model was developed to predict NO_x from two different engines, based on the experimental data. The number of data patterns required for training the network were chosen in such a way that the network was sufficiently trained to produce consistent results, and concurrently the remaining data were enough to test the established model. In addition, some data patterns were set aside for validating the network during the process. A total of 70% of total experimental data were selected for training the neural network, 15% for the network's validation, and the remaining 15% data were used for testing the performance of the trained network. The input data were fed into the neural network toolbox and model parameters adjusted to determine the optimum network. Then, the accuracy of the network was presented using R-values and absolute errors calculated by comparing the predicted values of NO_x emissions with the experimentally measured values. Initially, the designed network was trained by selecting a minimum number of neurons in the hidden layer. Then the numbers of neurons were increased until the R-value reached a maximum value, and the results showed better reproducibility (lowest error). The number of neurons in the hidden layer for which the error was minimized was selected as the optimum condition. Of all the networks trained, only one satisfied this condition, which was the simplest network. A network with one hidden layer and 21 neurons proved to be an optimum ANN for the non-EGR engine (called 4-21-1). In this notation, four represents the number of input variables and one corresponds to the resultant NO_x concentration. The same optimum network was obtained for the EGR engine with 26 neurons in the hidden layer (7-26-1). The R-values did not improve or converge beyond 21 and 26 neurons in the hidden layer, and therefore, the networks with these numbers of neurons in the hidden layer were considered satisfactory.

To ensure precision, a regression analysis of outputs and desired targets was performed as shown in Figures 31 and 32 for the selected engines. The graphs obtained from MATLAB toolbox clearly show how well the variation in the output (predicted values) coincided with the targets (experimental values). If this number is equal to 1, then the targets and outputs are perfectly correlated. Thus a strong correlation is seen between the values predicted by the ANN model and the measured values resulting from experimental tests. The ANN model for the non-EGR engine displayed excellent overall agreement with the experimental data where it showed excellent R-values: 0.99567, 0.99479, and 0.99668 for training, validation, and testing, respectively. The same trend was observed for the EGR engine as shown in Figure 32. For the EGR engine, the R-values were 0.99955, 0.99784 and 0.99968 for training, validation, and testing, respectively. This is corroborated by the consistent concurrency of the ANN predicted values with the experimental data for the entire range of observations.

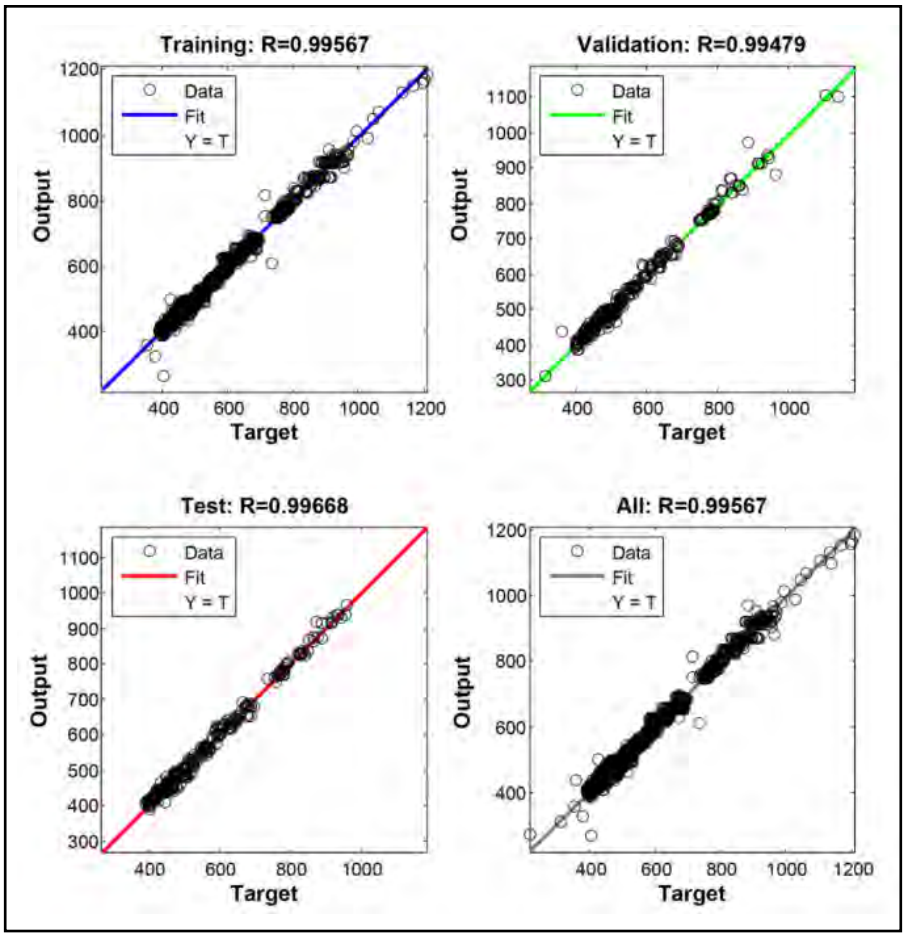

Figure 31. Overall R-Values of the Developed Network for Non-EGR Engine

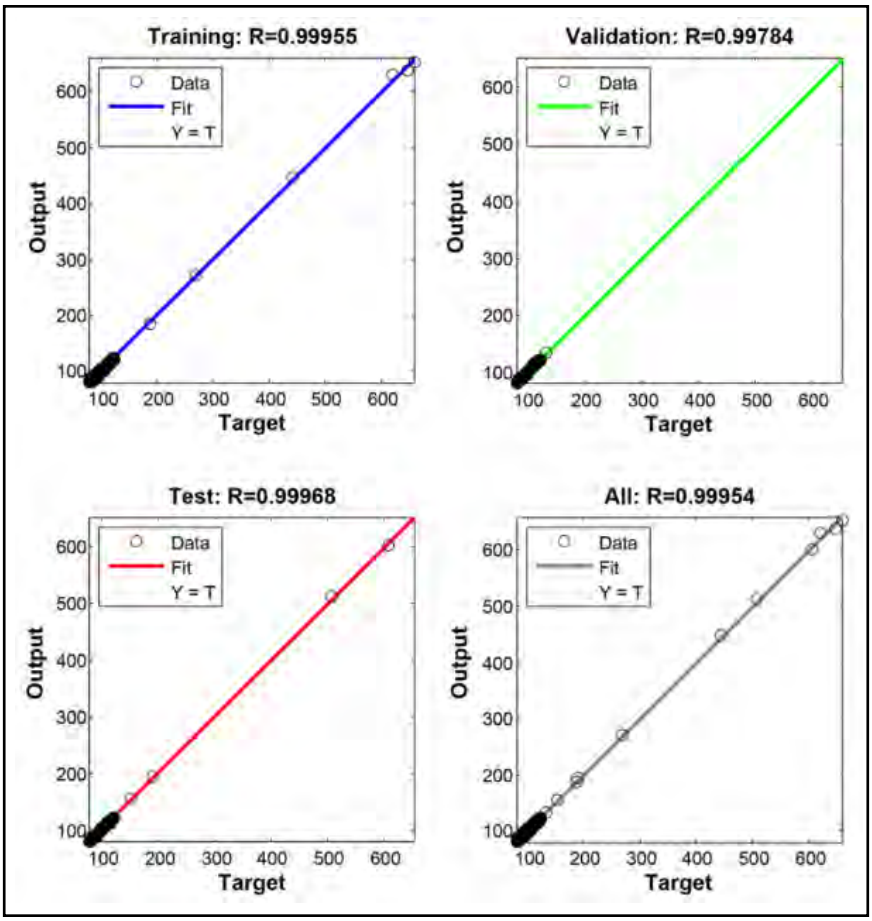

Figure 32. Overall R-Values of the Developed Network for EGR Engine

A comparison of ANN predictions for NO_x emissions with the experimental data is shown in Figures 33 and 34 for the non-EGR and EGR engines, respectively. The results confirmed that the ANN modeling with the standard feed forward back-propagation algorithm and LM training algorithm represented the experimental data very well from different idling engines with various input parameters (Ghobadian et al., 2009; Kiani et al., 2010; Najafi et al., 2009; Taghavifar et al., 2014). Major discrepancies were observed at the beginning of the running process when the engines were not stable and engine load was being increased. It can be observed that the agreement of the prediction increases slightly in the engine equipped with EGR compared to the non-EGR engine. EGR increased the correlation between the input and output parameters and slightly reduced the error. In other words, EGR is thought to reduce the combustion peak temperature as well as the intake oxygen concentration that resulted in the lowering of NO_x emissions. In addition, because EGR can control NO_x formation and dampen sudden variations (Figures 33 and 34), the pattern of NO_x emissions obtained from the EGR engine is less complicated and smoother than that of the non-EGR engine, hence it can be predicted by the model with less error. The RMSE values were confirmed for the impact of EGR on NO_x emissions, with the values being 22.1 and 1.7 ppm for non-EGR and EGR engine series, respectively. The relatively high value of RMSE for the 700 series (non-EGR) compared to the 800 series (EGR) was due to the engine conditions at the beginning of the combustion, when the engines was cold. The RMSE value for the 800 series showed that the engine was relatively stable

even in cold conditions, due to the recirculating portion of the engines' exhaust (<10%) returning back to the cylinder as discussed earlier.

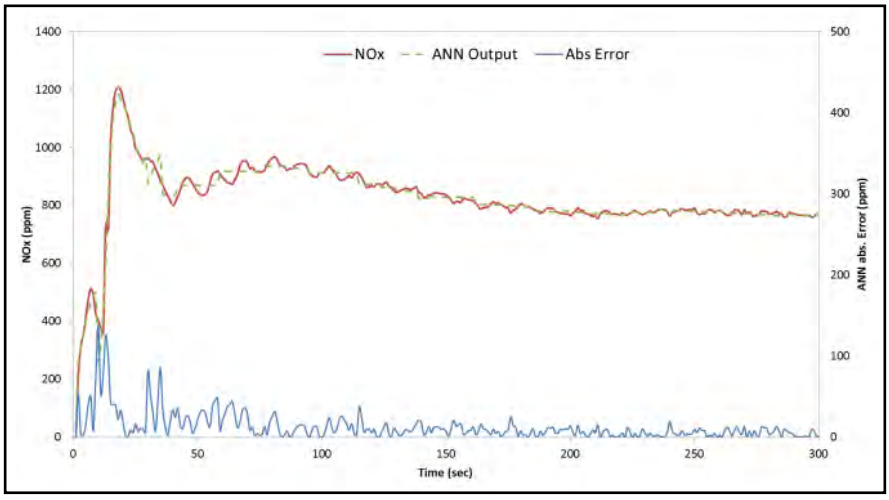

Figure 33. Comparison of Experimental and ANN Predicted NO_x for the Non-EGR Engine in Cold Idle Mode

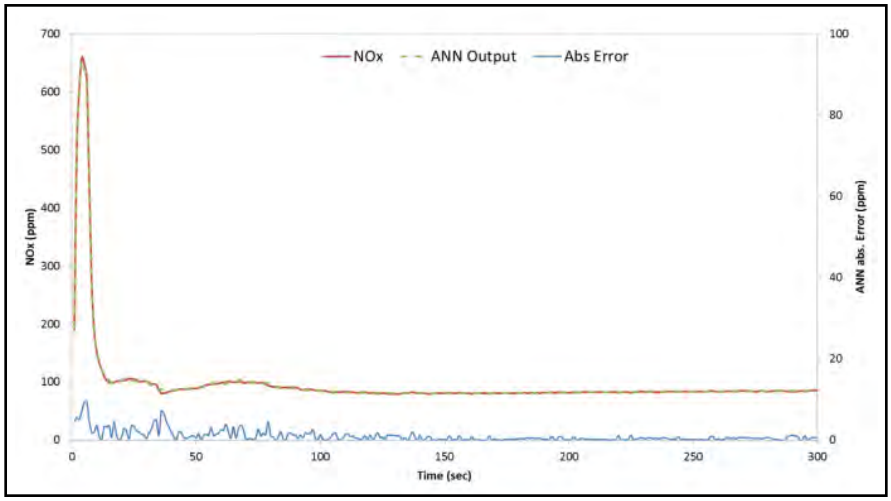

Figure 34. Comparison of Experimental and ANN Predicted No_x for the EGR Engine in Cold Idle Mode

Modeling Results, SSA Study

To evaluate the performance of the SSA model, the simplified ND/MD/MD5D mechanism is used to simulate NO_x emissions. Experimental data that have been collected from combustion of selected pure biodiesel fuels with different range of unsaturation (46.2%–85.1%) are used for comparison (Omidvarborna et al., 2015c). Among the tested biodiesel fuels, SME is the most unsaturated, WCO is medium unsaturated, and TO least unsaturated (Omidvarborna et al., 2015c). SME has the longest chain length, and WCO and TO are relatively short chain fatty acids (Omidvarborna et al., 2015c). The simulation was performed using the SSA at the temperature range below 700 K, which was also used

in the experiments. Because NO_x formation is related to high oxygen concentration, the air-fuel ratio was set as 1.0, the same condition used in the experiments (Shu et al., 2013).

Figure 35(a) shows the SSA modeling result (blue line) and experimental results (triangular marks) for pure biodiesel fuels ranging from highly unsaturated (SME in red) to relatively medium-unsaturated (WCO in purple) and low-unsaturated (TO in green) fuels. The mole fraction of NO_x in the exhaust is plotted in terms of the peak combustion temperature, where it is affected by the composition of FAME for each feedstock. The NO_x concentrations calculated in the simulation follow a similar trend as the experimental data.

Figure 35(b) shows the prediction of the SSA model when the biodiesel fuels were blended with ULSD in proportions of B20 (20% biodiesel, 80% ULSD) and B50 (50% biodiesel, 50% ULSD). The results are plotted with their SDs for the NO_x mole fraction in terms of the peak combustion temperature (x-axis). As the content of ULSD increases in the blends, the peak combustion temperature increases (Omidvarborna et al., 2015c). This temperature increase may result in the formation of thermal NO_x. The SSA model is a good predictor of the mole fraction of NO_x from B50, B20, and ULSD fuels, which means that the ND mechanisms are well suited in the simulation. Although the NO_x values are overestimated, the agreement between the SSA model and experimental results are reasonable. It is thought that the differences in the C/H/O ratio and ester group concentration between the surrogate model and real biodiesel fuels may be responsible for the discrepancies.

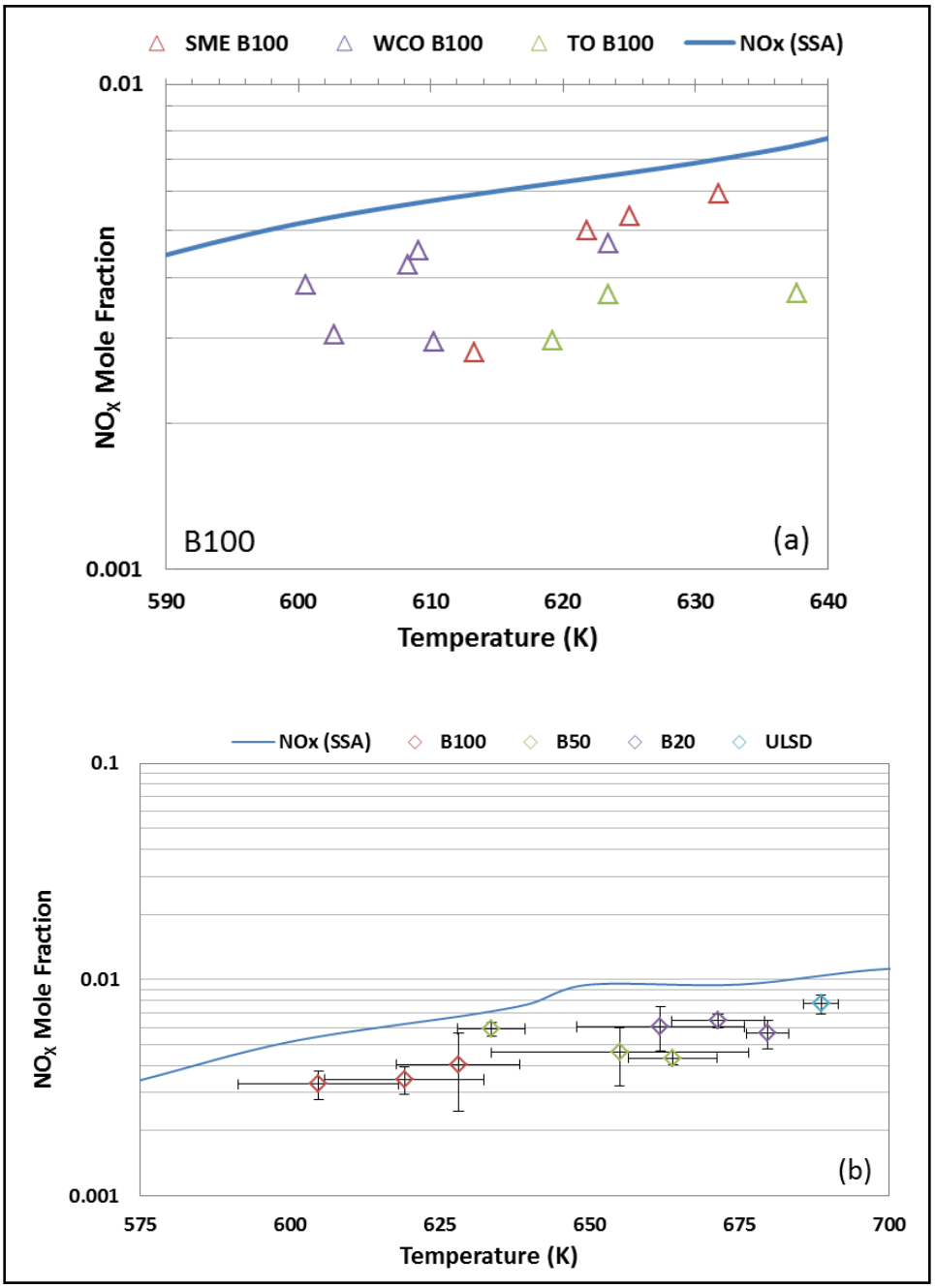

Figure 35. Comparison of Experimental (Omidvarborna et al., 2015c) (symbols) and Predicted (lines) NO_x Concentrations at Φ = 1.0 and Initial Pressure of 200 psi (13.8 bar)

The experimental values of pure biodiesel fuels (Omidvarborna et al., 2015c) versus the predicted values from the SSA are plotted along the diagonal line, as shown in Figure 36. The diagonal lines represent the equality between the experimental and simulation values. The data points located close to the line indicate agreement of the simulation results with the experimental results. Nearly all the experimental data are located within the scatter bands of +20% for SME and WCO fuels. The results for TO are greater than +20%, meaning the model over predicted the NO_x emissions. MD and MD5D have shorter chains than methyl esters in biodiesel fuels (C_{12}-C_{18}), which is thought to occur because

the selected surrogate provides extra oxygen for combustion (because of the short chain and high oxygen-to-carbon ratio) compared with the experimental results. Therefore, a biodiesel surrogate should have a higher peak combustion temperature and possibly emit more NO_x emission than that seen in the experimental data. The over prediction of exhaust emissions at LTC also can be seen in the work of Chang et al. (2015) with a reduced mechanism. The differences in the C/H/O ratio and ester group concentration between the surrogate model and real fuels may be responsible for this over prediction. In addition, the SSA shows better prediction of NO_x concentrations for the biodiesel with unsaturated fatty acids than the ones with saturated fatty acids. It is suggested that the reaction pathways be expanded to include possible side reactions, especially for saturated fatty acids, to reduce the deviations. However, considering the possibility that the semidetailed NO_x formation mechanisms may result in a better prediction on NO_x, it will make the model more complex. For the current model, the RMSE values confirm the dependence of the unsaturation degree on better agreement of the SSA model with the experimental values. The RMSE values for SME (highly unsaturated), WCO, and TO (saturated) are 0.0020, 0.0019, and 0.0029, respectively. The RMSE values show that the overall agreement between the experimental data and the predictions from the biodiesel surrogate (ND/MD/MD5D) is considered satisfactory.

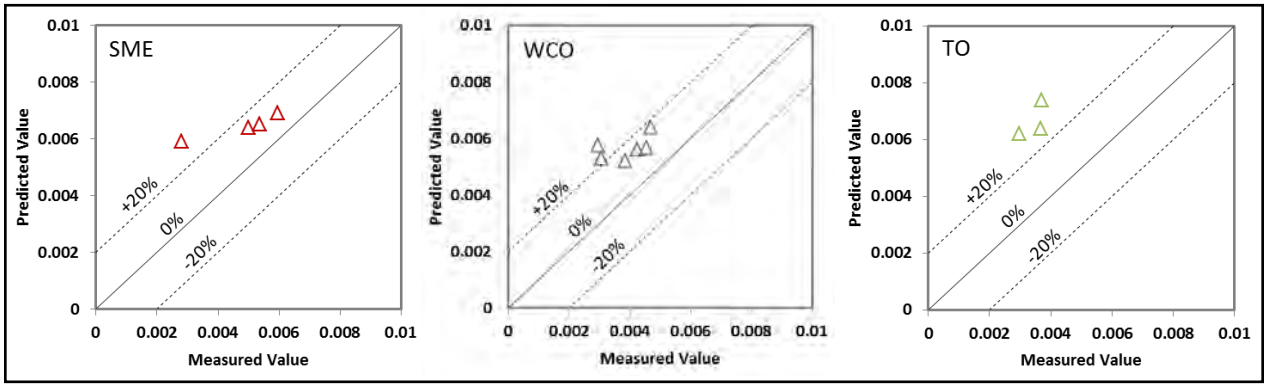

Figure 36. Measured Values versus Predicted Values by SSA for Pure Biodiesel Fuels (SME, WCO, and TO)

V. CONCLUSION

Biodiesel, produced from renewable sources, is a more sustainable source of energy and plays an increasingly significant role in meeting energy demands. Therefore, research on the different feedstocks and their influence on emissions and PM size distribution are increasingly important. Biodiesel from different sources have various physical and chemical properties compared to diesel fuel. These fuel properties have an impact on combustion, emission, and PM size characteristics. Based on the laboratory/field experiments and modeling studies carried out, the following conclusions can be drawn.

From the laboratory study, the FTIR results showed different functional groups in biodiesels from ULSD, which resulted in variation of emission characteristics. The FTIR spectra of biodiesel fuels showed C=O stretching bond of methyl ester at 1700 to 1800 cm^{-1} and C-O bonds at 1000 to 1300 cm^{-1}, respectively. FTIR results indicate that it is not possible to establish any significant difference between biodiesel fuels. Under LTC conditions, the ignition delay time and ignition temperature increased and decreased, respectively, when the percentage of biodiesel in the blends increased. The ignition temperatures of neat biodiesel samples decreased relatively in the order of SME (the highest), TO, and WCO (the lowest). It was found that all neat biodiesel samples produced almost no soot after combustion and as the portion of ULSD increased in the blends, the mass of soot increased. TEM conducted on 100 soot particles showed that ULSD emitted larger particles than biodiesel fuels under test conditions. The oxygen content of biodiesel is thought to reduce the size of soot particles through enhanced oxidation, which also made the size distribution of soot narrower than that of ULSD. The high content of oxygen in the biodiesel samples is thought to change the internal structure of soot particles by interfering with the process of soot formation (e.g., soot inception, nucleation, and growth), which eventually leads to reduced soot production.

Elemental analysis showed the presence of aluminum, calcium, copper, iron, magnesium, molybdenum, sodium, and potassium in soot from biodiesel samples. These are the major inorganic elements in biodiesel soot that directly originate from the fuel. FTIR analysis of soot particles clearly showed that soot produced from biodiesel combustion contained oxygen molecules. Having oxygen in the soot structure may enhance the oxidation of the soot produced due to possible reactions involving oxygen bonds.

TGA analysis was divided into two parts, unburned HC and carbon. The reactivity of soot from various fuels was investigated and the results indicated that biodiesel blends showed a faster rate of oxidation compared with ULSD. Blends of biodiesel fuels showed a lower temperature peak, indicating a greater soot oxidation in comparison to ULSD. Among biodiesel fuels, WCO had the lowest temperature peak.

The laboratory results confirmed that the degree of unsaturation may be related to oxygen content in biodiesel fuels. As unsaturation degree increased, the oxygen content in FAMEs increased. SME, the most highly unsaturated biodiesel compared with WCO and TO, emitted smaller soot particles under TEM study as well as a stronger FTIR spectrum of OH bonds in collected soot.

The difference in NO_x emissions between neat biodiesel samples and ULSD was validated. The degree of unsaturation of biodiesel appeared to have a relationship with NO_x emissions. In a comparison of average values, SME produced more NO_x emissions than TO and WCO. Highly unsaturated molecules in biodiesel such as C18:2 and C18:3 appear to cause more NO_x emissions. Biodiesel with a small amount of unsaturated HCs would help reduce NO_x emissions. The paired t-test results indicated that there were significant differences in NO_x emissions between the neat biodiesel samples, e.g., TO100, WCO50, and WCO100, and ULSD. Additionally, there were pairs of fuels that may cause partially significant differences in NO_x reduction.

Carbon emission analysis gives valuable knowledge on the combustion characteristics, fuel properties, and carbon emissions of three biodiesel fuels from various feedstock under fuel-rich LTC conditions. This investigation confirmed that the variation in the properties of the biodiesel led to the different carbon emissions over a range of combustion conditions. CO and CO_2 emissions are well correlated with the chemical characteristics of the fuels. The highest value of CO emissions and the lowest value of CO_2 emissions were observed for ULSD. For biodiesel fuels, high oxygen-to-carbon ratios and short saturated chains of methyl esters are thought to attribute to more complete combustion and less CO and more CO_2 production compared to ULSD. More CO_2 was produced in the order of TO (the shortest and the most saturated), WCO, and SME (the longest and the least saturated). The CH_4 content in the emissions seemed to be enhanced by the addition of biodiesel in the blends. Saturated FAMEs with short chains such as in WCO and TO resulted in lower emissions of CH_4 than longer chain biodiesel fuels with unsaturated bonds. The results suggest that more saturated fuel with high levels of short FAMEs produce low emissions of CO, CO_2, and CH_4, especially in fuel-rich conditions and during incomplete combustion.

From the field study, more PM deposition is observed from buses running on ULSD than buses running on SME B20. Moreover, cold idling releases comparatively larger quantities of PM than hot idling mode. In both hot and cold idling modes, PM_{10} was released regardless of the type of fuel combusted, but the PM size range for hot idling had lower particle concentrations than that for cold idling. The NO_x emission changes were directly proportional to engine speed; that is, they increased with higher engine speed and decreased with lower engine speed.

From the modeling study, the ANN results showed that three-layer neural network modeling along with the back-propagation feed-forward neural network, combination of logsig transfer functions, and the LM training algorithm predicted NO_x emissions in close agreement with the experimental data. R values were very close to 1 for training, validating, and testing of the network, when 21 (4-21-1) and 26 (7-26-1) neurons in hidden layers were selected for the non-EGR and EGR engines. R-values were very close to 1, thus indicating that ANN modeling could predict the experimental data (average R-value of 0.99567 (without EGR) and 0.99954 (with EGR) for tested engines). RMSE analysis of the experimental data and calculated data was performed and the RMSE values were 22.1 and 1.7 ppm for non-EGR and EGR engine series, respectively. Thus, EGR proved to be a useful tool to control NO_x emissions from idling engines. Therefore, ANN has the potential to predict engine emissions under idling conditions. However, appropriate training data and input parameters must be used. With sufficient data and parameters available for input, the use

of ANN may be a powerful tool for predicting engine exhaust emissions without conducting complicated, expensive, and time-consuming experiments.

Understanding of the oxidation mechanism and kinetics of biodiesel surrogates significantly contributes to the development of reliable kinetic models for methyl esters and consequently real biodiesel fuels. Thus, the need for larger methyl esters, including both saturated and unsaturated, in practical biodiesel is imperative. In this study, a simplified chemical reaction mechanism for combustion of biodiesel fuels is simulated using the SSA and Monte Carlo simulation. The results are validated against the experimental data for the mole fraction of NO_x in the exhaust emissions. Biodiesel surrogates, MD and MD5D, are used as representatives of saturated and unsaturated methyl ester, and ND is included to match the energy content of the surrogates with ULSD. The SSA can be a simple and feasible algorithm for simplified surrogates to predict the combustion byproducts of biodiesel with relatively good agreement. By varying the ratios of surrogates, it is possible to simulate the combustion of different types of biodiesel that have different compositions of saturated and unsaturated fatty acids. The overall agreement between the SSA predictions and experimental data is satisfactory, but the current model underestimates NO_x concentration for TO by more than 20% compared to SME and WCO, which have more unsaturated fatty acids than TO. It is thought that the difference between chemical characteristics of the surrogate and real FAMEs as well as the simplified reaction pathways has a major impact on this deviation. Moreover, a careful selection of side reactions and inclusion of them in the combustion mechanisms would increase the model performance. Lastly, more detailed analysis and comparison of biodiesel surrogates are required to improve the prediction through SSA simulation.

The results presented here also provide additional justification for the use of biodiesel as an alternative fuel. In addition to providing a renewable energy source to the transportation sector and reducing exhaust emissions, biodiesel use may have the advantage of reducing the size and number of soot particles emitted.

VI. PUBLICATIONS

- Hamid Omidvarborna, Ashok Kumar, and Dong-Shik Kim, Pavan Kumar Penumalla Venkata, Venkata Siva Prasad Bollineni, Characterization and Exhaust Emission Analysis of Biodiesel in Different Temperature and Pressure: Laboratory Study, Journal of Hazardous, Toxic, and Radioactive Waste, 19 (2), 2015, 04014030.

- Hamid Omidvarborna, Ashok Kumar, and Dong-Shik Kim, Characterization of particulate matter emitted from transit buses fueled with B20 in idle modes, Journal of Environmental Chemical Engineering, 2 (4), 2014, 2335–2342.

- Hamid Omidvarborna, Ashok Kumar, and Dong-Shik Kim, Recent Studies on Soot Modeling for Diesel Combustion, Renewable and Sustainable Energy Reviews, 48, 2015, 635–647.

- Hamid Omidvarborna, Ashok Kumar, and Dong-Shik Kim, NO_x emissions from low-temperature combustion of biodiesel made of various feedstocks and blends, Fuel Processing Technology, 140, 2015, 113-118.

- Variation of diesel soot characteristics by different types and blends of biodiesel in a laboratory combustion chamber, Science of Total Environment, 544, 2016, 450-459.

- Hamid Omidvarborna, Ashok Kumar, and Dong-Shik Kim, ANN of NO_x emission from EGR and non-EGR transit buses in cold and hot idling modes, Environmental Progress & Sustainable Energy, In press (DOI: 10.1002/ep.12376).

- Hamid Omidvarborna, Ashok Kumar, and Dong-Shik Kim, The effect of unsaturated bonds and chain lengths on combustion and carbon emissions of biodiesel fuels from different feedstocks, (under review).

- Hamid Omidvarborna, Ashok Kumar, and Dong-Shik Kim, Prediction of NO_x emissions from a simplified biodiesel surrogate by applying stochastic simulation algorithms (SSA), (under review).

BIBLIOGRAPHY

Abd-Alla, Gamal Hassan “Using Exhaust Gas Recirculation in Internal Combustion Engines: A Review.” *Energy Conversion and Management* 43 (2002): 1027-1042.

Abdel-Rahman, AA. “On the Emissions from Internal-Combustion Engines: A Review.” *International Journal of Energy Research* 22 (1998): 483-513.

Aceves, Salvador M., Joel Martinez-Frias, Daniel L. Flowers, J. Ray Smith, Robert W. Dibble, John F. Wright, and Randy P. Hessel. *A decoupled model of detailed fluid mechanics followed by detailed chemical kinetics for prediction of iso-octane HCCI combustion*. No. 2001-01-3612. SAE Technical paper, 2001.

Adi, Gaytari, Carrie Michele Hall, David Snyder, Michael Bunce, Christopher Satkoski, Shankar Kumar, Phanindra Garimella, Donald Stanton, and Greg Shaver. “Soy-Biodiesel Impact on NOx Emissions and Fuel Economy for Diffusion Dominated Combustion in a Turbo Diesel Engine Incorporating Exhaust Gas Recirculation and Common Rail Fuel Injection.” *Energy and Fuels* 23 (2009): 5821–5829.

Agarwal, Avinash Kumar, and Lalit Das. “Biodiesel Development and Characterization for Use as a Fuel in Compression Ignition Engine.” *Journal of Engineering for Gas Turbines and Power* 123 (2001): 440–447.

Agarwal, Avinash Kumar, Shrawan Kumar Singh, Shailendra Sinha, and Mritunjay Kumar Shukla. “Effect of EGR on the Exhaust Gas Temperature and Exhaust Opacity in Compression Ignition Engines.”*Sadhana* 29, no. 3 (2004): 275-284.

Agarwal, Deepak, Shrawan Kumar Singh, and Avinash Kumar Agarwal. “Effect of Exhaust Gas Recirculation (EGR) on Performance, Emissions, Deposits and Durability of a Constant Speed Compression Ignition Engine.” *Applied Energy* 88 (2011): 2900–2907.

Ahn, Tae-Hyuk, Yang Cao, and Layne T. Watson. “Stochastic Simulation Algorithms for Chemical Reactions.” In *BIOCOMP*, pp. 431-436. 2008.

Barabas, I., A. Todoruţ, and D. Băldean. “Performance and Emission Characteristics of a CI Engine Fueled with Diesel–Biodiesel–Bioethanol Blends.” *Fuel* 89 (2010): 3827-3832.

Bari, Saiful. “Performance, Combustion and Emission Tests of a Metro-Bus Running on Biodiesel-ULSD Blended (B20) Fuel.” *Applied Energy* 124 (2014): 35-43.

Basha, Syed Ameer, K. Raja Gopal, and S. Jebaraj. “A Review on Biodiesel Production, Combustion, Emissions and Performance.” *Renewable and Sustainable Energy Reviews* 13 (2009): 1628-1634.

Benjumea, Pedro, John R. Agudelo, and Andrés F. Agudelo. “Effect of the Degree of Unsaturation of Biodiesel Fuels on Engine Performance, Combustion Characteristics, and Emissions.” *Energy & Fuels* 25 (2010): 77-85.

Betha, Raghu, and Rajasekhar Balasubramanian. “Emissions of Particulate-Bound Elements from Biodiesel and Ultra Low Sulfur Diesel: Size Distribution and Risk Assessment.” *Chemosphere* 90 (2013): 1005-1015.

Boehman, Andre L., David Morris, James Szybist, and Etop Esen. “The Impact of the Bulk Modulus of Diesel Fuels on Fuel Injection Timing.” *Energy & Fuels* 18 (2004): 1877-1882.

Boehman, André L., Juhun Song, and Mahabubul Alam. “Impact of Biodiesel Blending on Diesel Soot and the Regeneration of Particulate Filters.” *Energy & Fuels* 19 (2005): 1857-1864.

Brakora, Jessica L., Youngchul Ra, Rolf D. Reitz, Joanna McFarlane, and C. Stuart Daw. “Development and validation of a reduced reaction mechanism for biodiesel-fueled engine simulations.” *SAE International Journal of Fuels and Lubricants* 1, no. 1 (2009): 675-702.

Burrage, Kevin, Tianhai Tian, and Pamela Burrage. “A Multi-Scaled Approach for Simulating Chemical Reaction Systems.” *Progress in Biophysics and Molecular Biology* 85, no. 2 (2004): 217-234.

Cain, Jeremy P., Paul L. Gassman, Hai Wang, and Alexander Laskin. “Micro-FTIR Study of Soot Chemical Composition—Evidence of Aliphatic Hydrocarbons on Nascent Soot Surfaces.” *Physical Chemistry Chemical Physics* 12 (2010): 5206-5218.

Cardone, Massimo, Maria Vittoria Prati, Vittorio Rocco, Maurizia Seggiani, Adolfo Senatore, and Sandra Vitolo. “Brassica Carinata as an Alternative Oil Crop for the Production of Biodiesel in Italy: Engine Performance and Regulated and Unregulated Exhaust Emissions.” *Environmental Science & Technology* 36 (2002): 4656-4662.

Caresana, Flavio. “Impact of Biodiesel Bulk Modulus on Injection Pressure and Injection Timing. The effect of residual pressure.” *Fuel* 90 (2011): 477-485.

Chang, Yachao, Ming Jia, Yaodong Liu, Yaopeng Li, and Maozhao Xie. “Development of a New Skeletal Mechanism for N-Decane Oxidation under Engine-Relevant Conditions Based on a Decoupling Methodology.” *Combustion and Flame* 160, no. 8 (2013): 1315-1332.

Chang, Yachao, Ming Jia, Yaopeng Li, Yanzhi Zhang, Maozhao Xie, Hu Wang, and Rolf D. Reitz. “Development of a Skeletal Oxidation Mechanism for Biodiesel Surrogate.” *Proceedings of the Combustion Institute* 35 (2015): 3037-3044.

Chattopadhyay, Soham, and Ramkrishna Sen. “Fuel Properties, Engine Performance and Environmental Benefits of Biodiesel Produced by a Green Process.” *Applied Energy* 105 (2013): 319-326.

Chauhan, BS, Kumar N, and Cho HM. “A Study on the Performance and Emission of a Diesel Engine Fueled with Jatropha Biodiesel Oil and its Blends.” *Energy* 37 (2012):616-622.

Chien, Yi-Chi, Mingming Lu, Ming Chai, and F. James Boreo. “Characterization of Biodiesel and Biodiesel Particulate Matter by TG, TG− MS, and FTIR.” *Energy & Fuels* 23 (2008): 202-206.

Demirbas, Ayhan. “Importance of Biodiesel as Transportation Fuel.” *Energy Policy* 35, (2007): 4661-4670.

Dieselnet website (2015). https://www.dieselnet.com/tech/diesel_emiform.php (*Accessed October 17, 2015*).

Diévart, Pascal, Sang Hee Won, Stephen Dooley, Frederick L. Dryer, and Yiguang Ju. “A Kinetic Model for Methyl Decanoate Combustion.”*Combustion and Flame* 159, no. 5 (2012): 1793-1805.

Dooley, Stephen, Henry J. Curran, and John M. Simmie. “Autoignition Measurements and a Validated Kinetic Model for the Biodiesel Surrogate, Methyl Butanoate.” *Combustion and Flame* 153, no. 1 (2008): 2-32.

Durrett, Timothy P., C. Benning, and J. Ohlrogge. “Plant Triacylglycerols as Feedstocks for the Production of Biofuels.” *The Plant Journal* 54 (2008): 593-607.

Fazal, M. A., A. S. M. A. Haseeb, and H. H. Masjuki. “Biodiesel Feasibility Study: An Evaluation of Material Compatibility; Performance; Emission and Engine Durability.” *Renewable and Sustainable Energy Reviews* 15 (2011): 1314-1324.

Fernando, Sandun, Chris Hall, and Saroj Jha. “NOx Reduction from Biodiesel Fuels.” *Energy & Fuels* 20 (2006): 376-382.

Fisher, Elizabeth M., William J. Pitz, Henry J. Curran, and Charles K. Westbrook. “Detailed Chemical Kinetic Mechanisms for Combustion of Oxygenated Fuels.” *Proceedings of the Combustion Institute* 28, no. 2 (2000): 1579-1586.

Gaïl, Sandro, Murray J. Thomson, S. Mani Sarathy, Sajid A. Syed, Philippe Dagaut, Pascal Diévart, Anthony J. Marchese, and Frederick L. Dryer. “A Wide-Ranging Kinetic Modeling Study of Methyl Butanoate Combustion.” *Proceedings of the Combustion Institute* 31, no. 1 (2007): 305-311.

Gaïl, S., S. M. Sarathy, M. J. Thomson, P. Diévart, and P. Dagaut. “Experimental and Chemical Kinetic Modeling Study of Small Methyl Esters Oxidation: Methyl (E)-2-Butenoate and Methyl butanoate.” *Combustion and Flame* 155, no. 4 (2008): 635-650.

GHG Data 2006, Highlights from greenhouse gas (GHG) emissions data for 1990–2004 for Annex I Parties, United Nations Framework Convention for Climate Change. Available at: http://unfccc.int/files/essential_background/background_publications_htmlpdf/application/pdf/ghg_booklet_06.pdf (Accessed on December 20, 2015).

Ghobadian, Barat, H. Rahimi, A. M. Nikbakht, G. Najafi, and T. F. Yusaf. “Diesel Engine Performance and Exhaust Emission Analysis Using Waste Cooking Biodiesel Fuel with an Artificial Neural Network.” *Renewable Energy* 34 (2009): 976-982.

Gillespie, Daniel T. “A General Method for Numerically Simulating the Stochastic Time Evolution of Coupled Chemical Reactions.” *Journal of Computational Physics* 22, no. 4 (1976): 403-434.

Gillespie, Daniel T. “Exact Stochastic Simulation of Coupled Chemical Reactions.” *The Journal of Physical Chemistry* 81, no. 25 (1977): 2340-2361.

Golovitchev, Valeri I., and Junfeng Yang. “Construction of Combustion Models for Rapeseed Methyl Ester Bio-Diesel Fuel for Internal Combustion Engine Applications.” *Biotechnology Advances* 27, no. 5 (2009): 641-655.

Haas, Michael J., Karen M. Scott, Teresa L. Alleman, and Robert L. McCormick. “Engine Performance of Biodiesel Fuel Prepared from Soybean Soapstock: A High Quality Renewable Fuel Produced from a Waste Feedstock.” *Energy & Fuels* 15 (2001): 1207-1212.

Hansen KF and Jensen MG. “Chemical and Biological Characteristics of Exhaust Emissions from a DI Diesel Engine Fuelled with Rapeseed Oil Methyl Ester (RME).” SAE paper, 971689, 1997.

Harris, Stephen J., and M. Matti Maricq. “Signature Size Distributions for Diesel and Gasoline Engine Exhaust Particulate Matter.” *Journal of Aerosol Science* 32 (2001): 749-764.

Herbinet, Olivier, William J. Pitz, and Charles K. Westbrook. “Detailed Chemical Kinetic Oxidation Mechanism for a Biodiesel Surrogate.” *Combustion and Flame* 154, (2008): 507-528.

Hill, S. C., and L. Douglas Smoot. “Modeling of Nitrogen Oxides Formation and Destruction in Combustion Systems.” *Progress in Energy and Combustion Science* 26 (2000): 417-458.

Hoekman, S. Kent, and Curtis Robbins. “Review of the Effects of Biodiesel on NOx Emissions.” *Fuel Processing Technology* 96 (2012): 237-249.

Hountalas, D. T., G. C. Mavropoulos, and K. B. Binder. “Effect of Exhaust Gas Recirculation (EGR) Temperature for Various EGR Rates on Heavy Duty DI Diesel Engine Performance and Emissions.” *Energy* 33 (2008): 272-283.

Ishiguro, Tomoji, Noritomo Suzuki, Yoshiyasu Fujitani, and Hidetake Morimoto. “Microstructural Changes of Diesel Soot during Oxidation.” *Combustion and Flame* 85 (1991): 1-6.

Ismail, Harun Mohamed, Hoon Kiat Ng, Suyin Gan, Tommaso Lucchini, and Angelo Onorati. “Development of a Reduced Biodiesel Combustion Kinetics Mechanism for CFD Modelling of a Light-Duty Diesel Engine.” *Fuel* 106 (2013): 388-400.

Kaden, Debra A., Ronald A. Hites, and William G. Thilly. “Mutagenicity of Soot and Associated Polycyclic Aromatic Hydrocarbons to Salmonella Typhimurium.” *Cancer Research* 39 (1979): 4152-4159.

Kegl, Breda. “Influence of Biodiesel on Engine Combustion and Emission Characteristics.” *Applied Energy* 88 (2011): 1803-1812.

Kiani, M. Kiani Deh, Barat Ghobadian, T. Tavakoli, A. M. Nikbakht, and G. Najafi. “Application of Artificial Neural Networks for the Prediction of Performance and Exhaust Emissions in SI Engine Using Ethanol-Gasoline Blends.” *Energy* 35 (2010): 65-69.

Kleeman, Michael J., James J. Schauer, and Glen R. Cass. “Size and Composition Distribution of Fine Particulate Matter Emitted from Motor Vehicles.” *Environmental Science & Technology* 34 (2000): 1132-1142.

Klippenstein, Stephen J., Lawrence B. Harding, Michael J. Davis, Alison S. Tomlin, and Rex T. Skodje. “Uncertainty Driven Theoretical Kinetics Studies for CH_3OH Ignition: HO_2+ CH_3OH and O_2+CH_3OH.” *Proceedings of the Combustion Institute* 33, no. 1 (2011): 351-357.

Knothe, Gerhard. “Dependence of Biodiesel Fuel Properties on the Structure of Fatty Acid Alkyl Esters. “*Fuel Processing Technology* 86 10 (2005): 1059-1070.

Knothe, Gerhard, Christopher A. Sharp, and Thomas W. Ryan. “Exhaust Emissions of Biodiesel, Petrodiesel, Neat Methyl Esters, and Alkanes in a New Technology Engine.” *Energy & Fuels* 20 (2006): 403-408.

Kohse-Höinghaus, Katharina, Patrick Oßwald, Terrill A. Cool, Tina Kasper, Nils Hansen, Fei Qi, Charles K. Westbrook, and Phillip R. Westmoreland. “Biofuel Combustion Chemistry: from Ethanol to Biodiesel.” *Angewandte Chemie International Edition* 49 (2010): 3572-3597.

Korn, Maria das Graças Andrade, Denilson Santana Sodré dos Santos, Bernhard Welz, Maria Goreti Rodrigues Vale, Alete Paixão Teixeira, Daniel de Castro Lima, and Sérgio Luis Costa Ferreira. “Atomic Spectrometric Methods for the Determination of Metals and Metalloids in Automotive Fuels–A Review.” *Talanta* 73 (2007): 1-11.

Köylü, Ümit Özgür, G. M. Faeth, Tiago L. Farias, and Maria da Gracia Carvalho. “Fractal and Projected Structure Properties of Soot Aggregates.” *Combustion and Flame* 100 (1995): 621-633.

Krzyżanowski, Michał, Birgit Kuna-Dibbert, and Jürgen Schneider. *Health Effects of Transport-Related Air Pollution*. WHO Regional Office Europe, 2005.

Kumar, Ashok, Dong-Shik Kim, Hamid Omidvarborna, and Sudheer Kumar Kuppili. *Combustion Chemistry of Biodiesel for Use in Urban Transport Buses: Experiment and Modeling*. No. CA-MNTRC-14-1146. 2014.

Kumar, Ashok, and Vinay Kumar V. Nerella. “Experimental Analysis of Exhaust Emissions from Transit Buses Fuelled with Biodiesel.” *Open Environmental Engineering Journal* 2 (2009): 81-96.

Laden, Francine, Lucas M. Neas, Douglas W. Dockery, and Joel Schwartz. “Association of Fine Particulate Matter from Different Sources with Daily Mortality in Six US Cities.” Environmental Health Perspectives 108 (2000): 941–947.

Lai, Jason YW, Kuang C. Lin, and Angela Violi. “Biodiesel Combustion: Advances in Chemical Kinetic Modeling.” *Progress in Energy and Combustion Science* 37 (2011): 1-14.

Lapuerta, Magin, Octavio Armas, and Jose Rodriguez-Fernandez. “Effect of Biodiesel Fuels on Diesel Engine Emissions.” *Progress in Energy and Combustion Science* 34 (2008b): 198-223.

Lapuerta Magin, Octavio Armas, and Jose Rodriguez-Fernandez. “Effect of the Degree of Unsaturation of Biodiesel Fuels on NOx and Particulate Emissions.” *SAE International Journal Fuels Lubricants* 1 (2009): 1150–1158.

Lapuerta, Magin, José Rodríguez-Fernández, and John R. Agudelo. “Diesel Particulate Emissions from Used Cooking Oil Biodiesel.” *Bioresource Technology* 99 (2008a): 731-740.

Lapuerta, Magín, Francisco J. Martos, and José M. Herreros. “Effect of Engine Operating Conditions on the Size of Primary Particles Composing Diesel Soot Agglomerates.” *Journal of Aerosol Science* 38 (2007): 455-466.

Lapuerta, Magín, Fermín Oliva, John R. Agudelo, and André L. Boehman. “Effect of Fuel on the Soot Nanostructure and Consequences on Loading and Regeneration of Diesel Particulate Filters.” *Combustion and Flame* 159 (2012): 844-853.

Leung, D. Y. C., and Y. Guo. “Transesterification of Neat and Used Frying Oil: Optimization for Biodiesel Production.” *Fuel Processing Technology* 87 (2006): 883-890.

Liberman, Michael A. *Introduction to Physics and Chemistry of Combustion: Explosion, Flame, Detonation*. Springer Science & Business Media, 2010.

Liu, W., R. Sivaramakrishnan, Michael J. Davis, S. Som, D. E. Longman, and T. F. Lu. “Development of a Reduced Biodiesel Surrogate Model for Compression Ignition Engine Modeling.” *Proceedings of the Combustion Institute* 34, no. 1 (2013): 401-409.

Luo, Zhaoyu, Max Plomer, Tianfeng Lu, Sibendu Som, Douglas E. Longman, S. Mani Sarathy, and William J. Pitz. “A Reduced Mechanism for Biodiesel Surrogates for Compression Ignition Engine Applications.” *Fuel* 99 (2012): 143-153.

Macor, A., F. Avella, and D. Faedo. “Effects of 30% v/v Biodiesel/Diesel Fuel Blend on Regulated and Unregulated Pollutant Emissions from Diesel Engines.” *Applied Energy* 88 (2011): 4989-5001.

Maiboom, Alain, Xavier Tauzia, and Jean-François Hétet. “Experimental Study of Various Effects of Exhaust Gas Recirculation (EGR) on Combustion and Emissions of an Automotive Direct Injection Diesel Engine.” *Energy* 33 (2008): 22-34.

Majewski, W. (2001). Diesel Particulate Filters. DieselNet Technology Guide. www.DieselNet.com

Marques, Antonio, Eliseu Monteiro, Nuno Afonso Moreira, and Salvador Malheiro. *NOx Emissions Reduction in a Biodiesel Engine by Means of EGR Technology*. No. 2007-01-0078. SAE Technical Paper, 2007.

McCormick, Robert L., Michael S. Graboski, Teresa L. Alleman, Andrew M. Herring, and K. Shaine Tyson. “Impact of Biodiesel Source Material and Chemical Structure on Emissions of Criteria Pollutants from a Heavy-Duty Engine.” *Environmental Science & Technology* 35 (2001): 1742-1747.

Metcalfe, Wayne K., Stephen Dooley, Henry J. Curran, John M. Simmie, Ahmed M. El-Nahas, and Maria V. Navarro. “Experimental and Modeling Study of C5H10O2 Ethyl and Methyl Esters.” *The Journal of Physical Chemistry A* 111, no. 19 (2007): 4001-4014.

Metropolis, Nicholas, Arianna W. Rosenbluth, Marshall N. Rosenbluth, Augusta H. Teller, and Edward Teller. “Equation of State Calculations by Fast Computing Machines.” *The Journal of Chemical Physics* 21, no. 6 (1953): 1087-1092.

Monyem A. and Van Gerpen JH. “The Effect of Biodiesel Oxidation on Engine Performance and Emissions.” *Biomass and Bioenergy* 20 (2001):317-325.

Morimune, Takaaki, Hajime Yamaguchi, and Yukio Yasukawa. “Study of Catalytic Reduction of NOx in Exhaust Gas from a Diesel Engine.” *Experimental Thermal and Fluid Science* 18 (1998): 220-230.

Mueller, Charles J., André L. Boehman, and Glen C. Martin. “An Experimental Investigation of the Origin of Increased NOx Emissions When Fueling a Heavy-Duty Compression-Ignition Engine with Soy Biodiesel.” *SAE International Journal of Fuels and Lubricants* 2 (2009): 789-816.

Najafi, G., B. Ghobadian, T. Tavakoli, D. R. Buttsworth, T. F. Yusaf, and M. Faizollahnejad. “Performance and Exhaust Emissions of a Gasoline Engine with Ethanol Blended Gasoline Fuels Using Artificial Neural Network.” *Applied Energy* 86 (2009): 630-639.

Neer, Adam, and Umit O. Koylu. “Effect of Operating Conditions on the Size, Morphology, and Concentration of Submicrometer Particulates Emitted from a Diesel Engine.” *Combustion and Flame* 146 (2006): 142-154.

Ng, Jo-Han, Hoon Kiat Ng, and Suyin Gan. “Advances in Biodiesel Fuel for Application in Compression Ignition Engines.” *Clean Technologies and Environmental Policy* 12 (2010): 459-493.

Ng, Hoon Kiat, Suyin Gan, Jo-Han Ng, and Kar Mun Pang. “Development and Validation of a Reduced Combined Biodiesel–Diesel Reaction Mechanism.” *Fuel* 104 (2013): 620-634.

Obodeh, O., and C. I. Ajuwa. “Evaluation of Artificial Neural Network Performance in Predicting Diesel Engine NOx Emissions.” *European Journal of Scientific Research* 33 (2009): 642-653.

Omidvarborna, Hamid, Ashok Kumar, and Dong-Shik Kim. “Characterization of Particulate Matter Emitted from Transit Buses Fueled with B20 in Idle Modes.” *Journal of Environmental Chemical Engineering* 2 (2014): 2335-2342.

Omidvarborna, Hamid, Ashok Kumar, and Dong-Shik Kim. “Recent Studies on Soot Modeling for Diesel Combustion.” *Renewable and Sustainable Energy Reviews* 48 (2015a): 635-647.

Omidvarborna, Hamid, Ashok Kumar, Dong-Shik Kim, Pavan Kumar Penumalla Venkata, and Venkata Siva Prasad Bollineni. “Characterization and Exhaust Emission Analysis of Biodiesel at Different Temperatures and Pressures: Laboratory Study.”*Journal of Hazardous, Toxic, and Radioactive Waste*19, no. 2 (2015b): 04014030.

Omidvarborna, Hamid, Ashok Kumar, and Dong-Shik Kim. “NOx Emissions from Low-Temperature Combustion of Biodiesel Made of Various Feedstocks and Blends.” *Fuel Processing Technology* 140 (2015c): 113-118.

Omidvarborna, Hamid, Ashok Kumar, and Dong-Shik Kim. “Variation of Diesel Soot Characteristics by Different Types and Blends of Biodiesel in a Laboratory Combustion Chamber.” *Science of The Total Environment* 544 (2016a): 450-459.

Patel, Amar, Song-Charng Kong, and Rolf D. Reitz. *Development and Validation of a Reduced Reaction Mechanism for HCCI Engine Simulations*. No. 2004-01-0558. SAE Technical Paper, 2004.

Pinzi S, Rounce P, Herreros JM, Tsolakis A, and Dorado MP. “The Effect of Biodiesel Fatty Acid Composition on Combustion and Diesel Engine Exhaust Emissions.” *Fuel* 104 (2013):170-182.

Plee, S. L., T. Ahmad, J. P. Myers, and G. M. Faeth. “Diesel NOx Emissions—A Simple Correlation Technique for Intake Air Effects.” In *Symposium (International) on Combustion* 19 (1982): 1495-1502.

Pradeep, V., and R. P. Sharma. “Use of Hot EGR for NOx Control in a Compression Ignition Engine Fuelled with Bio-diesel from Jatropha Oil.” *Renewable Energy* 32 (2007): 1136-1154.

Puhan, Sukumar, N. Saravanan, G. Nagarajan, and N. Vedaraman. “Effect of Biodiesel Unsaturated Fatty Acid on Combustion Characteristics of a DI Compression Ignition Engine.” *Biomass and Bioenergy* 34 (2010): 1079-1088.

Riediker, Michael, Wayne E. Cascio, Thomas R. Griggs, Margaret C. Herbst, Philip A. Bromberg, Lucas Neas, Ronald W. Williams, and Robert B. Devlin. “Particulate Matter Exposure in Cars is Associated with Cardiovascular Effects in Healthy Young Men.” *American Journal of Respiratory and Critical Care Medicine* 169 (2004): 934-940.

Robert, Michael A., Saskia VanBergen, Michael J. Kleeman, and Christopher A. Jakober. “Size and Composition Distributions of Particulate Matter Emissions: Part 1—Light-Duty Gasoline Vehicles.” *Journal of the Air & Waste Management Association* 57 (2007): 1414-1428.

Rosenberg, H. S., L. M. Curran, A. V. Slack, J. Ando, and J. H. Oxley. “Post Combustion Methods for Control of NOx Emissions.” *Progress in Energy and Combustion Science* 6 (1980): 287-302.

Rounce, P., A. Tsolakis, and A. P. E. York. “Speciation of Particulate Matter and Hydrocarbon Emissions from Biodiesel Combustion and Its Reduction by Aftertreatment.” *Fuel* 96 (2012): 90-99.

Roweis, S. (2004). *Levenberg Marquardt Optimization*, Cambridge University Press, 2nd edition.

Salamanca, Maurin, Fanor Mondragón, Jhon Ramiro Agudelo, Pedro Benjumea, and Alexander Santamaría. “Variations in the Chemical Composition and Morphology of Soot Induced by the Unsaturation Degree of Biodiesel and a Biodiesel Blend.” *Combustion and Flame* 159 (2012a): 1100-1108.

Salamanca, Maurin, Fanor Mondragón, John R. Agudelo, and Alexander Santamaría. “Influence of Palm Oil Biodiesel on the Chemical and Morphological Characteristics of Particulate Matter Emitted by a Diesel Engine.” *Atmospheric Environment* 62 (2012b): 220-227.

Saleh, H. E. “Effect of Exhaust Gas Recirculation on Diesel Engine Nitrogen Oxide Reduction Operating with Jojoba Methyl Ester.” *Renewable Energy* 34 (2009): 2178-2186.

Santamaria, Alexander, Nancy Yang, Eric Eddings, and Fanor Mondragon. “Chemical and Morphological Characterization of Soot and Soot Precursors Generated in an Inverse Diffusion Flame with Aromatic and Aliphatic Fuels.” *Combustion and Flame* 157 (2010): 33-42.

Sarathy, S. M., S. Gaïl, S. A. Syed, M. J. Thomson, and P. Dagaut. “A Comparison of Saturated and Unsaturated C4 Fatty Acid Methyl Esters in an Opposed Flow Diffusion Flame and a Jet Stirred Reactor.” *Proceedings of the Combustion Institute* 31 (2007): 1015-1022.

Schönborn, Alessandro, Nicos Ladommatos, John Williams, Robert Allan, and John Rogerson. “The Influence of Molecular Structure of Fatty Acid Monoalkyl Esters on Diesel Combustion.” *Combustion and Flame* 156 (2009): 1396-1412.

Schwartz, Joel. “Air Pollution and Daily Mortality: A Review and Meta-analysis.” *Environmental Research* 64 (1994): 36-52.

Shah, Sandip D., David R. Cocker, J. Wayne Miller, and Joseph M. Norbeck. “Emission Rates of Particulate Matter and Elemental and Organic Carbon from In-Use Diesel Engines.” *Environmental Science & Technology* 38 (2004): 2544-2550.

Shandilya, Kaushik, and Ashok Kumar. “Particulate Emissions from Tailpipe During Idling of Public Transit Buses Fueled with Alternative Fuels.” *Environmental Progress & Sustainable Energy* 32 (2013): 1134-1142.

Shandilya, Kaushik, and Ashok Kumar. “Carbon Speciation of Exhaust Particulate Matter of Public Transit Buses Running on Alternative Fuels.” *Fuel* 115 (2014): 678-684.

Shu, Gequn, Biao Xu, Wei Zhang, Wei Zhao, Haiqiao Wei, and Tianyu Zhu. “Chemical Kinetic Modeling for the Effects of Methyl Ester Moiety in Biodiesel on PAHs and NOx Formation.” *Transactions of Tianjin University* 19 (2013): 168-173.

Slepoy, Alexander, Aidan P. Thompson, and Steven J. Plimpton. “A Constant-Time Kinetic Monte Carlo Algorithm for Simulation of Large Biochemical Reaction Networks.” *The Journal of Chemical Physics* 128, no. 20 (2008): 205101.

Smekens, Anne, Ricardo Henrique Moreton Godoi, Patrick Berghmans, and René Van Grieken. “Characterisation of Soot Emitted by Domestic Heating, Aircraft and Cars Using Diesel or Biodiesel.” *Journal of Atmospheric Chemistry* 52 (2005): 45-62.

Song, Juhun, Mahabubul Alam, André L. Boehman, and Unjeong Kim. “Examination of the Oxidation Behavior of Biodiesel Soot.” *Combustion and Flame* 146 (2006): 589-604.

Stöber, Werner, and Ulrich R. Abel. “Lung Cancer Due to Diesel Soot Particles in Ambient Air?” *International Archives of Occupational and Environmental Health* 68 (1996): S3-S61.

Stratakis, G. A., and A. M. Stamatelos. “Thermogravimetric Analysis of Soot Emitted by A Modern Diesel Engine Run on Catalyst-Doped Fuel.” *Combustion and Flame* 132 (2003): 157-169.

Su, Jianye, Haoyue Zhu, and Stanislav V. Bohac. “Particulate Matter Emission Comparison from Conventional and Premixed Low Temperature Combustion with Diesel, Biodiesel and Biodiesel–Ethanol Fuels.” *Fuel* 113 (2013): 221-227.

Szybist, James P., Andre L. Boehman, Joshua D. Taylor, and Robert L. McCormick. “Evaluation of Formulation Strategies to Eliminate the Biodiesel NOx Effect.” *Fuel Processing Technology* 86 (2005): 1109-1126.

Szybist, James P., Juhun Song, Mahabubul Alam, and André L. Boehman. “Biodiesel Combustion, Emissions and Emission Control.” *Fuel Processing Technology* 88 (2007): 679-691.

Taghavifar, Hamid, Hadi Taghavifar, Aref Mardani, and Arash Mohebbi. “Modeling the Impact of In-Cylinder Combustion Parameters of DI Engines on Soot and NOx Emissions at Rated EGR Levels Using ANN Approach.” *Energy Conversion and Management* 87 (2014): 1-9.

USEPA (2002). A comprehensive analysis of biodiesel impacts on exhaust emissions, US Environmental Protection Agency, p02001.

USEPA website (2016). https://www3.epa.gov/climatechange/ghgemissions/sources/transportation.html (Accessed on Jan 19, 2016).

Vander Wal, Randy L., Vicky M. Bryg, and Michael D. Hays. “Fingerprinting Soot (towards source identification): Physical Structure and Chemical Composition.” *Journal of Aerosol Science* 41 (2010): 108-117.

Vander Wal, Randy L., and Aaron J. Tomasek. “Soot Nanostructure: Dependence Upon Synthesis Conditions.” *Combustion and Flame* 136 (2004): 129-140.

Varatharajan, K., and M. Cheralathan. “Influence of Fuel Properties and Composition on NOx Emissions from Biodiesel Powered Diesel Engines: A Review.” *Renewable and Sustainable Energy Reviews* 16 (2012): 3702-3710.

Vijayan, A. Characterization of Vehicular Exhaust Emissions and Indoor Air Quality of Public Transport Buses Operating on Alternative Diesel Fuels, Ph.D. Dissertation, The University of Toledo, Toledo, 2007.

Wang, Wei-Guang, Donald W. Lyons, Nigel N. Clark, M. Gautam, and P. M. Norton. “Emissions from Nine Heavy Trucks Fueled by Diesel and Biodiesel Blend without Engine Modification.” *Environmental Science & Technology* 34 (2000): 933-939.

Westbrook, Charlie K., Chitral V. Naik, Olivier Herbinet, William J. Pitz, Marco Mehl, S. Mani Sarathy, and Henry J. Curran. “Detailed Chemical Kinetic Reaction Mechanisms for Soy and Rapeseed Biodiesel Fuels.” *Combustion and Flame* 158, no. 4 (2011): 742-755.

Xue, Jinlin, Tony E. Grift, and Alan C. Hansen. “Effect of Biodiesel on Engine Performances and Emissions.” *Renewable and Sustainable Energy Reviews* 15, (2011): 1098-1116.

Yaakob, Zahira, Binitha N. Narayanan, and Silija Padikkaparambil. “A Review on the Oxidation Stability of Biodiesel.” *Renewable and Sustainable Energy Reviews* 35 (2014): 136-153.

Yamane, Koji, Atsushi Ueta, and Yuzuru Shimamoto. “Influence of Physical and Chemical Properties of Biodiesel Fuels on Injection, Combustion and Exhaust Emission Characteristics in a Direct Injection Compression Ignition Engine.” *International Journal of Engine Research* 2 (2001): 249-261.

Yoshikawa, Takeshi, and Rolf D. Reitz. “Development of an Improved NOx Reaction Mechanism for Low Temperature Diesel Combustion Modeling.” *SAE International Journal of Engines* 1, no. 1 (2009): 1105-1117.

Yusaf, Talal F., D. R. Buttsworth, Khalid H. Saleh, and B. F. Yousif. “CNG-Diesel Engine Performance and Exhaust Emission Analysis with the Aid of Artificial Neural Network.” *Applied Energy* 87 (2010): 1661-1669.

Zeldovich, Ya B. “The Oxidation of Nitrogen in Combustion and Explosions.” *Acta Physicochim. URSS* 21 (1946): 577-628.

Zhang, Yu, and André L. Boehman. “Impact of Biodiesel on NOx Emissions in a Common Rail Direct Injection Diesel Engine.” *Energy & Fuels* 21 (2007): 2003-2012.

Zheng, Ming, Mwila C. Mulenga, Graham T. Reader, Meiping Wang, David SK Ting, and Jimi Tjong. “Biodiesel Engine Performance and Emissions in Low Temperature Combustion.” *Fuel* 87 (2008): 714-722.

Zheng, Ming, Graham T. Reader, and J. Gary Hawley. “Diesel Engine Exhaust Gas Recirculation–A Review on Advanced and Novel Concepts.” *Energy Conversion and Management* 45 (2004): 883-900.

ABOUT THE AUTHORS

ASHOK KUMAR, PH.D.

Dr. Ashok Kumar is a professor and department chairman of Civil Engineering at The University of Toledo, Toledo, Ohio. Before coming to Toledo, he worked for Syncrude Canada Ltd. as an atmospheric physicist where he developed, planned, and conducted studies related to the dispersion of emissions of a tar sands plant.

Dr. Kumar received his Bachelor of Science in Engineering (Honors) from Aligarh University in India (1970), his Master of Applied Science from University of Ottawa, Canada (1972), and his Ph.D. from the University of Waterloo, Canada (1978). He is registered as a Professional Engineer in the Province of Alberta, Canada, and is a Diplomat of the American Academy of Environmental Engineers. He is a fellow member of Air and Waste Management Association (A&WMA).

Air and Waste Management Association presented him with L. A. Ripperton Award for distinguished achievement as an educator in the field of air pollution control in June 2003. He was conferred honorary membership in A&WMA in 2014. His research work has focused on finding innovative solutions to fundamental and applied problems in air quality, risk analysis, and environmental data analysis. He was a Co-PI on the TARTA grant and a PI on the MIOH grant on the use of alternative fuels.

DONG-SHIK KIM, PH.D.

Dr. Kim is associate professor of Chemical and Environmental Engineering at University of Toledo. Since joined the faculty, Dr. Kim has worked on several research projects supported by Federal, State, and international funding agencies including NSF, NASA, USDA, Air Force, Ohio Board of Regents, and KIST (Korea Institute of Science and Technology).

His research has focused on biomaterials development and biomass energy. Dr. Kim earned his Bachelor of Science and Master of Science degrees in chemical engineering at Seoul National University, Korea, and his doctorate in chemical engineering at the University of Michigan, Ann Arbor. Dr. Kim is an active member of the American Institute of Chemical Engineers, American Chemical Society, and American Society of Engineering Education.

Recognized for his achievements in research and education, he received deArce Memorial Endowment Award, Kohler Junior Faculty Award, and Outstanding Undergraduate Research Mentor Award. He is a recipient of the Air Force Summer Faculty Research Award in 2010, 2012, and 2013. He has published 50 articles in peer-reviewed journals and presented his work in domestic and international conferences. He received a US Army Achievement Medal in 1987 after 3 years of military service in Korea. He is a registered professional engineer in Michigan.

HAMID OMIDVARBORNA, PH.D.

Hamid Omidvarborna received his PhD in 2016 from The University of Toledo on alternative fuels and air pollution. He has extensive knowledge as a process and quality control engineer. He received his Bachelor of Science in Chemical Engineering from Razi University (2005) and his Master of Science from Isfahan University of Technology (2008), both in Iran. His main research interests are biofuel combustion chemistry, vehicle emission analysis, air pollution monitoring, and atmospheric modeling.

MANIDEEP YARLAGADDA

Manideep Yarlagadda is an environmental graduate student at The University of Toledo and is in the process of completing his MS. His research focus is in the area of variations in NO_x and PM emissions from transit buses running on biodiesel with EGR and non-EGR engines. Manideep received his bachelor's degree in civil engineering from Jawaharlal Nehru Technological University (JNTU), Hyderabad, India, in 2014.

SUDHEER KUMAR KUPPILI

Sudheer Kumar Kuppili is a masters student at The University of Toledo. Sudheer received his Bachelors of Technology in Civil Engineering in 2012 from Chaitanya Engineering College, JNT University, Visakhapatnam, India. He worked as a summer lecturer in 2012 at Chaintanya Engineering College. His work emphasizes biodiesel properties while focusing on the characterization and sensitive analysis of particulate matter and nitrogen oxides released from TARTA buses, which use biodiesel fuel. He conducts relative experiments in the laboratory and also teaches air pollution dispersion modelling. He is interested in air quality regulations and compliances, and has been involved in this project since August 2012.

NADER SAWTARIE

Nader Sawtarie is a chemical engineering graduate student at The University of Toledo and is pursuing his MS. His research focus is in modeling particulate matter (PM) formation from the combustion of biodiesel, and also the synthesis of bio-derived nanoparticles. Nader received his bachelor's degree in chemical engineering from Bucknell University (Lewisburg, PA) in 2012.

PEER REVIEW

San José State University, of the California State University System, and the MTI Board of Trustees have agreed upon a peer review process required for all research published by MNTRC. The purpose of the review process is to ensure that the results presented are based upon a professionally acceptable research protocol.

Research projects begin with the approval of a scope of work by the sponsoring entities, with in-process reviews by the MTI Research Director and the Research Associated Policy Oversight Committee (RAPOC). The research draft is reviewed by the Research Committee of the Board of Trustees and may include invited critiques from other professionals in the field. The review is based on the professional propriety of the research methodology.

MTI FOUNDER

Hon. Norman Y. Mineta

MTI/MNTRC BOARD OF TRUSTEES

Directors

MNTRC
MINETA NATIONAL TRANSIT RESEARCH CONSORTIUM

SAN JOSÉ STATE
UNIVERSITY

Funded by U.S. Department of
Transportation